C A P C I S

Corrosion & Protection Centre Industrial Services
University of Manchester Institute of Science & Technology

Capcis Limited
Bainbridge House, Granby Row,
Manchester, M1 2PW, United Kingdom.
Telephone: 061-236 6373
Telefax: 061-228 7846
Telex: 668610 CAPCIS G

NON-DESTRUCTIVE METHODS FOR FIELD INSPECTION OF EMBEDDED OR ENCASED HIGH STRENGTH STEEL RODS AND CABLES.

PHASE 2
FINAL REPORT
NCHRP PROJECT 10-30(3)

Prepared for:

National Co-operative Highway Research Programme
Transportation Research Board
National research Council

UMIST/CAPCIS 706015, May 1991

Prepared by:

Prof. F.M. Burdekin, Dr. D.G. John, Prof. P.A. Payne,
Mr. T.A. Smith & Dr. P.A. Gaydecki.

Acknowledgement

This work was sponsored by the American Association of State Highway and Transportation Officials, in co-operation with the Federal Highway Administration and was conducted in the National Co-operative Highway Research Programme, which is administered by the Transportation Research Board of the National Research Council.

TABLE OF CONTENTS

LIST OF FIGURES

Main Text

Appendix B

Appendix D

Appendix G

LIST OF TABLES

Main Text

Appendix D

Appendix E

LIST OF PLATES

ACKNOWLEDGEMENTS

The research team included the following members:

Professor F.M. Burdekin	-	Principal Investigator and Project Director
Dr. D.G. John	-	Principal Investigator and Project Manager
Professor P.A. Payne	-	Senior Consultant
Mr. T.A. Smith	-	Senior Consultant
Dr. K. Hladky	-	Senior Project Officer
Dr. P. Gaydecki	-	Project Officer
Mr. P. Nedwell	-	Experimental Officer

The team also gratefully acknowledges the support and help received from the following persons:

Dr. Walid Damaj, for his dedicated assistance in the experimental and theoretical work over the course of the project;

Mr. Martin Doyle and Mr. John Wall for organizing the preparation of all the concrete specimens;

Mr. Lee Sherwood, Mr. Robert Kean, Dr. Morph Jafar and Mr. Harvey Turner for assistance on potential measurements and force-corrosion experiments;

Mr. Ding for help in investigating the possibility of using pseudo-random code generation techniques;

Mr. Peter Aylott for assistance and advice on computer related aspects of the project.

ABSTRACT

This report documents and presents the results of a study to develop an ultrasonic testing method for non-destructive evaluation of deterioration in the condition of embedded steel components in concrete. Theoretical and experimental studies have been carried out on ultrasonic wave propagation in concrete and reflection from interfaces representing different conditions of deterioration in embedded steel components. Extensive scatter and attenuation of ultrasonic waves in concrete, and signal strength on reflection from different conditions of embedded component, depend highly on signal frequency. Advanced signal processing methods have been developed involving fast Fourier transformation to the frequency domain, block filtering to give signal content within discrete frequency bands, and inverse transformation to enable analysis of signal content reflected from embedded components.

A prototype scanning system, using rolling transducers, has been developed which is capable of detecting significant voids, cable breaks or major corrosion deterioration.

SUMMARY

The definition study NCHRP Project 10-30(1) which preceded the current project, had identified the capabilities and limitations of different non destructive testing methods for providing information on the condition of steel components embedded in concrete. Whilst radiographic and magnetic methods could be useful in certain circumstances, the problem of detecting major corrosion deterioration of pre-stressing tendons inside metal ducts remained extremely difficult and expensive, except for limited circumstances where radiography might be practical. Preliminary trials of ultrasonic testing techniques have shown that breaks, or partial fractures, in steel wires could be detected over lengths of several metres of wire when the ultrasonic signal was introduced by direct contact of transducers at the ends of the wire. The early stages of the present programme showed that when wires and cables were embedded in concrete, severe attenuation of the signal occurred, such that defects in the wires could only be detected within a distance of the order of one metre from the end of the wire. It was therefore clear from an early stage that any successful system for interrogating the condition of embedded steel components in concrete would have to operate by transmitting and receiving signals from the surface of the concrete, which were returned from embedded components, with information in either the amplitude, frequency or phase content of the signal about the condition of the component. Since concrete is itself an inhomogeneous material, consisting of a cement matrix with different aggregate particle sizes and perhaps porosity/microfissures, severe attenuation and scattering of ultrasonic signals occurs in concrete.

Literature surveys and theoretical and experimental studies were carried out to determine the nature of the attenuation and scattering of ultrasonic waves in concrete and the factors which controlled the reflected signal strength from embedded components. The critical factor to enable a signal to be returned from an embedded component is the ratio of the transverse dimension of the component to the ultrasonic wavelength. For detection of deterioration in the surface condition of an embedded component, such as by pitting corrosion, the critical dimension is reduced to perhaps one tenth of the component transverse dimension, which in turn implies a requirement to use signals of higher and higher frequencies. Unfortunately, attenuation and scattering of the signal in concrete are highly frequency dependent, such that high frequencies are much more severely attenuated than lower frequencies. Much effort has therefore been expended in the present programme in developing signal processing methods and experimental techniques which enable the relative signal strength, at different frequency levels and positions in the time domain, to be identified.

Efforts to analyse the whole of the signal content using ultrasonic transducers with nominal frequencies in the range 50 kHz to 350 kHz were generally unsuccessful for either time domain or frequency domain analysis. The basic reason for this was that the high frequency content information was totally swamped by the relatively insensitive low frequency content, which gave little information about embedded components because of the relatively large wavelength inherent to low frequencies. Attempts to develop transducers which gave required frequency characteristics in concrete did not overcome the problem. However, substantial progress and success was achieved with a sophisticated signal processing system which enabled the signal content in different frequency bands to be separated out and examined.

This signal processing technique involved identification of the signal content of interest in the time domain (usually the first part of the signal received) and transformation of this signal to the frequency domain by Fourier analysis. The transformed signal was then subject to block filtering so that only the signal content within the required frequency bands remained. Thus, even though the signal content at high frequencies was several orders of magnitude less than the signal content at low frequencies, the low frequency signal could be eliminated and the residual high frequency content then transformed back to the time domain for analysis of characteristic. By taking products and ratios of signal content in different frequency bands it has proved possible to identify the signal content returned from embedded features.

The practical results of these techniques are that major voids, cable breaks and severe corrosion damage can be identified with confidence but it is unlikely that the early stages of deterioration can be so identified.

In the final stages of the project, a prototype system has been developed using a pair of rolling transducers mounted on a bogie for scanning the surface of concrete beams. Further development work is necessary to take this prototype system to a practical field survey system. It is considered that the ultrasonic system developed here, should be used in conjunction with other non-destructive systems to obtain fullest information about the condition of steel components buried in concrete, but such systems are now within reach of commercial development.

CHAPTER 1: INTRODUCTION AND RESEARCH APPROACH

1.1 PROBLEM STATEMENT AND RESEARCH OBJECTIVE

In many highway bridge structures, the integrity of the entire structure depends critically upon high strength steel rods and/or cables. In suspension bridges and cable stayed bridges, the supporting cables may be from the order of 25 mm (1") diameter to the order of 1 m (39") diameter, made up of multiple individual wires. In concrete structures, reinforcement is usually in the form of steel bars of diameter perhaps 10 mm (3/8") to 50 mm (2"). The strength of steel being typically in the range 250 N/mm^2 (36000 psi) to 460 N/mm^2 (65000 psi). With prestressed concrete, the systems adopted may be either pre-tensioned or post-tensioned but in both cases, it is common to use much higher strength steel for pre-stressing tendons. Bars of 100 mm (3/8") to 50 mm (2") in strengths of 1000 N/mm^2 (144000 psi) to 1500 N/mm^2 (216000 psi) are commonly used. Pre-stressing tendons often consist of multiple wires or strands made up from wires of individual diameter 5 to 7 mm (3/16" to 5/16") with strengths in excess of 1500 N/mm^2 (216000 psi).

Bridge structures are designed for very long lives (of the order of 100 to 120 years) and may be subject to a number of deterioration mechanisms. The most serious of these, as far as steel rods and cables are concerned, are likely to be corrosion or fatigue. Corrosion will occur in any steel component exposed to a wet environment in air, unless satisfactory protection mechanisms are effective. In the case of the exposed cables, such as suspension and cable stayed bridges, protection is usually applied by zinc coatings and/or paint. In the case of components embedded in concrete, protection is normally afforded by the alkaline environment provided by cement, giving a pH value in the range 12 to 14. However, both the zinc or other protective coatings on free cables and the alkaline protection for components embedded in concrete can deteriorate due to various degradation mechanisms in service. Corrosion of the critical steel components may then take place by general loss of cross sectional area, by pitting corrosion, or, particularly in high strength steels, by a hydrogen induced stress corrosion cracking. Corrosion problems for steel rods and cables in bridges are aggravated by the use of de-icing salts, which tend to reduce the effectiveness of corrosion protection measures. Undetected ongoing corrosion of critical steel components can eventually lead to complete collapse of the structure, as has occurred in a small number of cases.

The objective of the present research project is to develop a non-destructive testing method, suitable for field inspection of bridges to detect serious deterioration of high strength rods and cables, particularly for the case of such components embedded in concrete. The case of post-tensioned, prestressed concrete structures, with cables inside metal ducts, was regarded as a critical case for which the only existing practical method was radiography with serious limitations, restrictions and cost implications.

1.2 SCOPE OF STUDY

An earlier phase of this project (NCHRP Project 10-3(1), 1987) had reviewed different non-destructive testing methods, and their capabilities and limitations for detecting the condition of embedded or encased steel rods and cables (Phase I Final Report). It was concluded from that study that whilst magnetic and radiographic based methods could give some information about the presence and condition of embedded steel components, there were severe

limitations inherent with these techniques, particularly for the case of post-tensioned cables in metal ducts. It was therefore proposed that the present study should seek to develop a non-destructive testing method based on ultrasonics/acoustic pulsing to give information about the condition of embedded steel components. The study was intended to investigate the theoretical basis for a satisfactory ultrasonic testing technique, including modelling analysis where necessary and to develop the necessary signal processing and experimental techniques to enable a prototype system to be developed from the theoretical and experimental findings.

It was originally intended that the final stage of the programme should involve practical field trials of the prototype system, when successfully developed, on examples of pre-stressed concrete bridges.

1.3 RESEARCH APPROACH

It was recognised from the start that the basic alternatives were either to transmit ultrasonic signals down the length of steel components from one end to the other, or to interrogate the steel components from the external surfaces of the concrete structure. In both cases, it was recognised that serious difficulties would arise from confusion of different signals for different ultrasonic wave types and reflections from different boundaries, together with inherent scatter and attenuation problems for ultrasonic waves in concrete.

It was necessary therefore, to carry out a thorough study of the literature to establish the problems encountered by others attempting to develop ultrasonic testing systems for steel components in concrete. It was then necessary to carry out theoretical studies and model analysis to understand the basic behaviour of ultrasonic waves of different types, either transmitted in steel embedded in concrete, or transmitted from the concrete surface to reflect from interfaces with embedded components back to the surface. In this objective, assistance was provided by a PhD research student from within the Department of Civil Engineering, UMIST, working on the theoretical and practical aspects of ultrasonic interrogation of steel components embedded in concrete. It was considered particularly important in the theoretical analysis to establish the effect of wave type, frequency and wave length on scatter, attenuation and reflection behaviour. To assist in understanding these phenomena, various series of experiments were planned which would look at the behaviour of steel components immersed in water, or embedded in mortar, or embedded in concrete. The purpose of these experiments was to try to identify that part of the signal which contained information about the condition of the steel component without the presence of the scattering/attenuation effects of concrete, and then try to develop signal processing means of separating out that same signal content when the complexities of scatter/attenuation in concrete were added.

To try and optimise the identification of breaks or serious local corrosion of embedded cables, it was planned to develop a system in which a signal transmitted from a single central transducer would be received at a surrounding array of transducers, in such a way that the signal at each receiving transducer would be reflected from different parts of the embedded steel component. By comparison of the signals received, it was hoped that when one of the transducers received a signal from a deteriorated/broken piece of cable it would immediately be clear, from comparison with other transducers receiving signals from sound cable, that a significant defect was present.

Initial studies suggested that the theoretical analysis would be likely to show the importance of signals at different frequencies and it was originally hoped to be able to develop transducers or pulse systems which would enable a range of frequencies to be applied or analysed. In this task, collaboration was arranged between CAPCIS and a PhD student working in the Department of Instrumentation and Analytical Sciences (DIAS), UMIST, on the topic of pseudo-random code generation and its application to ultrasonic excitation/reception systems. Considerable effort was therefore planned for signal processing techniques to enable signals received by up to four transducers to be analysed in the time domain, and transformed to the frequency domain, with the ability to manipulate and compare various aspects of the received signals.

It was always recognised that the critical requirement was to be able to develop a system which could interrogate the condition of post-tensioned cables in grouted ducts. An extensive experimental programme was therefore planned, in which laboratory samples of beams with embedded wires, strands, ungrouted ducts, grouted ducts and cables in grouted ducts were prepared. A small number of larger scale samples of slabs and beams with embedded components and deliberate voids was also planned. To move to the larger scale, a pre-tensioned standard bridge beam, rejected from a pre-cast manufacturer's works because of local damage to the concrete, was also obtained. All these specimens underwent extensive testing during the course of the project.

When the theoretical modelling and experimental work and the signal processing systems had been developed into a satisfactory technique, it was planned to develop a prototype scanning system which, although not suitable for commercial field use, would be sufficient to demonstrate the basis of a system suitable for development to form a commercial field tool.

CHAPTER 2: FINDINGS

2.1 STATE-OF-THE-ART SUMMARY

2.1.1 Introduction

The initial State-of-the-Art review in the Final Report on Phase 1 of NCHRP Project 10-30(1) detailed the various data bases - later to include the relatively new ICONDA system - and keywords which were used to obtain information. It also listed a number of organisations known to be concerned with the application of non-destructive examination techniques and which have been contacted to ascertain what development and progress was being made but not yet reported.

Appendix A is a bibliography of the more appropriate references selected from some hundreds of titles listed in the literature searches carried out during Phase II of this project. Extended abstracts of many of these documents have been published in Progress Reports.

The basic problem of detecting deterioration in reinforcement steel is posed in a number of references. It is commonly agreed that there is a need for a non-destructive system capable of interrogating the condition of reinforcing steel embedded in concrete. An assessment of available literature however shows that there is no consensus opinion on a preferred system for fulfilling this requirement.

Several techniques are available for development and various authors (investigators) have published papers on the status of their particular system.

Following a review of this literature and after discussion with various users and interested parties, a considered conclusion was that an ultrasound system offered the best prospect that a successful system could ultimately be developed and built.

Thus, the ultrasound systems which formed the basis of subsequent literature searches were:

- The Impact Echo Method
- Acoustic Emission
- Acoustic Pulsing
- Radar/Microwave System
- Stress waves generated by Moderate Speed Gun or Schmidt Hammer
- Electromagnetic Impact Driving Method

Subsequent literature surveys therefore concentrated on reported developments and progress in the application of ultrasound to the examination of reinforced concrete structures.

2.1.2 Review of Publication Since 1986

A complete bibliography of all references reviewed since the Final Report of 10-30(1) 1987 is given in Appendix A.

As a general observation, these surveys showed that little success in the detection of rebar deterioration has been achieved with any of the systems described. Rebar deterioration is presumed to occur beneath cracks or defects in the concrete cover. Much of the reported investigative effort has

therefore concentrated on developing techniques aimed at establishing concrete quality and condition. It is also acknowledged that reinforcement corrosion can be induced by the properties and quality of the concrete cover. Several references [18,36,106] described ultrasound techniques for determining the condition of the concrete by measuring permeability and crack control capability. Other references [30,109] were concerned with the detection of voids in cable duct grouting as these can provide corrosion sites for pre-stressing steel.

Theoretical modelling of conditions within a concrete specimen for comparison with experimental results has been undertaken by several organisations, although most papers describing this work were provided by the National Testing Institute (formally the National Bureau of Standards) in Washington. A number of references from this source [78,79,80,81,82] described the generation of a stress pulse by mechanical impact of a steel ball dropped on to the test surface and an analysis of echoes reflected from features within the test specimen.

Test specimen geometries included flat plate, plain concrete beams, beams containing disc shaped flaws, beams with surface breaking cracks and a concrete beam containing a duct, half the length of which was filled with grout. A wave form analyser captures and analyses the transient frequencies and wave forms and performs signal analysis in the frequency domain. A two dimensional finite element method was developed to predict the expected echo response from a known impact and to study the interaction of transient stress waves with planar discontinuities in elastic solids. It is claimed that the theoretical model and the analysis of diffracted waves produced good agreement, but basic measurements require the provision of a high fidelity transducer capable of measuring small surface displacements. Waveforms and frequency spectra are also influenced by specimen composition, impact contact time and distance between impact and response points. Success is claimed for the detection of relatively large defects such as holes and delaminations and the ability to differentiate between filled and empty ducts.

Following an earthquake in India an impact echo system, using a free falling hammer to generate low frequencies (200 - 500 kHz) was used to examine a dam wall. It was claimed [81] that reflections 100 m away from the source were detected and also that a crack 15 m long was identified.

Impact testing on reinforced concrete slabs has also been carried out in Japan [64,65] to investigate the propagation of stress waves. These tests were significantly less sensitive than the NTIS programme and eventually included heavier impact loadings used to determine ultimate impact capacity of reinforced concrete and modes of fracture.

The impact-echo method uses acoustic and low frequency ultrasonic test equipment and, apart from the method of introducing a stress wave into the specimen, was initially thought to parallel the research described in this report. However, this is not the case as the research described herein has had to concentrate on the detection of small changes of state of reinforcing bar induced by forced corrosion, strand breakage in a multi-strand cable and the detection of voids in grouting rather than empty ducts. This has necessitated the exploration of frequency bands giving the most readily interpreted signals, either in the time or frequency domain. It was found that higher frequencies were needed than those used for the impact-echo method.

Acoustic emission has been a subject for several researchers [35,38,52,66,77,91,97,99] The system requires the installation of permanently attached sensors and is essentially a monitoring technique rather than a periodic inspection tool. Some success has been reported in detecting noise from within reinforced concrete test specimens and structures but recent current literature [66,106,109] it is not clear whether this noise can be identified as being generated by concrete cracking due to expansive forces resulting from a build up of corrosion products, breaking of wires or wire strands, or movement at the concrete/wire interfaces. Interpretation of signals is therefore difficult without subsequent intrusive investigation.

It is generally concluded that although some success has been achieved with laboratory specimens, acoustic emission techniques for use on full scale structures is still very much an area of research.

A Japanese reference [66] reported extensive acoustic emission tests on reinforced concrete samples, subjected to bend and torsion loading, with a frequency range of 10 kHz to 300 kHz. Field tests confirmed that although acoustic emission events (counts) were highly sensitive to local instabilities, the elimination or prevention of other noise was the most important problem yet to be solved with in-situ acoustic observations.

Acoustic emission surveys have been carried out in bridges in Holland [62,66,109] but it proved impossible to identify the extent or position of damage.

Work in Germany, which has been comprehensively reported, [30] refers to the necessary role of inspection of reinforced concrete structures. Particular emphasis is placed on the adequacy of grouting and the corrosion condition of pre-stressing steel in the assessment of the condition of pre-stressed structures.

Various methods have been used to check the corrosion condition of pre-stressing members and the position and filling of ducting. Methods of investigation are classified into three groups: destructive, partially destructive and non destructive. The ultrasonic technique came under the second category, since acoustic pulsing - the preferred method - could only be carried out if access was available to the bar end which must also be flat to accommodate the probe which contains both the transmitter and receiver. Difficulties arose during test work with respect to concrete and material within concrete due to its greater inhomogeneity compared with metals. There were consequent problems in matching probes and electronics and in the unambiguous identification of signals. The suitability of the pulse echo method for checking grouting in post-tensioned members was also studied. The method was found to be limited by short, jointed or sharply angled pre-stressing bars and also by multibar systems. In common with references from other countries, risks of defects associated with grouting deficiencies in the grouting of post-tensioned structures is discussed. Demolition and modification work has revealed many inadequately filled ducts, giving rise to warnings from safety organisations. Long term durability due to faulty grouting is threatened by a reduction of failure strength due to corrosion of pre-stressing steel caused by the ingress of water and oxygen.

Ultrasonic methods used in Holland [109] to detect voids in cable duct grouting required transmitters and receivers attached to opposite faces of the concrete and velocities were measured directly. The method proved unreliable, particularly where the voids were small compared with concrete thickness or where cables shadowed each other.

The role of radar has been the subject of several references [13,14,26,27,92,101]. Extensive application of this technique has been described by several authors who have reported comprehensively on work with ground penetrating systems used to establish the thickness and connection of concrete and slab pavings. A recent reference [42] described a mobile radar system used to examine the condition of bridge decks in Canada. The technique uses high frequency electromagnetic waves, reflections from which change as electromagnetic discontinuities are encountered. The system is operated from a specially adapted prototype vehicle and is claimed to be a viable rapid scan contact method of conducting bridge inspection surveys. The system detects cracking and spalling of concrete, some of which may be the result of the expansion of corrosion products around embedded reinforcement and also bond fracture between the concrete and asphalt surfacing.

2.1.3 Summary Statement

It is universally recognised that there is a need to obtain early identification of pre-stressing cable deterioration in reinforced concrete structures if realistic assessments of structural integrity are to be made. The State of the Art, as indicated by extensive literature reviews, suggests that progress towards solutions of the problems posed is slow and difficult: none of the techniques reviewed are capable of providing a simple mobile system that can be operated by non-expert personnel. Work undertaken at CAPCIS/UMIST and reported in this document is unique in the field of experimentation and details the significant progress made towards a viable solution.

2.2 ULTRASONIC PROPAGATION IN CONCRETE

This research has been based upon the principle that by transmitting an ultrasonic pulse through concrete reinforced with steel, it is possible, by analysing the various characteristics of the detected signal, to gain information regarding the internal composition of the concrete and the condition of the reinforcing components. Before proceeding to a discussion of the findings of that research, Section 2.2 presents a review of some of the more important aspects of the science of acoustics; it is emphasised that this review is in essence a non-technical statement on a subject which is, after all, a highly complex matter, and inevitably some simplification will result. For a fuller and more mathematical treatment of the subject, the reader is referred to Appendix B, which is concerned with the topics of propagation, signal losses and signal-to-noise enhancement techniques in significant detail.

2.2.1 Basic Principles

Acoustic waves travel through a medium by propagating a disturbance of particles about a mean position. Ultrasonic waves are, of course, a class of acoustic waves, the classification being given because they lie beyond the limits of human hearing with regard to frequency (normally, this limit is said to be 20 kHz, although this is in fact rather high, especially where adults are concerned). The velocity at which the disturbance travels is known as the propagation velocity of the medium, usually denoted as ζ (the symbol used in this document), although v is also used. Since the displacement has a directional component and an oscillatory component, the displacement is said to be a function of both time and space. At any given position therefore, the degree of particle compression or rarefaction is a said to be a sinusoidal

function of time; at any given time it is sinusoidal function of space. The amplitude of the maximum displacement (peak to peak) is denoted by the symbol λ. The wavelength, λ is defined as the distance between adjacent regions of similar amplitude or slope. The frequency, f, is defined as the number of wavefronts passing a particular point in one second, and is expressed in Hertz, or Hz. Velocity, wavelength and frequency are related by the expression:

$$c = f\lambda \qquad (2.1)$$

Whilst it is often assumed that velocity, c, is independent of frequency, certain media are dispersive (including concrete), that is, different frequencies travel with different velocities. For the moment, however, the above assumption will be accepted.

Strictly speaking, this work has been concerned with the propagation, detection and analysis of low amplitude ultrasonic waves. The term "low amplitude" is used here to describe that category of waves whose magnitude is such that the medium returns to its original physical state after the disturbance has passed, i.e., there is a linear relationship between the applied stress and the resultant strain. Large amplitude waves, often referred to as shock waves, induce permanent changes in the medium through which they travel and are not dealt with in this work. This makes the subject a little easier to handle, since the equations appearing in Appendices B to E approximate more closely the situation in practical circumstances.

Ultrasonic testing has been used for many years, and used highly successfully, to inspect the internal condition of metal components and castings. Metals, as far as ultrasonic waves below 10 Mz are concerned, are homogeneous in structure and isotropic (implying that the sound travels with equal velocity regardless of orientation). Concrete, on the other hand, is highly inhomogeneous. Although, in principle, the effects of the medium on the waves are no different from those produced under homogeneous conditions, the sheer number of interfaces gives rise to such a variety of scattering and absorption mechanisms that it is impossible, without detailed and careful signal processing, to identify or interpret the information in a meaningful way. This, in essence, has been the nature of the project.

2.2.2 Wave Modes

A bulk or infinite solid medium will sustain two, and only two, wave modes; these are the compression (also known as the longitudinal wave), and the shear wave (also known as the transverse wave). In the compressional wave, the direction of particle displacement takes place in parallel to the direction of propagation. By contrast, in shear waves, the particle displacement is perpendicular with respect to the direction of propagation. It is worth mentioning at this point that in almost all pictorial representations of waveforms, for ease of interpretation, the wave is shown as a shear wave, as in Figure 1 which depicts a typical ultrasonic signal generated in this kind of work. Since shear forces can, in general, only be generated between particles in solid media, liquids cannot sustain shear waves, except for very short periods and for particularly viscous substances. A unique feature of shear waves is that they have no regions of wave compression or rarefaction. Because of this, there are no localised fluctuations in density such as occur in all other types of waves.

In solids possessing a boundary, or a surface in contact with the air, other more complex modes of propagation may exist. The most important of these "second order" waves is the surface wave (Rayleigh wave) which, incidentally, has given rise to considerable problems of interference during the earlier stages of the research. Surface wave particle displacement is elliptical in nature, and as the name suggests, this kind of wave attenuates rapidly with depth, following an exponential relationship. At a depth of one wavelength for example, the amplitude of displacement is 10% of that at the surface. The presence of surface waves can be easily verified by, for instance, placing a finger on the surface in the space between two transmit-receive transducers. This tends to damp out propagation in this mode. Another significant feature of surface waves is that, given an undamped and even surface, their attenuation occurs more gradually than waves travelling in bulk media since they only travel, essentially, in two dimensions.

In media constituting a thin layer on a substratum, long wave propagation is possible. In this case the direction of displacement of the particles takes place parallel to the surface but perpendicular to the direction of wave propagation. This kind of wave has not been encountered in this work, owing to the large dimensions of the structures under test.

In an unbounded plate whose thickness is comparable to the wavelength, plate wave (or Lamb wave) propagation can occur. Two types of plate mode can exist. The first kind, the symmetrical plate wave, propagates as a compressional wave along the centre line of the plate causing perpendicular expansion and rarefaction. The second kind, the asymmetrical plate wave, consists of particle motion whose displacement along the centre line is transverse and elliptical at the surface. Again however, Lamb waves were rarely generated in the specimens used in this project.

It is worth considering that in practical circumstances an ultrasonic system may - desirably or otherwise - generate a number of wave modes which ultimately make the analysis more complex. In such cases the arrival times of signals is of crucial importance, since each wave mode has its own characteristic velocity (see Appendix B). Furthermore, when an ultrasonic wavefront is partially reflected and refracted at the boundary between two media, mode conversion will occur.

In addition to the wave modes described above, it is necessary to consider certain wave transferal mechanisms whose nature are strongly dependent upon the dimensions of the medium in relation to the wavelength. **In particular, the propagation of acoustic waves in rods is of special significance to the project, since single, solid tendons are frequently employed to reinforce a structure.**

In rods whose diameter is less than the wavelength, compressional, transverse and torsional waves can be generated. The first kind is often referred to as the rod wave since its velocity is lower than compressional waves travelling in bulk media. In a tensioned rod, transverse waves may exist, in which the particle displacement takes place in a direction perpendicular to the direction of propagation and to the axis of the rod (string vibrations). In torsional waves, displacement occurs in a rotational manner about the axis, as the wave travels forward. The torsional wave velocity is equal to the shear wave velocity in the bulk medium.

When the diameter of the rod exceeds that of the wavelength, bulk longitudinal waves may be propagated. However, there may now also theoretically exist an infinite number of other transverse and torsional type

wave modes, grouped in families and sub-families of the basic rod. With the exception of the principle torsional wave, all are dispersive, that is, their velocity is frequency dependent. Hence a short regular sine wave transmitted into such a rod will be received as a signal whose duration is many times longer than the original pulse.

It is important to note that if an acoustic signal is transmitted along a rod embedded in a medium, in general, severe attenuation will result as the rod radiates energy into the surrounding matter. It is possible, under certain conditions, to induce loss-free propagation (see Appendix B), but the criteria to realize this phenomenon are never satisfied given the nature of the work described in this report.

2.2.3 Reflection and Refraction

When an acoustic wave travels from one medium to another, providing there is no gap at the interface, some of the energy will be reflected and some of the energy will be transmitted through to the second medium. The amount of energy reflected will depend, initially, upon the difference of the acoustic impedances between the two materials. For instance, the acoustic impedances of water and steel are so different that an ultrasonic wave travelling through water and incident on a steel plate will experience almost total reflection. Furthermore, The amount of energy transmitted into the second medium will depend upon the angle of incidence of the sound wave; maximum transmission occurs at normal incidence, and, at progressively more acute angles, progressively less energy travels into the second material. In addition, at angles other than normal incidence the transmitted wave will experience a change in its angle of penetration - hence it is refracted.

2.2.4 Signal Attenuation

Acoustic waves travelling through a real medium suffer attenuation; the causes of this phenomenon are principally scatter, absorption and divergence. These are highly complex processes, but must be addressed because, without question, they have determined the limits of accuracy and reliability of the present prototype system.

Signal scattering is primarily a function of:

- The ratio between the insonating wavelength and the mean diameter of the scatterers.

- The difference in acoustic impedance between the scatterers and the matrix in which they are embedded.

The manner in which an ultrasonic wave is scattered changes fundamentally as the mean diameter of the scatterers increases. Suffice it to say however, that the size of the scattering particles in concrete - the aggregate - excludes the use of ultrasonic interrogation frequencies above 500 kHz. This is because signal loss is proportional to the square of the frequency for stochastic scattering (where the aggregate diameter is approximately the same as the wavelength), and proportional to the fourth power of the frequency for Rayleigh scattering (where the particle diameter, such as for sand, is very much less than the wavelength).

Ultrasonic signals are also attenuated by thermal-absorptive processes, whereby the acoustical energy is ultimately converted to heat. This mechanism

generally becomes limiting at very high operating frequencies (in the MHz range), and is responsible for the eventual decay of a signal within a body.

Beam divergence is the term used to describe the way in which the sound waves spread out from their point of origin; it is dealt with more fully in the following section.

2.2.5 Transducer Considerations

The devices used in the project to generate and detect the ultrasonic waves are fabricated from piezoelectric synthetic crystals. When an electric field is applied to the upper and lower faces of a disc of this material, the crystal undergoes mechanical strain, this strain being proportional to the intensity of the applied field. The effect is reversible since an applied mechanical stress induces equal and opposite charges to appear on each face. If the crystal is excited with a short, high voltage impulse (typically several hundred volts) lasting 1μs or less, it will resonate at its natural frequency, this being proportional to the thickness of the material. The rate of decay of the oscillations is determined by the degree of damping which is applied (by the use of backing material). Generally, highly damped crystals will both generate and respond to a broader range of frequencies lying about the central resonance, but they are less sensitive than their undamped counterparts.

Disc-shaped ultrasonic transducers radiate a beam whose angle of divergence is governed by the relationship between the wavelength and the disc diameter; the smaller the wavelength in comparison to this diameter, the smaller the angle of divergence will be. Naturally it is desirable, for the purposes of energy optimization and image clarity, that the beam be as narrow as possible, at least in the case of conventional ultrasonic interrogation. In order to realize this objective the system should generate the highest frequency that does not result in intolerable losses due to scatter and absorption. As will be seen, it is virtually impossible to propagate any kind of well-defined beam into concrete with transducers of a sensible diameter; this has resulted in the development of an unconventional but successful approach to the application of ultrasonic analysis in this problem, with emphasis being placed on signal processing, analysis and data interpretation. In any non-destructive inspection system employing ultrasound, the transducers are the most important components. Considerable time has therefore been expended in attempting to find the most suitable devices.

2.3 EQUIPMENT, SAMPLES AND SOFTWARE

2.3.1 Equipment Purchased

The items of equipment that have been purchased or obtained for the purposes of the project, are listed as follows:

1. One Ferranti 286 AT IBM compatible personal computer, with 640 kbytes of main memory, 20 Mbyte hard disc and 80287 mathematics co-processor.

2. One Solartron digital storage oscilloscope, with 40 MHz digitization speed, 100 MHz display capability and 8-bit A/D resolution.

3. One Steinkamp ultrasonic pulser system with low-frequency probes.

4. Five CNS 125 kHz ultrasonic probes.

5. One pair of Steinkamp 200 kHz probes.

6. One pair of Steinkamp 500 kHz probes.

7. One pair of CNS rolling transducers.

8. One Analogic 6100 waveform analyser, with model 630 A/D converter, comprising dual channel input, independent time base, 9-bit linear digitizing resolution with 12-bit resolution in signal compression mode, 36 MHz sampling speed. Fully programmable, with time domain and frequency domain analysis functions.

Not all of these devices are used in the current prototype system; this has been a gradual refinement process involving the considered selection, over many months, of the most suitable components for the task at hand.

2.3.2 Equipment Manufactured

In addition to the above mentioned items of purchased equipment, several devices have been designed and built within UMIST/CAPCIS since suitable commercial equivalents did not exist or were not readily available. These are listed as follows:

1. One low voltage pulse-echo unit, with fast rise-time and variable pulse repetition frequency.

2. One single-cycle sine wave generator, used to excite ultrasonic transducers with one cycle of a sine wave, with a variable period facility.

3. One four channel, low-noise instrumentation grade amplifier. This featured differential-type inputs and incorporated a logic-switched gain system to improve noise immunity.

4. One four-to-two channel signal multiplexer. The CANDI system is intended, finally, to analyse signals from an array of four receiving probes. The waveform analyser has only two input channels however, and a device was required to switch between pairs of signals. The synchronisation was derived from the pulser unit.

Full constructional details of the various devices are included in Appendix G of this report.

2.3.3 Software Developed

The software that has been written during the period of the contract comprises three distinct categories: modelling, analysis and control.

In order to understand more fully the manner in which ultrasonic waves are reflected, refracted and attenuated within inhomogeneous media, programs were written that simulated how these signals travel through concrete, and how the presence of buried steel components influenced both the strength and the spectral composition of waves that travelled over various distances and sample geometries. In particular, this work has been carried out within the Department of Civil Engineering, UMIST, as part of a Ph.D. research programme.

Emphasis has also been placed on simulating signal-to-noise improvements derived from the application of specialist signal processing techniques, such as temporal and spatial signal averaging, auto- and cross-correlation, frequency domain deconvolution and successive energy trend multiplication. Both the ultrasonic modelling process and the signal-enhancement simulation have contributed greatly to the development of a practical inspection system; in other words, they have not been merely academic exercises. Without the understanding gained from this work, it is likely that the progress have the experimental programme would not have proceeded as quickly and design optimisation would have taken considerably longer.

The most important analysis software was written during the early phase of the project, i.e. before 1989. After that point, minor improvements were continually made to the signal processing programs but there were no new major enterprises in this area. It was decided as a matter of policy early in the project that, because of the particular requirements of the system, software would be written in-house rather than purchased; this ensured total compatibility with the hardware and meant that the software could be written around the most relevant signal-processing operations. In this way, maximum efficiency was assured.

The key item of software used in this early phase was ULTRAMATH™, a program that acquired data through the use of a digital storage oscilloscope (Solartron 5602), and performed a variety of time domain and frequency domain operations on the raw signals. Because it was PC based, it could not operate in real-time nor could it analyse batches of readings representing a full scan of a large scale test structure. However, it was a vital component of the early research since it identified those signal processing operations that were most relevent to the task at hand.

Once this objective had been realised, the key signal processing operations were transfered to a dedicated waveform analyser (the Analogic 6100), which has both the speed and the memory to process large numbers of sequential time records. At this stage in the project, the emphasis was therefore placed on writing software that would control the analyser, instructing it to carry out specific operations in a specific sequence, as well as storing and retrieving the data. This became known as the CANDI-scan supervisor system, CANDI being an acronym for Cable Analysis by Non-Destructive Inspection.

2.3.4 Samples Prepared

This project has been notable for the number and variety of concrete test specimens that have been manufactured within the Department of Civil Engineering, UMIST. Except when specified otherwise (such as in samples made from mortar alone), the concrete mix design used for the test specimens consisted of ordinary portland cement to BS12, water, fine aggregate and coarse aggregate (up to 20 mm) in the proportions 1 : 0.6 : 1.3 : 2.3, with a nominal cube strength at 28 days of 30 N/mm^2. Where concrete containing chloride was required, this was added at 4% chloride as calcium chloride per weight of cement. Rather than list every single sample that has been fabricated (the list would probably exceed 100), the catalogue below is a description of the types of samples on a generic basis.

a. Cylindrical samples, 50 mm diameter, various lengths to 500 mm.
   - Mortar
   - Fine aggregate
   - Coarse aggregate

b. Cylindrical samples, 150 mm diameter, various lengths to 1 m.
   - Plain
   - With single 7 mm wire, cut, uncut and corroded
   - Chloride contaminated

c. Square section samples, 150 X 150 mm, up to 1 m.
   - Mortar
   - Plain concrete
   - With 7-wire strand, cut, uncut and corroded
   - With cracked or broken surfaces
   - With voids and wire gaps
   - With solid bars up to 40 mm diameter

e. Ducted samples, 40 mm steel duct, mainly 800 - 1000 mm in length.
   - 150 X 150 mm in section
   - 150 X 300 mm in section
   - Empty
   - Filled with mortar
   - Filled with mortar and 7-wire strand, one or several
   - With void

f. Concrete slabs, 700 X 700 X 150 mm, with and without voids.

g. One full size, 9 m bridge beam (see below).

h. One large scale, 5 m test beam (see below).

The full size bridge beam is 8.79 m in length and a maximum width of 495 mm, measured at the base. The structure is pretensioned along its length by ten 15 mm diameter 7-wire strand steel tendons, each tensioned to 115 kN. See Figure 2 and Plate 1. It is a reject unit and was obtained from Buchan's to whom this assistance is acknowledged.

The large-scale test beam was fabricated at the Department of Civil Engineering, UMIST, using an existing steel mould 5.0 m long by 150 mm wide and 300 mm deep (see Plate 2). Special end plates were also machined with openings to accommodate the six equispaced 7-wire strand prestressing cables. The tendons used were supplied by British ropes Bridon Wire Division and were 15.7 mm super prestressing strand, relaxation class 2 to BS 5896/3: 1980. The strand end grips were supplied by CCL Systems of Leeds as was the stressing jack and pump system. Concrete for the beam was designed using the standard procedure set out in Design of Normal Concrete Mixes (BRE 1988). The characteristic strength was 40 N/mm^2, with a slump of 75 mm, a water cement ratio of 0.43 and a cement content of 510 kg/m^3. Figure 3 shows the test beam and provides details of the stresses in each of the tendons, the positions of additional reinforcement and locations of defects on the wires and simulated voids.

2.3.5 Transducers Evaluated

The following list catalogues all the transducers that have been used at some stage during the project.

1. 40 kHz 20 mm diameter Steinkamp transducers.
2. 50 kHz 50 mm diameter CNS transducers.
3. 125 kHz 25 mm diameter CNS transducers.

4. 170 kHz 15 mm diameter AET transducers.
5. 200 kHz 20 mm diameter CNS transducers.
6. 200 kHz 25 mm diameter Steinkamp transducers.
7. 250 kHz 40 mm diameter Krautkramer transducers.
8. 360 kHz 80 mm diameter CNS rolling transducers.
9. 400 kHz 30 mm diameter wide-band DIAS transducers.
10. 500 kHz 25 mm diameter Steinkamp transducers.

It was rapidly established in the early stages of the project that transducers generating frequencies below 100 kHz were unsuitable for detecting small-scale changes that had occured inside the concrete. At 50 kHz (types 1 and 2) for example, the wavelength of sound in concrete is approximately 80mm. The longer the wavelength, the larger the obstacle in its path must be before substantial reflection occurs. Although it was found that it was possible to transmit and receive such frequencies over very substantial distances (9 m for instance) spectral analysis suggested that they were little affected either by the internal aggregate profile or indeed by steel cables used to reinforce the samples.

None of the transducers listed above oscillated monotonically; instead they generated a range of frequencies about a centre frequency whose value was not only governed by the nominal resonance of the crystal but also by the backing material (which affects the bandwidth) and by the filtering effects of the concrete. For example, the C.N.S. rolling transducers (now incorporated into the current CANDI prototype) have a strong nominal resonance of 360 kHz, with much smaller amplitude frequencies extending down to 20 kHz and up to 450 kHz (type 8). However, when these transducers are used to insonate concrete, the signal detected over just a short distance (such as 70 mm) bears little resemblance, in the frequency domain, to the original output. Because concrete rapidly attenuates high frequencies the spectrum now contains a low amplitude peak at the nominal resonance with most of the energy being concentrated in the bands lying between 70 kHz and 100 kHz; it is not that these frequencies have been amplified (although non-linear spectral transposition is possible), rather the high frequencies have been reduced to levels below those of the lower bands.

Conventional ultrasonic inspection systems are, almost exclusively, pulse-echo systems. A short-duration signal is emitted by a transducer, reflected from an obstacle or back wall, and received either by the same transducer or by a receiving probe immediately adjacent to the transmitter. If a single transducer acts as both transmitter and receiver, it is necessary that it ceases to radiate (or "ring") before the echo returns, or at least, for the output to be at a level that is significantly weaker than the returning signal. Similarly, if two probes are employed, it is necessary that the outgoing signal be contained within a narrow beam, so as to minimize any "cross-talk" between the transmitter and receiver.

During the course of the project, there was a period of time when it was thought that a pulse-echo system might be used to locate embedded cables and regions of delamination. To this end, a number of highly-damped, medium frequency transducers (400 kHz, type 9) were fabricated by the transducer-group within the Department of Instrumentaion and Analytical Science (DIAS). With high-frequency probes used on steel (say 5 MHz), the outgoing signal will typically decay after 6 cycles, or 1.2μs. Since the speed of sound in steel is 5940 m/s there is a layer immediately below the transducer face, 3.0 mm in thickness (not 7.1 mm since the path length is

twice the outward distance), which is inaccessible because any echoes originating from this layer will be convolved with the output pulse. This is known as the dead-zone.

By comparison, the 200 kHz C.N.S. transducers (type 5) on concrete have a decay time of 150μs. The speed of sound in concrete is approximately 4000 m/s giving a dead-zone in this case of 300 mm. Most of the concrete samples used in the project have contained steel cables embedded at a depth of 70 mm. This would require a pulse echo system to cease ringing after 36μs, representing 14.4 cycles for a 400 kHz transducer. Not only was this impossible to achieve as far as the transducers were concerned, it was also found that, because of multiple internal reflections from the aggregate, a short duration ultrasonic pulse introduced in the concrete and, lasting for perhaps only 2μs (generated by laser induced plasma shock), took several hundred microseconds to decay. Because of the weakness of the echo signals, it was impossible to recover them from this background noise. Furthermore, this not only eliminated single transducer pulse-echo configurations, it also eliminated twin-probe systems. These not only suffered from the noise problems associated with back-scatter, they were also limited by surface wave effects.

The philosophy that was finally adopted involved accepting that the transducers were always going to act, effectively, as spherical wave radiators, and that the decay time of the signal was going to be much longer than was acceptable for pulse-echo systems. Emphasis was therefore placed on developing sophisticated signal processing and analysis techniques to recover the information content of the composite signal transmitted through the concrete. The central hypothesis of the current methodology in signal processing is that different wavelengths (i.e. different frequencies) will be reflected with different energies depending upon the size and nature (interface or boundary conditions) of the defect encountered.

2.4 EXPERIMENTAL METHODS

2.4.1 Early Configurations

Figure 4 and Plate 3 depicts the experimental configuration that was used for most of the tests prior to the introduction of the first CANDI prototype. A single transmitting ultrasonic probe was connected to either a C.N.S. pulser, having an excitation voltage of 1000 V, with a pulse repetion (PRF) of 10 Hz, or a Steinkamp pulser, having an excitation voltage of 600 V and a PRF of 1 Hz. Both the transmitting and the receiving probes were acoustically coupled to the concrete surface using either a medium grade petroleum based grease or an acoustic coupling gel (in practice it was found that neither had any particular advantage over the other).

The output from the receiving probe was then amplified using a single channel low-noise medium gain (up to 60 dB) preamplifier, and thence to the input of the Solartron 5602 digital storage oscilloscope. The oscilloscope was triggered to sample the data by a synchronisation signal generated by the pulser, coinciding with the probe excitation pulse. In order to improve the signal-to-noise ratio, especially where weak signals were concerned, waveform averaging was performed. Once digitised the data were transferred to a Compaq II portable PC for storage onto floppy disc and then to a the Ferranti PC for processing and final analysis.

2.4.2 The Final System (CANDI)

The CANDI system underwent two distinct stages in its evolution. In the first stage, a broad band transmitting probe with a centre frequency of 170 kHz was mounted at the centre of a cruciform style frame, with four broad band acoustic emission receivers mounted at its vertices. The design allowed the receivers to be independently located relative to the transmitter, and a variety of insertion-rings were also manufactured to allow the use of a range of transducers. Each transducer was acoustically isolated from the steel frame assembly (and thus from the transmitter) by the use of rubber 'O'-rings. These rings held the transducers inside the outer aluminium rings which were fastened to the frame with the aid of spring-loaded grub-screws. This provided each probe with independent flexibility, a feature which was deemed necessary to minimize the effects of surface irregularities.

The outputs from the four receivers were fed to the inputs of a low-noise, four channel, instrumentation grade amplifier, the outputs of this in turn being routed to a four-to-two channel multiplexer. The Analogic waveform analyser has the capability to handle only two channels, not four. Hence the multiplexer alternated its output between channels 1 & 2 and 3 & 4, deriving its synchronisation from the trigger signal generated by the pulser. The Compaq II portable PC was interfaced to the analyser and was used to control its function and to store the data onto both floppy and hard disc. Figure 5 shows the first CANDI prototype.

In the final stage, the four-transducer probe frame was replaced by two rolling transducers travelling in parallel and spaced 70 mm apart, with one probe acting as transmitter and the other as receiver; these probes were 80 mm in diameter, 40 mm in width and had a nominal resonance of 360 kHz. Good acoustical coupling was assured by the soft neoprene tyres which rolled across the surface of the concrete, this having been initially sprayed with water. The water film ensured that consistent contact was maintained with the surface of the sample, unlike earlier static grease coupled systems, thereby greatly reducing the random element in signal strength from one reading to the next. Indeed, tests revealed that the signal variation arose mainly because of changes in the aggregate profile through which the sound waves passed. Figure 6 shows these probes. Not only did these devices obviate the requirement for the muliplexer, they also substantially improved the scanning speed and spectral response of the system. Amplification was still necessary but with two channels rather than four.

2.5 FINDINGS OF EARLY EXPERIMENTS

2.5.1 Introduction

The results in this section are not necessarily presented in the chronological order in which they were conducted; rather, they are presented in a logical sequence from the simple to the fairly complex. All of the early experimental analysis was performed using static coupled probes, the digital storage oscilloscope and the PC based software.

This early stage in the project was characterised by the reasonable assumption that the presence of steel in concrete would reduce the high frequency losses normally encountered by a broad band signal when travelling through plain concrete. Because of the homogeneous nature of most metals, these signals, which did not extend beyond 500 kHz, experienced no significant frequency reduction when travelling, for instance, through 1 m of 7 mm

diameter steel wire in air (see Figure 7). By contrast, the same signal travelling through the same distance in plain concrete is radically altered, as shown by Figure 8. The first objective therefore, was to quantitatively establish the acoustic attenuation as both a function of distance and frequency.

2.5.2 Attenuation Analysis: Implications for Pulse-Echo Systems

Two broad band transducers with a nominal centre frequency of 500 kHz were coupled to either end of a solid concrete cylinder using a medium grade grease. One transducer was excited to resonance by a 600 V spike and the other, acting as a receiver, was connected directly to the input of the oscilloscope. No amplification was used. The cylinders were 50 mm in diameter and ranged in length from 100 mm to 500 mm, in 100 mm increments. Three mixes were investigated. Mix 1 contained no aggregate but was composed entirely of sand and cement. Mix 2 contained aggregate with a diameter <10 mm, and mix 3 contained aggregate with a diameter <20 mm. the signals acquired were analysed for their amplitude, energy and spectral content. The results of these experiments are described in detail in Appendix D.

Generally speaking the signal strength was found to decline not only with length of sample, but also with increase in frequency. In the case of mix 1, for the frequency band 25 kHz 50 kHz, the acoustic pressure is halved for every 100 mm travelled. Between 225 kHz 250 kHz, over the same distance the acoustic pressure falls by a factor of 4. However, although the weakest signals were associated with samples containing the largest mean aggregate size it was also discovered that the attenuation versus frequency gradient in this case did not decline as rapidly.

As theory indicates, it is Rayleigh scattering, in which the mean particle diameter is much smaller than the wavelength, that affects the higher frequency components most severely. The attenuation in this instance is proportional to the fourth power of the frequency. Whilst this scattering mode was responsible for most energy losses arising from absorption and thermal conversion, the stochastic and diffusion (or specular) scattering, occuring for particle diameters equivalent to and greater than the wavelength, gave rise to coherent noise at the receiving stage because each scattering interface produced an echo essentially similar to any echo from actual regions of delamination or corrosion (ignoring spectral shifts).

Using the attenuation statistics provided by this series of experiments, it was possible to estimate the strength of an echo that would be expected from a small area of delamination (25 mm in diameter) lying 100 mm below the surface of concrete specimen. It was also possible to estimate how much smaller the amplitude of this echo would be than the noise produced by the aggregate back-scatter. This process involved taking into account the losses incurred as a result of beam divergence, scatter and absorption. It was found that the echo was reduced in strength by a factor of approximately 1300, and beyond the limits of resolution of the detection system if signal enhancement techniques were not employed.

What makes this situation intolerable, as far as pulse-echo systems are concerned, is the presence of back-scatter noise which is always present and very much stronger than the echo amplitude. Random electronic-thermal noise can be eliminated by the use of temporal signal averaging, since the echo signal is temporally invariant and the noise is not. However, back scatter noise is also temporally invariant and can only be minimised by spatial

averaging. The number of averages that would be required to give workable signal-to-noise figures has been estimated to be in excess of 3000. Given the nature of the task, this is clearly not feasible and an alternative to the pulse-echo approach was required.

2.5.3 Cylindrical Sample Tests

Two CNS probes with a nominal resonance of 200 kHz were coupled to each face of a plain concrete cylinder, 150 mm in diameter and 1 m in length. The ultrasonic pulse that propagated through the concrete was compared to a pulse produced by the same system when the transducers were spaced 3 mm apart and immersed in water. Three major differences were observed:

a. The duration of the signal was some ten times longer, due to multiple internal reflections from the aggregate.

b. The signal was severely attenuated, by a factor of 200 or 46 dB.

c. The attenuation was most noticeable for the high frequencies; thus at 134 kHz, the attenuation was some 70 dB whereas at 35 kHz it was 18 dB. In absolute terms therefore, the ratio between the magnitudes of the lower and upper harmonics was reversed.

When the experiment was repeated but with a single 7 mm diameter steel wire embedded along the axis of the cylinder (and the transducers displaced to a position 40 mm from the wire), it was found that, although the overall signal attenuation was similar, both the propagation velocity was greater and the high frequency components had been preserved, as can be seen by comparing Figures 8 and 9.

If the transducers were mounted directly on the wire, the attenuation of the high frequency components was lessened still further (Figure 10a). This signal will not, however, resemble a signal which has travelled through wire in air since energy will be lost as radiation takes place into the surrounding medium. The extent to which the high frequencies are selectively removed will naturally depend on the quality of acoustical coupling between the wire and the concrete. During the early stages of corrosion of steel reinforcement, corrosion products accumulate at the steel/concrete interface, generating high pressures due to the volumetric increase. This results in a more intimate acoustical coupling, and has been demonstrated by examining the changes to signals passed along wire embedded in chloride contaminated samples after 0, 3 and 6 months. After each successive reading, the reduction in high frequency signal strength had become more severe (Figure 10b).

This does not necessarily imply, however, that the process would continue indefinitely as long as the corrosive action progressed. At some stage the quality of the acoustical coupling coupling would deteriorate, the increased pressure causing the concrete to crack and spall. Under such circumstances the high frequency components would be expected to experience considerably less attenuation.

The configuration whereby the transducers were attached directly to the wire ends was not successful in detecting partial cuts to the wire. In these experiments the wire was cut to a depth of 6 mm, that is, the area of contact was reduced to 8.8% of the cross-section of the wire. Apart from a slight reduction in signal amplitude, there were no indisputable spectral effects. Certainly a flaw of this kind will cause a scattering of the signal but

because of the long wavelength in comparison to the flaw dimension, no definitive conclusions could be drawn (a pulse-echo system operating at 1.25 MHz and attached to the wire was successful in locating the cut but was entirely useless once coupled to the concrete).

Table 1 contains some of the more pertinent statistics associated with the cylindrical sample experiments. Having established the parameters that were most likely to be of use in any subsequent analysis system (energy, frequency and velocity), it was necessary to conduct experiments using transmitters and receivers mounted on the same flat surface and positioned over the reinforcing steel, in order to reproduce, as far as possible, the conditions under practical circumstances.

2.5.4 Prewaveform Optimisation Analysis: Square-Section Samples

Early experimental results suggested, and this was supported by preliminary theoretical work, that the spectral content of the received signal changed as the signal decayed. Since the above results showed that the presence of steel in a concrete sample increased the measured propagation velocity, a series of tests were conducted in which the first tens of microseconds of the wave were analysed for spectral content and also compared against the spectral content for the rest of the signal.

By using significant levels of preamplification and by selectively analysing discrete sections or windows of the waveform, it proved possible, under certain circumstances, to isolate the contribution of the steel with regard to the spectral information. "Prewaveform optimisation" actually involves expanding the time base of the oscilloscope so that the window of interest encompasses the whole screen and hence the data record. Since the amplitude of this initial section of the wave is small, the oscilloscope is also used at a higher sensitivity. Table 2 contains a summary of the findings for tests on the square-section samples.

Using the same equipment as before, the transducers spaced 1 m apart were mounted on one face of a plain concrete square-section sample as illustrated in Figure 11. Both a prewave and a main wave reading were taken. The test was then repeated for a similar sample but one which contained a 15 mm 7-wire strand cable embedded along its axis. Figure 12 shows that the frequency spectra for the two main wave packets is similar in form (they will never be identical). By contrast, Figure 13 indicates that the spectra for the prewaves are markedly different; in particular, the data acquired from the sample with the cable retains significantly more energy at the higher frequency levels.

An attempt was then made to detect the presence of a single cut wire in a 7-wire strand embedded within the same type of square-section sample, using prewaveform analysis. However the dimension of this defect in comparison to the aggregate size and number, regardless of its higher acoustic impedance differential with respect to the mortar, meant that its effect on the prewave spectrum was so insignificant that no discernable difference could reliably be said to exist (Figure 14). This situation was not improved by moving the transducers closer together, since the noise arising from the aggregate back scatter was by far the most important contributory factor in determining the spectrum of the signal. Although it was not realised at that time, this experiment suggested that a level of signal processing beyond that which had been applied was required to identify the information content of the data.

In order to demonstrate that the ultrasonic wave front was actually reaching and travelling along the steel, a square-section sample was prepared with a 7-wire strand as before, and the concrete was then cut to expose the cable, as illustrated in Figure 15. With the transducers positioned on either side of the fault, the only route that the signal could take to arrive at the receiver was along the stand. This signal was measured and was found to be significantly weaker (by a factor of 50) than the signal received from an intact specimen. This again suggested that small, localised internal changes could not be identified by simply analysing the whole signal.

2.5.5 Ducted Sample Tests

Four square-section samples were fabricated with 40 mm diameter ducts embedded along their axes. The ducts themselves were made from 0.5 mm thickness steel having a corrugated-spiral surface with a peak-to-peak height of 2.5 mm. These samples were tested before and after the ducts were filled with grout. The difference between the two spectra was so apparent that prewaveform optimisation was not required; it was not that the spectra were altered, it was simply that the overall energy of the signals received from the ungrouted samples was much greater (by a factor of 10) than the energy from the grouted samples. Table 2 summarises the test statistics. The mechanism in this case is clear: the ungrouted duct acts as a void, with dimensions greater than the longest wavelength carrying any significant energy. Total reflection therefore occurs, unlike the grouted case where most of the signal will not be reflected and will experience further attenuation.

Again this result implied that small voids or areas of delamination due to corrosion might also be detected since they would reflect the shorter wavelengths rather than the longer ones. Filtering would be required since most of the energy of a broad band signal was contained in the range below 100 kHz.

2.5.6 Wedge Experiments

At this stage in the programme it was thought that two of the most serious problems which might ultimately limit the capability of a prototype system were its inability to launch a well defined beam into the concrete and hence into the steel, and the weakness of the high frequency components in comparison to the lower range of the spectrum. In an effort to improve this situation, mortar wedges were cast (Figure 16) which, it was hoped, would direct the energy at an oblique angle into the steel, rather than at normal incidence. Mortar was chosen as the wedge material in order to approximate the acoustic impedance of the concrete; this insured that the ultrasonic wave would only be slightly deflected as it left the wedge and entered the concrete. In particular it was hoped that the wave could be made to strike the steel at the first critical angle (defined as the angle at which the incident longitudinal wave does not refract through the steel but travels parallel to it along its surface). This angle for concrete/steel lies between 40° and 45°.

The wedges were not successful in improving the received energy content of the signal, mainly because losses were encured within them before the signals passed through to the concrete, due to multiple internal reflections. However, they did marginally improve the ratio of amplitudes between the low frequency and high frequency components, in favour of the high frequencies. The mechanism of this phenomenon is thought to be caused by the lower frequencies being more attenuated in the wedges because they have less directivity (higher

frequencies have smaller divergence), and therefore had a greater probability of striking the walls prior to entering the sample.

The use of wedges was eventually abandoned since the slight improvement in the above mentioned ratio was more than offset by the reduction in overall signal strength and the unnecessarily complex analysis that it entailed.

2.5.7 Main Wave and Prewaveform Optimisation Analysis: Bridge Beam Tests

The bridge beam, described in section 2.3.4 of this report, was composed of high quality concrete with a typical hardness of 50 N/mm^2 at 28 days. Its acoustic propagation velocity was unusually high at 4890 m/s. Using sensitive low frequency transducers and a moderate preamplifier gain of 40 dB (X100), signals of 40 kHz could be transmitted and received along its entire length (just less than 9 m) without difficulty. In contrast, a 140 kHz signal could only be detected to a distance of 2 m, and this with a gain of 60 dB (X1000). It was calculated that the attenuation in this case was of the order of 94 dB, i.e. involving a strength reduction of 50,000 times. For this reason, the pitch-catch experiments were conducted over distances of not more than 1 m. Table 3 provides the statistics for the bridge beam tests, and Figure 17 shows the beam and the probe locations used.

In the first experiment, a transmitting probe was coupled to the protruding end of a cable and the receiver was attached to the side of the beam with the relevant cable 64 mm below it. After acquiring a signal, the positions of the probes were reversed. Only the main waveforms were analysed. Because in both cases direct contact was made to the steel, the high frequency components were unusually strong, especially when the transmitter was attached to the steel. This was entirely expected since most of the high frequency content of the signal is scattered shortly after entering the concrete and therefore a smaller percentage will reach the buried cable, unless direct contact is made. Figure 18 shows the spectra for these tests.

Similarly the velocity in the first test was measured to be marginally higher than in the second, i.e. 5000 m/s as compared to 4975 m/s. Strictly speaking, the quantity which is being measured is the apparent velocity, since the transducers were now mounted on the same surface and the the calculations assume that the longitudinal wave travels from the transmitter to the receiver via the shortest direct path. Owing to signal scatter, these measurements will not be as precise as measurements taken with transducers mounted directly opposite each other. As a consequence, these apparent velocities have an uncertainty of approximately ±1%. It is worthy of mention that there is a greater signal pressure or amplitude associated with the first experiment than the second. Although the difference is small - 0.043 V (rms) as compared to 0.03 6 V (rms), the higher energy in the first instance is due to the containment effect of the steel.

Figure 19 shows the spectrum obtained from the prewave when the transducers were both coupled to the concrete on the edge of the beam, spaced 1 m apart with the cable lying 64 mm below the surface; it is a good example of the combined effect that both the cable and the beam geometry have on the frequency distribution. There is only one peak of significance, lying between 126 kHz and 130 kHz. The velocity, as accurately as can be measured, is 5000 m/s. This spectrum is of course very different from the spectrum of the main wave form (note the different scales on the x axes of the figures), which is dominated by the signal that has filtered through the concrete. It also

contrasts sharply with the prewave spectrum obtained when the transducers were coupled to a region of the beam where there was no underlying cable, although there were stirrups lying at right angles to the direction of propagation (Figure 20), but where the geometry of the structure was similar. The velocity in this experiment was measured to be 4890 m/s.

The strength and spectral composition of the prewave was thought to be influenced by the geometry of the concrete through which it travelled and by the presence of the steel cable. When the transducers were placed directly over the centre cable on the base of the beam (which had a cover of 40 mm), spaced 1 m apart, the lower frequencies in the prewave maintained their amplitudes but the 130 kHz band was weakened by 12 dB (Figure 21). This suggested that much of the energy had been scattered laterally before it entered the steel. Nevertheless, the spectrum is still significantly different from that obtained when no cable was present (Figure 20). In addition, the propagation velocity was measured to be 5050 m/s.

The final test conducted on the bridge beam involved placing the transducers 1 m apart on either side of the damaged area (see Figure 17). This experiment bore some similarities to the test on the square-section sample that had been cut to expose the cable (see section 2.5.4). The flaw on the beam only partially exposed the side cable but the effect on the prewave and main wave is noticeable in terms of amplitude and frequency content. Table 3 and Figure 22 show that the prewave rms value is weaker by 12 dB and its spectrum is no longer dominated by the harmonics above 120 kHz. These results are not consistent with the hypothesis that the steel alone is responsible for facilitating the transmission of high frequencies; rather, they support the idea that both the concrete and the cable interact in a complex manner and this should be taken into account when interpreting the data taken from this type of test.

2.5.8 Water Simulation Tests

The experiments described thus far were carried out in the period September 1987 to April 1988, that is, prior to the publication of the Interim Progress Report (1988). After this had been submitted, and approval had been given for a continuation of the programme, further tests on concrete were temporarily suspended in order that time could be spent on simplified and easily modified model experimental systems. In this manner it was hoped that an understanding of the mechanisms of ultrasonic propagation could be acquired using gradually more heterogeneous media.

These experiments were simulation trials, carried out in water, with steel bars located at different depths below the surface. In later tests scattering particles were added to the water to mimic the effects of aggregate in mortar. It must be said from the outset however, that meaningful results were relatively easy to obtain from water experiments, owing to the good transmission characteristics of liquid media, especially at these frequencies.

a. Method

Figure 23 and Plate 4 depict the experimental configuration. A linear transducer array, comprising two outer receivers and a central transmitter, were mounted above a water tank with their active faces in contact with the surface of the water. The spacing between the receivers and the transmitter was 76.2 mm. The transducers were selected to be as closely matched as possible with regard to spectral characteristics and sensitivity; their centre

frequency was nominally 125kHz. As before, the transmitter was excited to resonance using a 600V spike. The water depth in all experiments was 263mm.

When present, a 10mm diameter steel bar was placed at a depth of 52 mm. The transducers, having a diameter of 25mm, radiated a beam into water with a half-angle of divergence of 36°. The depth was chosen so that the receivers responded only to the echoes from the outer edge of the beam reflecting off the steel. Whilst this reduced the pressure to 28% of that measured along the axis of radiation, it ensured that the channel separation was maximised with respect to the receivers.

b. **Test Samples**

Seven major experiments were performed and analysed using this system. These were as follows:

1. Good steel, no defects.
2. Steel with saw-cut, 2.5mm width and 5 mm depth, with the flaw located between transmitter and right hand (B) receiver.
3. As (2) but with cut rotated through 90°.
4. Bar with radially corroded region, 30 mm long and 1 mm deep, located between transmitter and receiver B.
5. Naturally corroded bar.
6. Scan of force-corroded bar.

After satisfactory results were obtained from these tests, irregularly shaped polystyrene granules, with a mean diameter of 4 mm, were added to the water to scatter the ultrasonic beam. Polystyrene was chosen since the ratio of its acoustic impedance to that of water is similar to the acoustic impedance ratio between aggregate and water. Salt was added to the water in order that the beads floated in suspension; this increased the density slightly and also the propagation velocity, and so a small depth correction of the bar depth was required, from 52 mm to 50 mm.

Experiments using the polystyrene granules included the following:

1. Water with granules.
2. Good steel.
3. Scan of force-corroded bar.
4. Low-frequency (45kHz) interrogation.

The final set of water based experiments utilised a 4 channel system, with two additional receivers mounted at right angles to the original two. With the bar displaced towards one of these probes, it was hoped that positional information could be obtained enabling any future prototype system to be self-centring.

Because these experiments were simulations and the conditions differed somewhat from those in concrete, the analysis of the data also differed in form and were slightly more complex; for this reason, we restrict the discussion in this section to a qualitative summary of the experimental results. For more detailed information regarding the method of data analysis, the reader is referred to Appendix E.

c. **Test Results**

In the case of the good quality steel bar, the reflected signals arrived at receivers A and B at the same instant, i.e. the signals were in phase, as should be expected. Furthermore, the spectral compositions of these signals are very similar. Figure 24 shows these echoes.

i. **Good steel V steel cut between transmitter and receiver B**

The signal reflected from the saw-cut (positioned between the transmitter and receiver B) arrived fractionally sooner than the signal that travelled to receiver A, which was again reflected from a defectless surface. More significantly, the echo from the defect lost some of its high frequency content.

The attenuation of the high frequency components when a defect is present is readily explained since the shorter wavelengths are more susceptible to scattering in the region of discontinuity. What is perhaps surprising is the phase advancement. This implies that the signal entered the steel, travelled along it and partially re-emerged at the position of the saw-cut. Initially it was thought that experimental error had been responsible for this result, but repeated tests indicated that it was indeed a genuine phenomenon.

ii. **Good steel V steel cut and rotated through 90°**

Assuming that the wave front is most affected by the upper surface conditions of the bar, it is to be expected that the results obtained when the bar was axially rotated through 90° contained less contrast than did the results described above. The phase change was still detectable although less apparent, and the fall in the high frequency content occured again but not by the same extent.

iii. **Good Steel V Force Corroded Bar**

The region of force corrosion was a comparatively large defect, involving a 36% reduction in the steel cross-sectional area over a length of 30 mm. This feature was therefore readily identifiable both in the time and frequency domains.

The most important aspect of the analysis in this instance was the cross-correlation performed in the time domain between the signals arriving at receivers A and B. This provides an accurate measure, in terms of time, of the phase lag of signal B (that has travelled a slightly greater distance through the water owing to the defect) relative to signal A, and therefore gives a measure of the depth of the defect. The defective region represented a cross-sectional loss of 1 mm, and the estimate given by the cross-correlation lay between 0.7 and 1.3 mm. Although this may not seem, at first sight, a particularly significant finding, a cursory examination of the frequency involved reveals that the wavelength of the interrogating signal was at least 12 times greater than the dimension of the flaw detected. This gave considerable grounds for optimism regarding the proposed ultrasonic concrete inspection system for concrete, since all the preliminary experiments indicated that frequencies beyond 500kHz could not be used owing to the intolerable losses from scatter and absorption.

iv. **Good steel V naturally corroded bar**

In this experiment the bar was superficially corroded along its entire length by immersion in tap water for a period of two months. Although phase changes between the two sets of signals were detected, these were essentially random as a result of random changes in the surface condition of the steel. Because the corrosion that occured was fairly minimal, it was estimated that much greater detail would have been required in terms of sampling speed to resolve with certainty these phase changes.

One anomaly however, remained. In the case of the good steel, the amplitude of the high frequency (121 kHz) exceeded that of the low frequency (41 kHz) by a factor of 6. In the case of the corroded steel, this factor actually increased to 22. This is in direct contradiction of the theory, which states that reflection of a broad band pulse from a roughened surface causes preferential weakening of the higher frequencies. It is possible that the underlying trend has been masked by noise, since single frequency bands were used in the calculations rather than bands with several frequencies, the latter tending to reduce any random variability in the data.

v. **Scanning of force corroded bar**

After the static reading taken from the region of force corrosion, the bar was scanned by the linear array, a reading being taken every 35 mm. As the defect passed from under receiver B, the transmitter and finally receiver A, the phase lag discussed earlier gradually fell to zero and then reversed to become a phase advance (the phase was always measured relative to receiver A). This experiment was the first in the programme that incorporated a scan sequence, albeit with rather cumbersome techniques.

vi. **Simulated aggregate tests**

An attempt was made to simulate the condition of aggregate in concrete by introducing polystyrene granules into the water; by dissolving salt in the water in the correct ratio and hence increasing its density, the granules were made to float in suspension. Figure 25a shows the echoes returned from the base of the tank with clear water; by contrast, Figure 25b shows a much noisier signal, as the signal was scattered by the granules. Spectral analysis indicated a slight reduction in the strength of the high frequency components, in addition to a general attenuation of the overall echo.

However, using the 125 kHz probes there was still no difficulty in obtaining a strong echo from the good steel bar; although there was slightly more noise present in the data, the signal-to-noise ratio was far in excess of that encountered in concrete conditions.

Similarly, a repeat scan was performed of the force-corroded section of a bar in the manner described previously. Once again it was phase change that was of interest, and this was detected with no great difficulty, albeit with slightly more variation.

vii. **Low frequency analysis**

In all the above water-based experiments, the data analysis was facilitated by two major features:

- The wavelength was comparatively short (approximately 12 mm).
- The transducers always emitted a clearly defined beam, the half-angle of divergence being approximately 36°.

In concrete, neither of these two conditions are attainable using the equipment available. At 121 kHz for instance, the wavelength is approximately 35 mm and the transducers radiate in all directions. In order to reproduce these features in water therefore, a system was employed using transducers with a resonance of 45 kHz, and a diameter of 25 mm. In salt water the wavelength of these devices is 34.2 mm and the radiation pattern is omnidirectional. Despite the obvious presence of surface wave interference (Figure 26), calculated at 68% that of the pressure at the axis, the system was found to have extremely good penetration properties and could readily locate the base of the tank through a dense strata of aggregate in suspension 218 mm below the surface of the water.

Moreover, it also proved possible to identify the echoes returned from the 10 mm steel bar using the low frequency probes, and with precise alignment and careful signal processing, to isolate the phase discrepancy between signals reflected from an intact surface and one from a force-corroded defect (Figure 26b). It should be noted however, that the longer the wavelength the more difficult it becomes to identify change of this nature. It should be emphasised that, with respect to wavelength, 45 kHz in water is equivalent to 120kHz in concrete.

d. **Summary**

The water simulation trials were in some respects rather optimistic because the scattering effects produced by the polystyrene granules were not as severe as those produced by aggregate in concrete. However, they did suggest that, scattering aside, it was possible to use fairly low frequencies (i.e. not beyond 150 kHz) to identify relatively small defects in concrete. In these trials, the best results in water were obtained using a frequency of 120 kHz; in concrete this corresponds to approximately 325 kHz. At that time (November 1988) it was not thought possible that such a high frequency could be used to provide information because of the intolerable losses in signal strength it would sustain. In February 1990 however, it was successfully demonstrated using the CANDI prototype that frequencies extending to 400 kHz could be recovered having been transmitted through useful distances in concrete and the information content extracted from the background noise.

2.6 CANDI: THE FIRST PROTOTYPE SYSTEM

2.6.1 Phase 1 Software System Description

The data acquisition and analysis system used up to this point in the project was satisfactory for testing small scale samples when not more than a few readings were required to demonstrate the difference between defective and non-defective cases. It was however, entirely unsuitable for testing a large

structure approximating the size of an actual bridge beam when several hundred readings would be taken in a single scan.

The digital storage oscilloscope and PC based analysis software was therefore replaced by the Analogic 6100 waveform analyser, which could both store hundreds of time records in its RAM, and process them with considerable speed using its impressive repertoire of analysis functions. The analyser in turn was controlled by the PC, which also functioned as the mass storage device. This enabled data to be read back to the analyser for more detailed analysis once the experimentation had been completed.

Section 2.4.2 includes a description of the hardware configuration, for both the first and second stages of the CANDI prototype. Here we detail the signal processing operations that the system was instructed to perform after scanning a section of the test beam. These operations included the following:

a. Display of the collected waveforms for each receiver R1 to R4, in the time domain, for each scan position (see below for details of the scan procedure). Figure 27 shows an example of this, where each trace represents a signal received by transducer R1 within the period 28-29μs, and all the signals are displayed in a sequence corresponding to their position along the length of the beam. This form of presentation is known as a waterfall display enabling rapid identification of any difference between signals.

b. Calculation of the frequency spectrum for each waveform, R1 to R4, and display in waterfall mode of each scan position. An example of this is given in Figure 28.

c. Calculation of scalar quantities for each reading, to enable trends to be determined and displayed as plots. In such plots the x-axis represents position along the beam, and the y-axis the calculated signal quantity. These scalar quantities included rms, dominant frequency, average period, cycle number, duty cycle, mean voltage, energy, peak-to-peak voltage, maximum and minimum voltage and time of occurence of maximum signal amplitude. An example of a set of four trend plots is shown in Figure 29.

d. Calculation and display of waveforms derived by subtracting signal R2 from R1, and signal R4 from signal R3, and subsequent calculation of time and frequency domain and trend data on these new data sets, as outlined in (c) above.

In order to maximize the resolution of the frequency domain information, the conventional FFT was replaced by the chirp Z transform, known as a ZFFT. For more details on this technique, the reader is referred to Appendix F. Suffice it to say at this stage that the ZFFT offers much greater detail at the expense of computation time - typically 6 seconds for a 512 point record in comparison to 0.5 seconds for a conventional FFT.

2.6.2 Initial Results

A number of trial scans were made of the upper surface of the test beam, whose upper internal structure is shown in Figure 30. In the first scan, the frame comprising the central transmitter and four receivers was positioned with the fore and aft receivers (R1 and R2 respectively) directly over the upper centre cable (cable B). Receivers R3 and R4 were positioned over cables

A and C respectively. All receivers were spaced 100 mm from the central transmitter, the minimum distance that was required to allow the compressional wave reflected from the cable to reach the receivers before the surface travelling Rayleigh wave. This first scan used a transmitting probe with a central resonance of 200 kHz and wide-band acoustic emission receivers. The beam was scanned at intervals of 50 mm and 89 separate readings were taken for R1 to R4. The total length that was scanned was 4.45 m, since margins were left at either end to minimize edge effects (see Plate 5).

As stated, Figure 27 depicts the unprocessed waveforms collected by receiver R1, windowed between 28μs and 92μs for purposes of clarity. Each waveform represented a signal from one scan position. Unfortunately, although there was some (perhaps inconclusive) evidence to suggest an increase in amplitude over the area contaminated by salt (a paper towel saturated in salt solution was wrapped around the centre cable), and a decrease in the region of the stirrups, the dominant feature was the lack of coherence between successive waveforms, i.e. they did not rise and fall uniformly. Similarly, the 2FFT waterfall plots (Figure 28) contained so much variability that it was impossible to recover the information content (if indeed it existed) from the noise.

These data appeared to suggest that the interrogation frequency was high, the small wavelengths being scattered by the intervening aggregate, randomly distributed, giving random patterns in the shapes of the time record traces. The data collected by receivers R2 to R4 also displayed similar variability which would be superfluous to show as figures. As a consequence, a scan was performed along the centre cable using low frequency 45 kHz probes. This succeeded in eliminating the random appearence of the time records but did nothing to improve the information content of the data. Indeed, the speculated increase in energy associated with the salt contaminated region entirely disappeared.

In retrospect, the water simulation experiments showed that frequencies below 100 kHz in concrete (equivalent in wavelength to 37 kHz in water) would contain little information regarding small-scale changes. It was no surprise then, to find that the 45 kHz probes were not successful in locating any of the defects in the test beam.

2.6.3 Phase 2 Software Refinements: Frequency Domain Digital Filtering

In February 1990 tests were being conducted on small concrete samples in an attempt to understand why the CANDI system had so far failed to produce reliable information: it was suspected that if the high frequency components were affected by regions of change, their change in energy might be masked by the lower frequencies which were not only more immune to small scale defects but also contained considerably more energy. It was therefore decided to split the composite waveforms into discrete frequency bands and analyse each band separately.

Consider, then, a wide-band pulse, ranging from near d.c. to several hundred kilo-Hertz, travelling through concrete containing inclusions such as small voids and steel cables, with interface regions between the steel and the concrete.

This kind of signal rapidly loses high frequency energy due to the heterogeneous nature of the medium. Where these frequencies encounter boundary conditions, reflection will occur, the strength being dependent upon the size of the defect in relation to the wavelength. The total signal that

arrives at the receiver will include low frequency components of large amplitude and relatively little information content (this is not to say that these bands are without their uses - see Appendix B), and high frequency components that do change in strength according to the internal conditions but whose energy, in these tests, may be of the order of one thousandth of the whole signal.

For this reason, analysis of the total signal yielded rather limited success. What was required was a filter that rejected all but the specific band of interest. In electronics, an ideal filter is defined as a network which passes, without attenuation or phase distortion, those frequencies and only those frequencies for which it has been designed. In practice, such a filter is impossible to realise as totally sharp cut-off points are never achieved and attenuation and phase changes always occur.

In contrast, it is possible to implement ideal filters in the Fourier domain by setting unwanted harmonics to zero and performing an inverse transform to generate a time record composed only of the frequency bands of interest. This is termed "brick wall" filtering and has proven very successful in identifying areas containing voids, major cable breaks and areas of delamination.

2.6.4 Void In Ducts: Detection In Small Samples

Figure 31 shows the results obtained using this new method of analysis. A concrete specimen, 800 mm in length and 150 X 300 mm in cross section, containing a 50 mm steel corrugated duct lying along its axis, in turn containing a void at its mid point (formed by the insertion of two hollow plastic spheres 40 mm in diameter), the remainder of the duct being filled with grout on one side and four 7-wire strand in grout on the other, was scanned using two probes only. These were a 200kHz transmitter and an acoustic emission receiver, spaced 100 mm apart. The scan step was 20 mm, with the receiver innermost. A total of 35 readings was taken.

Each record was then high-pass filtered in the frequency domain to leave only those harmonics lying at 300 kHz and beyond. After re-transforming to the time-domain, the signal energy for each record was calculated. Figure 31 represents the energy (on the y axis) as a function of position (the x axis) on the beam. The first peak corresponds to the position of the receiver directly over the void, and the second to the transmitter directly over the same. The peak energy, about 0.00005 Vs, represents about one thousandth of the energy of the total signal.

2.7 CANDI: THE PRESENT PROTOTYPE SYSTEM

2.7.1 The C.N.S. Rolling Transducers

Numerous additional scans of small samples strongly suggested that these encouraging results were not chance effects but the logical outcome of processes that had, after all, been indicated by both the theoretical modelling and the simulation experiments. Rather than detail these numerous tests, we will concentrate on the the CANDI prototype as it is at present, its hardware description and its current capabilities and limitations.

The filtering work showed that frequencies beyond what was previously thought analyzable could be recovered; furthermore it was known that static coupled probes would not be suitable for a practical system. Therefore, in May 1990, a pair of rolling transducers was purchased. These probes are 80 mm

in diameter, 40 mm in width and have a nominal resonance of 360 kHz (see Plate 6). Good acoustical coupling was assured by the soft neoprene tyres which rolled across the surface of the concrete, this having been initially sprayed with water (Figure 32). Because of the physical properties of the neoprene tyres a continuous and consistent film built up between the probes and the surface of the concrete. Numerous tests showed that the apparently random variation in signal strength from one position to the next was now no longer due to variations in the quality of the coupling (a problem which had dogged the project for two years), but to variations in the aggregate profile through which the signal passed.

Although, as stated above, the nominal resonance of these devices is 360 kHz, considerable high frequency attenuation results when the signals travel through even a short distance in concrete. In the present configuration, the transmitter/receiver pair (the probes may function either as transmitters or receivers) roll in parallel with a spacing of 65 mm, centre line to centre line.

Figure 33a shows a typical signal received in this manner, and Figure 33b its corresponding spectrum. Note how most of the energy is confined to the frequency band lying between 80 and 100 kHz, with a small fraction between 350 kHz and 400 kHz. However, by Fourier domain block filtering and re-transforming to the time domain, the high frequency content is revealed, shown in Figure 34. This signal contains 2% of the energy of the total signal.

In the current system the received signal is partioned into eight frequency bands in 50 kHz increments, ranging from 0 kHz to 50 kHz up to 350 kHz to 400 kHz. The exact manner in which the individual energy traces from each frequency band are processed depends upon what is being looked for; rather than simply looking at the energy of the highest obtainable frequency, as was done initially, the bands may be cross-multiplied or ratios taken between the energies of the high and low frequencies. The details of the signal processing as well as the mathematical operations involved are described in Appendix B.

Thus, in summary, we can state:

The central hypothesis of the current methodology in signal processing is that different wavelengths - that is, different frequencies - will be reflected with different energies depending upon the size, geometry and acoustic impedance of the defect encountered. By partitioning the reflected signal into discrete frequency bands and by comparing the magnitudes of their energies, it is possible to derive information relating to the position, size and nature of the defect.

2.7.2 Broken Cable Detection in Small Samples

A concrete sample 890 mm in length and 150 X 150 mm in section was cast with a 7-wire strand cable embedded along its axis, with a central break, the ends being separated by 70 mm. Concrete was prevented from filling the gap by the insertion of a hollow plastic tube over the two ends of the cable, prior to casting. After a two week cure period the specimen was scanned using the rolling transducers and a scan increment of 10 mm. A total of 81 readings was taken, 45 mm margins being left at either end to minimize edge effects. Scan reading #40 corresponded to the mid-point of the defect.

Figure 35 shows how the energy varied in strength as a function of position along the sample. All frequency bands showed an increase in energy over the area of the defect, since is essentially similar to a void involving near total reflection of the signal at the concrete/plastic interface. By multiplying the respective energy traces, point for point (a form of cross-correlation), an enhanced line scan is produced. Note that the trace is not clear of noise, but the data corresponding to the defect lies well above the noise threshold.

2.7.3 Corrosion Detection In Small Samples

After scanning this sample, a small section of the cable was force corroded by applying a current of 10 mA for a period of 7 days. The point of maximum corrosion was estimated to be located at scan position #63. In order to avoid the effects of localized water penetration into the concrete around the region of corrosion, the sample was totally immersed in a water tank for a period of twenty four hours prior to scanning.

Unlike the case of the sample containing a void in a duct (Section 2.6.4), the energy reflected in the region of corrosion for each frequency band was only marginally greater than the background variability. No single energy trace in isolation could therefore be used as a reliable indicator of the affected region, as shown by Figure 36a. However, after processing the data by cross-multiplying the individual energy traces, the noise levels were greatly reduced and the resulting trace, given by Figure 36b, clearly shows the point at which maximum corrosion has taken place.

2.7.4 Transverse Scans of Ducted Samples

In Figure 37a, the trace shown represents a scan in which the transducers rolled over buried ductwork containing the following:

a. Solid grout (scan readings #0 - #24)
b. Grout with void (scan readings #25 - #49)
c. Grout with four 7-wire strands (scan readings #50 - #74)

In each case, the specimen was a concrete block 870 mm in length and 300 X 150 mm in section, with a 50 mm diameter steel duct embedded along its axis. The transducers were used to scan the width of the sample, with a scan increment of 10 mm. Margins of 30 mm were left on either side of the sample to minimise edge effects. For ease of comparison, the three separate traces have been concatenated to give plots shown in Figures 37a and 37b.

Figure 37a shows the energies detected in the frequency band lying between 50 kHz and 100 kHz, where the wavelength extends from 86 mm to 43 mm. Because of the large diameter of the duct, strong reflections were produced as the transducers passed over their mid-points, which lay at #12, #37 and #62 respectively. Moreover, the duct containing the void reflected more energy for a greater distance on either side of the peak. This was entirely to be expected since only in this case will near total reflection of the signal occur. In the grouted and grout/cable cases, the reflected energy will be weaker since partial transmission will also take place. Interestingly, the narrowest peak is returned by the duct containing the cables. In Figure 37b, the trace shows the energies detected using the same raw data but filtered to include only those frequencies lying between 300 and 350 kHz, i.e. wavelengths of between 14.3 mm and 12.3 mm.

Whilst this trace follows the same basic trend as Figure 37a, the peak associated with the duct containing the cables is now considerably attenuated. The reason for this remains obscure, since a concrete/steel interface has a higher reflectance ratio than a concrete/mortar interface. A possible explanation may be that the presence of the steel in the mortar represents yet another scattering mechanism. In any case, if these small-scale variations are genuine and not random artifacts, it implies that the system is not only capable of detecting voids in ducts, it may also have the potential to detect major breaks of cables within ducts.

2.7.5 Test Beam Scan Trials

After successfully demonstrating that the system was capable of detecting voids and defective regions in small samples, it was then used to examine all the flawed regions in the large scale test beam. These comprised two voids, three points at which paper towels, having been saturated in salt solution, were wrapped around the cables, and two points where one wire of the 7-wire strand cables had been cut and the ends separated by 60 mm. These last two cases did not, however, represent a fair challenge to the prototype system, since the concrete was poured after the wires had separated and the gap between the ends of the wires was filled with concrete. In each of the seven cases, a region 150 mm either side of the mid-point of the defect was scanned, with the transducers tracking along the length of beam.

With the exception of the last two cases mentioned above, in which the results were ambiguous, all the defective regions were successfully located. Figures 38a and 38b show typical results obtained from scans of two salt contaminated sections, using a method of signal processing that enhanced the high frequency energy content by attempting to neutralize the variations in background noise induced by the random nature of the aggregate profile and, to a lesser extent, the variations in signal strength resulting from changes in the coupling consistency. By using the same method of signal processing, the voids could also be located, as evidenced by Figures 39a and 39b.

2.7.6 Capabilities and Limitations Of The Current System

At present the system is capable of identifying moderately sized voids in ducts (greater than 40 mm in diameter) to a depth of 100 mm, major breaks in cables involving a total separation of not less than 60 mm to a depth of approximately 70 mm, and regions affected by chloride contamination to a similar depth. However, the reasons why the system is sensitive to this last factor remain uncertain; more is said of this matter in the next chapter. What it has not proven possible to achieve, so far, is detection of single wire breaks in a multi-wire strand. Given that a single wire is considerably smaller in diameter than the wavelengths concerned, it is not surprising that this should be the case. It may be possible, by the use of still higher frequency probes and continued refinement of the signal processing technique to improve the resolution of the system but this has yet to be successfully demonstrated.

In addition, experiments have shown that it is not possible to detect minor corrosion of fusion-bonded epoxy coated steel rebar, although, given the minimal extent of corrosion (300 mm^2 in this instance), and the quality of the coating, we do not consider this a particularly significant limitation. On the contrary, the failure of this test suggests that the system is capable of detecting the primary factors involved in salt-induced corrosion rather than the secondary effects such as deterioration in concrete quality (see Chapter 3).

2.7.7 Statistical Reliability of Analysed Data

Because the signal processing techniques are applied to data that have considerable random components convolved with coherent signal content, it is inevitable that the final traces generated by the system indicate only the likelihood of a defective or corroded region. The probability of the system correctly identifying such regions depends on the severity of the defects in question. On the basis of 95% probability levels (plus or minus two standard deviations of the quiescent noise level), it has been calculated that the system can detect the presence of voids, either as part of the concrete or within ducts, to a high level of confidence, and no special statistical tests are required to establish the reliability of the estimates (here we refer only to those defects that have been scanned as part of the experimental programme). The same is true of chloride contaminated regions.

Regarding smaller defects, such as the complete cable break indicated in Figure 35, here the central peak (which shows the break) has a magnitude of 7.41 standard deviations, the standard deviation having been calculated from the quiescent noise levels. However, the smaller noise peak to the right of the trace has a magnitude of 2.1 standard deviations, and strictly speaking this too might be interpreted as a fault condition. In order to reduce the number of false readings, it would be necessary, before using the system on a real structure, to characterise more closely the random energy variability of the resulting traces using a wide range of good quality (non-defective) samples.

Table 1

Basic Statistics Calculated From Tests on Cyclindrical Samples

Experiment (see note 1)	Velocity (m/s) (see note 2)	rms (V)	Attenuation (dB)	Preamplifier Gain (dB)
Transducers in water, 3 mm separation	-	0.50	0	0
Wire to Wire in air, 7 mm x 1 m	5540	0.92	5	0
Conc. to conc., no wire, cyl., 1 m	4464	0.01	-45	0
Conc. to conc., in line, with wire cyl, 1 m	4651	0.01	-51	0
Wire to wire in conc cyl, 1 m	5111	0.03	-25	0
Wire to wire 1m $CaCl_2$ conc. cyl, 2 months	4095	0.02	-50	20
Wire to wire 1m cyl, $CaCl_2$, 6 months	3942	0.05	-60	40
Wire to wire in cyl, 1 m 6/7 near Tx	4584	0.01	-34	0

Notes: for Table 1, 2 & 3.

1. Abbreviations:

conc:	concrete
cyl:	cylinder
PWO:	Prewaveform Optimisation
Rx:	Receiver
S1:	Sample 1
Trans:	Transverse
Tx:	Transmitter

2. Velocities normally accurate to $\pm$1%, depending upon signal strength.

3. Velocity statistic not valid since post-triggering used on oscilloscope.

4. Attenuation referenced to transducer output at 3 mm in water.

Table 2

Basic Statistics Calculated From Tests on Block Samples

Experiment (see note 1)	Velocity (m/2) (see note 2)	rms (V)	Attenuation (dB) (see note 3)	Preamplifier Gain (dB)
Plain conc, 0.945 m, trans, PWO	4047	0.03	-65	40
Plain conc, 0.94 m, trans	3730	0.22	-47	40
Conc 0.93 m, PWO, 7 wire good, trans	4061	0.19	-48	40
Conc 0.93 m, 7 wire good, trans	3843	2.32	-27	40
Conc 0.94 m, 7 wire 1 cut, trans, PWO	4113	0.07	-57	40
Conc 0.94 m, 7 wire 1 cut Rx, trans	3805	0.89	-45	40
Conc 0.5 m, 7 wire cut Rx, trans, PWO	See note 4	0.09	-55	40
Conc 0.5 m, 7 wire cut bypass, trans, PWO	See note 4	0.07	-67	40
Con 0.92 m, 7 wire $CaCl_2$ trans, PWO	3841	0.20	-48	40
Con 0.92 m, 7 wire $CaCl_2$ trans	3770	1.16	-33	40
Empty ducted, s1, trans, PWO	3937	0.06	-58	40
Empty ducted, s1, trans	3760	1.08	-33	40
Empty ducted, s2, trans, PWO	3974	0.13	-11	40
Empty ducted, s2, trans	3900	2.00	-28	40
Empty ducted, s3, trans, PWO	3734	0.10	-54	40
Empty ducted, s3, trans	3618	1.72	-29	40
Empty ducted, s4, trans, PWO	3899	0.12	-52	40
Empty ducted, s4, trans	3454	1.84	-29	40
Plain grout ducted, s2, trans, PWO	4109	0.03	-24	40
Plain grout ducted, s2, trans	3710	0.22	-47	40
Ducted, 7 wire and grout, s3, trans, PWO	3795	0.14	-51	40
Ducted, 7 wire and grout, s3, trans	2990	0.23	-47	40
Ducted, 7 wire 1 cut Tx, grout, trans, s4, PWO	3981	0.05	-60	40
Ducted, 7 wire 1 cut Tx, grout, trans, s4	3295	0.29	-45	40
Wedge 20°, conc 0.9 m, 7 wire, PWO	4026	0.02	-70	40
Wedge 20°, plain conc, 0.9 m	3982	0.01	-71	40
Conc 0.95 m, cut to 7 wire, trans PWO	3398	0.09	-76	40
Conc 0.95 m, cut to 7 wire, trans	2845	0.04	-61	40

The notes are appended to Table 1.

Table 3

Basic Statistics Calculated From Tests on Bridge Beam

Experiment (see note 1)	Velocity (m/s) (see note 2)	rms (V)	Attenuation (dB) (see note 3)	Preamplifier Gain (dB)
Conc to steel, 1 m	4975	0.03	-76	52
Steel to conc, 1 m	5000	0.04	-75	52
Conc to conc, 1 m, cable 0.064 m underneath PWO	5000	0.02	-78	52
Conc to conc, 1 m, no cable PWO	4608	0.58	-51	52
Conc to conc, 1 m, no cable PWO	4890	0.07	-70	52
Conc to conc, 1 m, cable 0.04 m underneath PWO	5050	0.01	-83	52
Conc to conc, 1 m, cable 0.04 m underneath	4854	0.19	-60	52
Conc to conc across flaw, 1 m, PWO	5000	0.01	-90	52
Conc to conc across flaw, 1 m	4878	0.07	-69	52

The notes are appended to Table 1

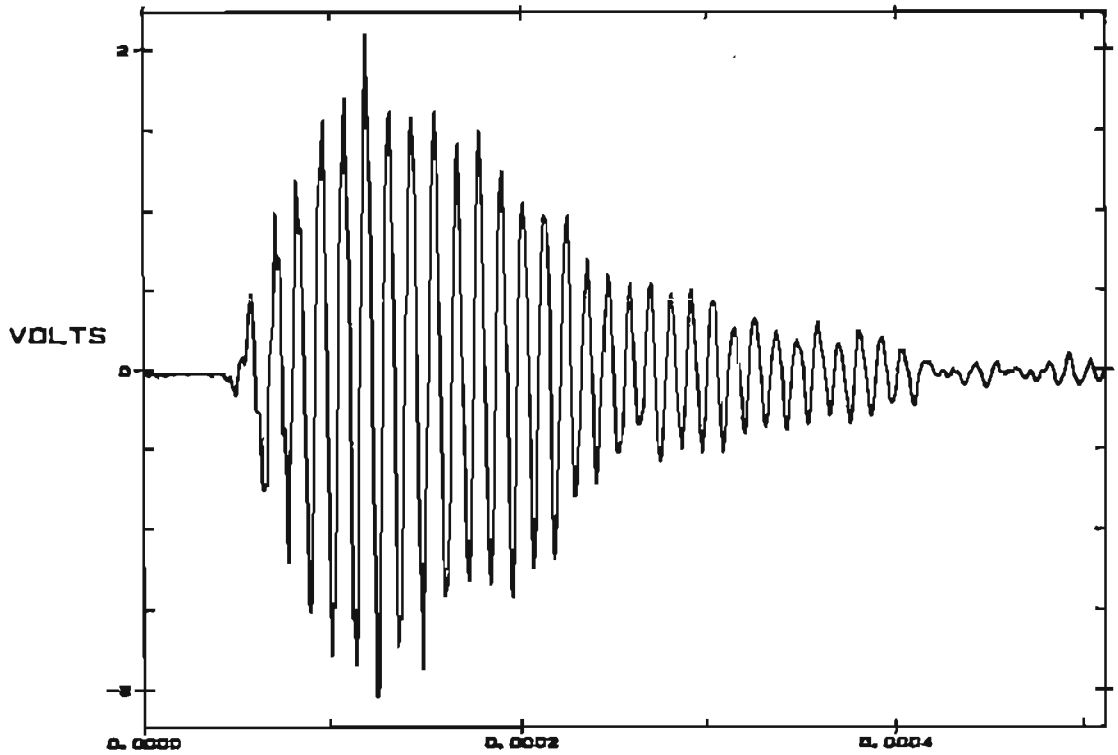

Figure 1. A typical ultrasonic pulse transmitted through concrete.

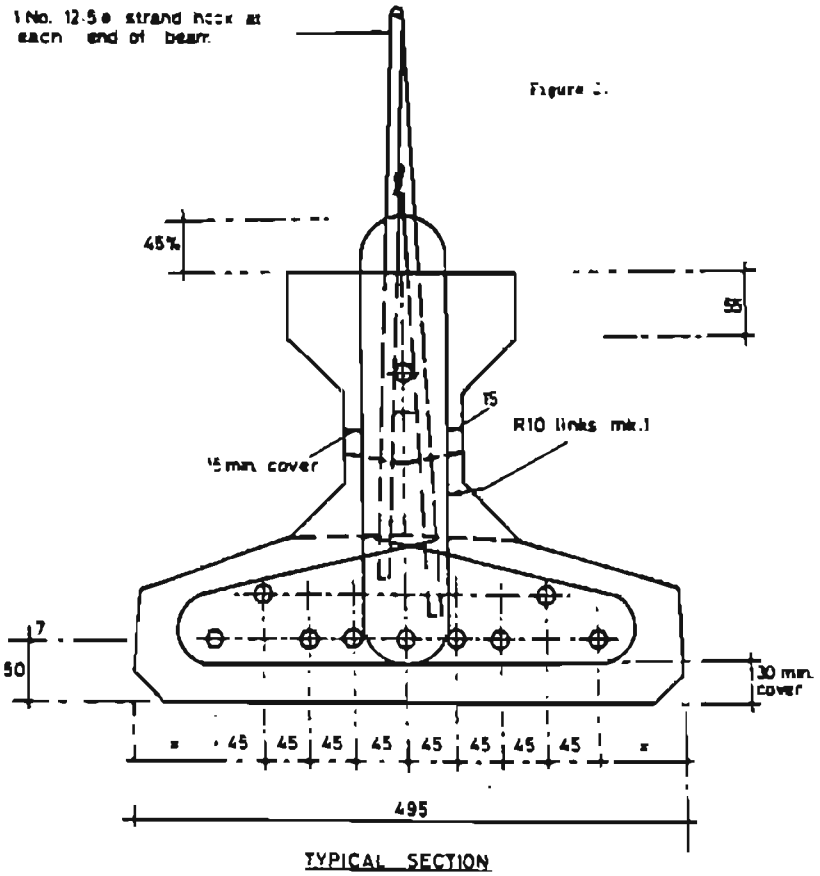

TYPICAL SECTION

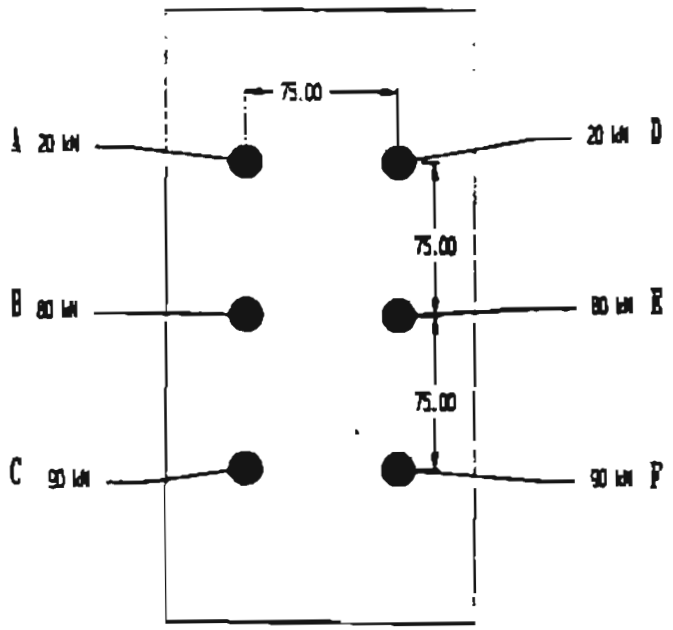

Section showing stresses in each Tendon

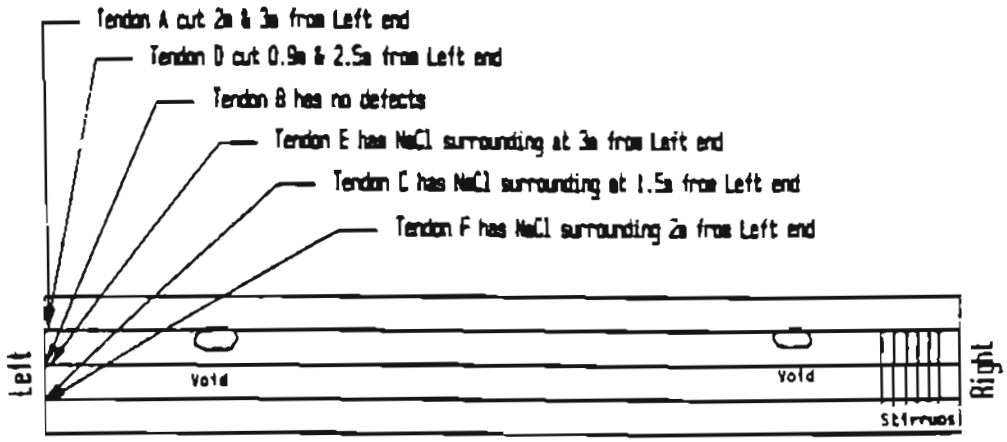

Elevation of beam showing Defect Positions

Figure 3. Large scale test beam, showing details of internal reinforcement and defect locations.

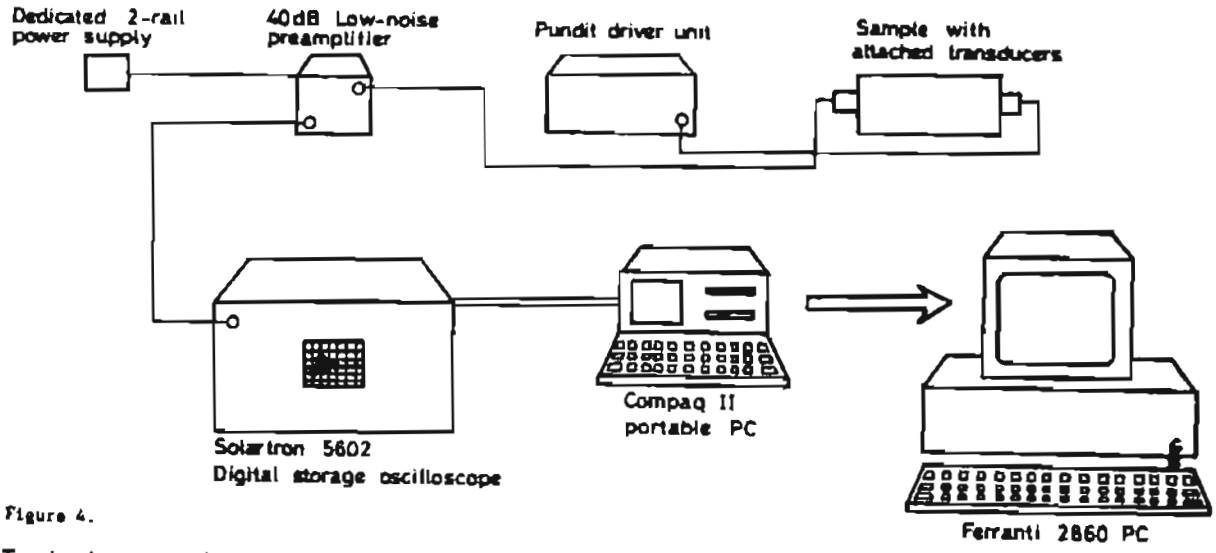

Figure 4.

Typical experimental configuration.

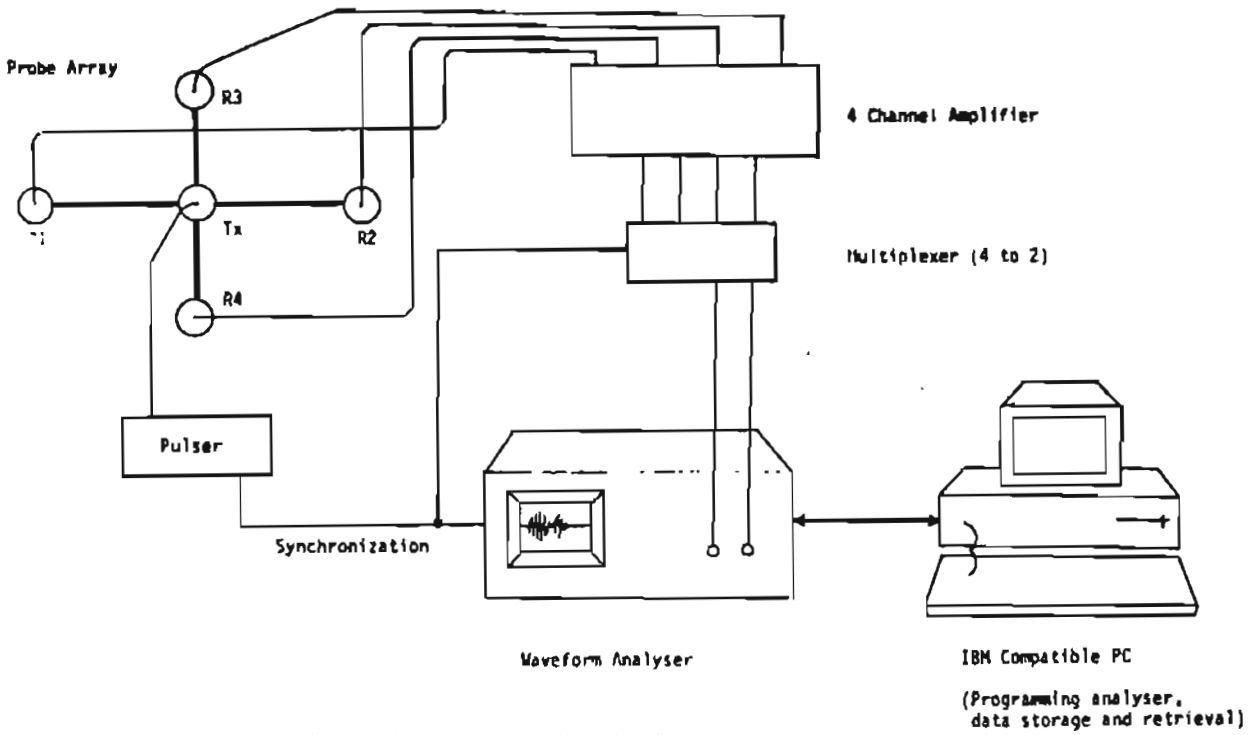

Figure 5. Schematic Diagram of Mk I Prototype Scanning System.

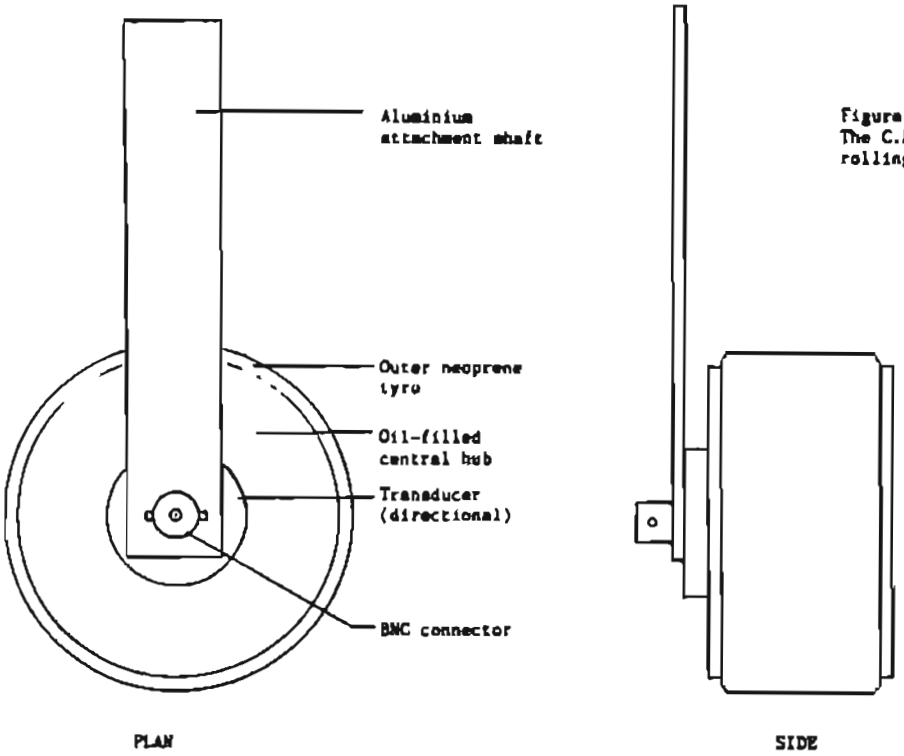

Figure 6.
The C.N.S. 360kHz rolling transducers.

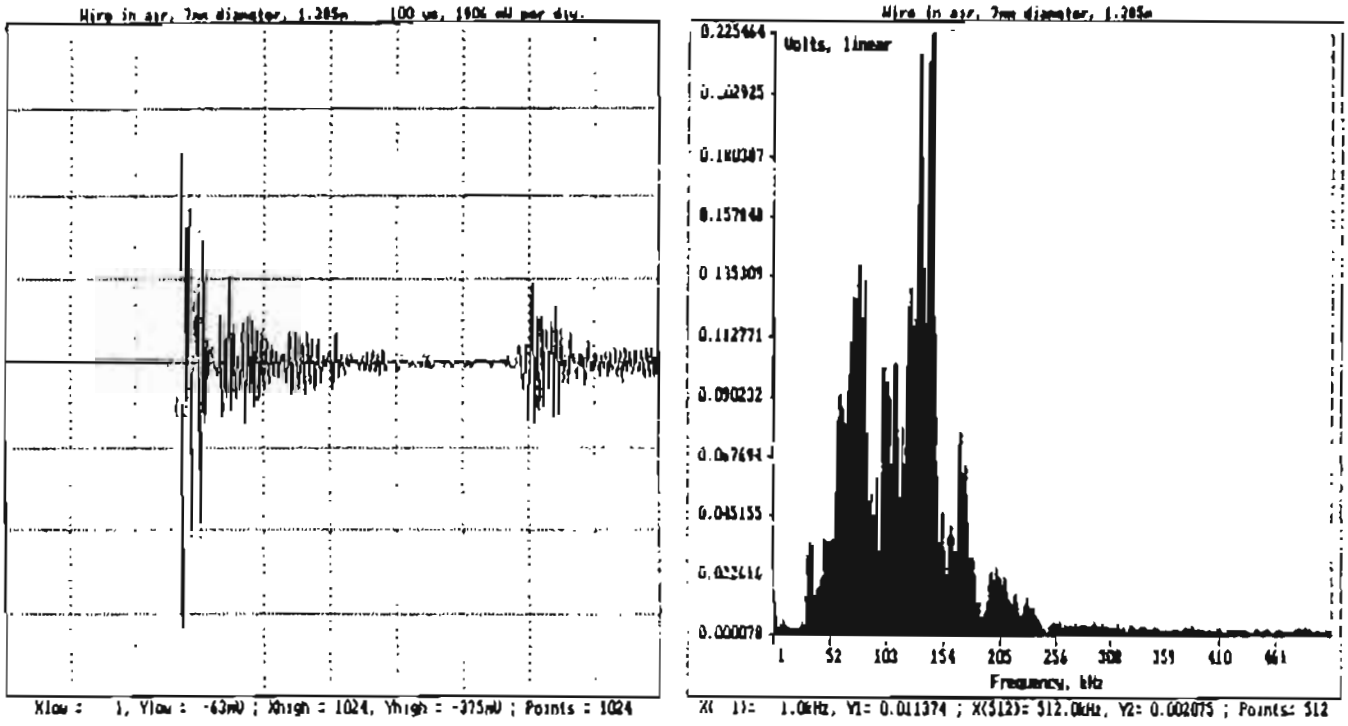

Figure 7. Signal and spectrum from pulse transmitted through wire in air.

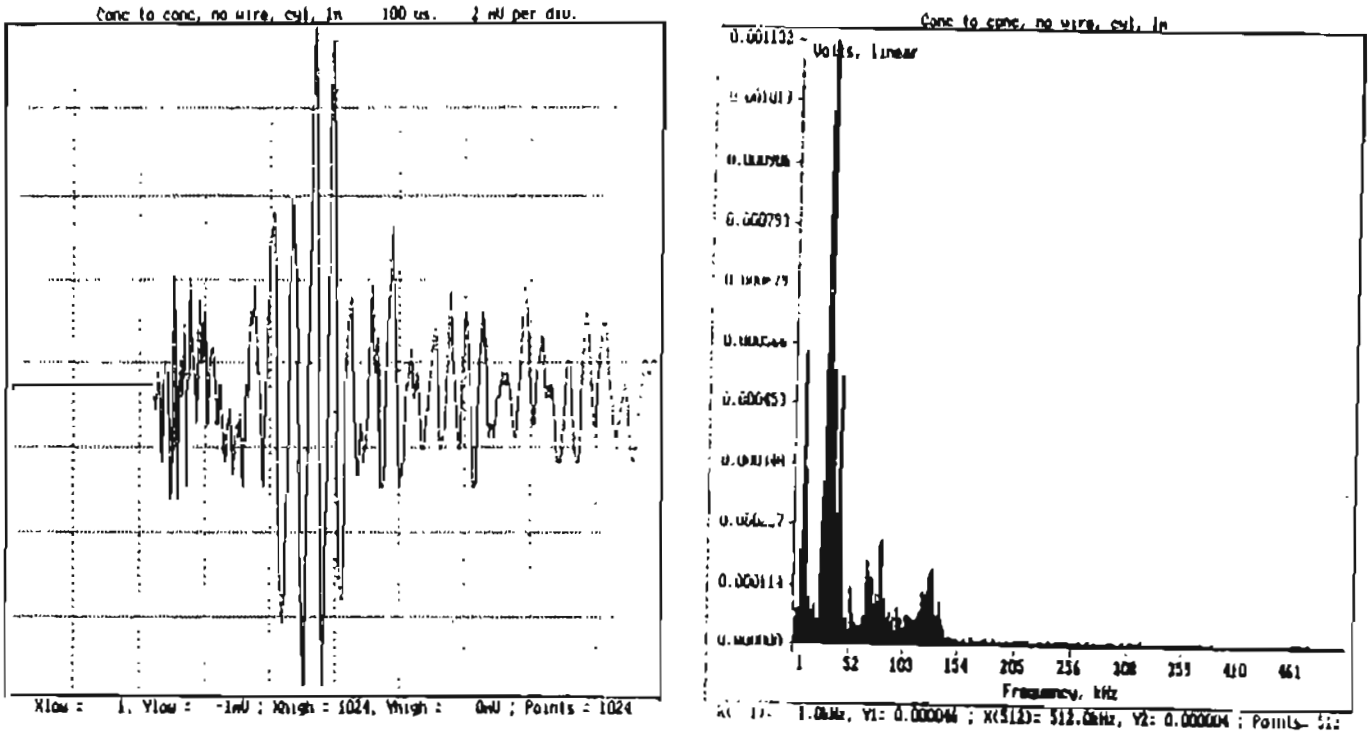

Figure 8. Signal and spectrum from pulse transmitted through plain concrete.

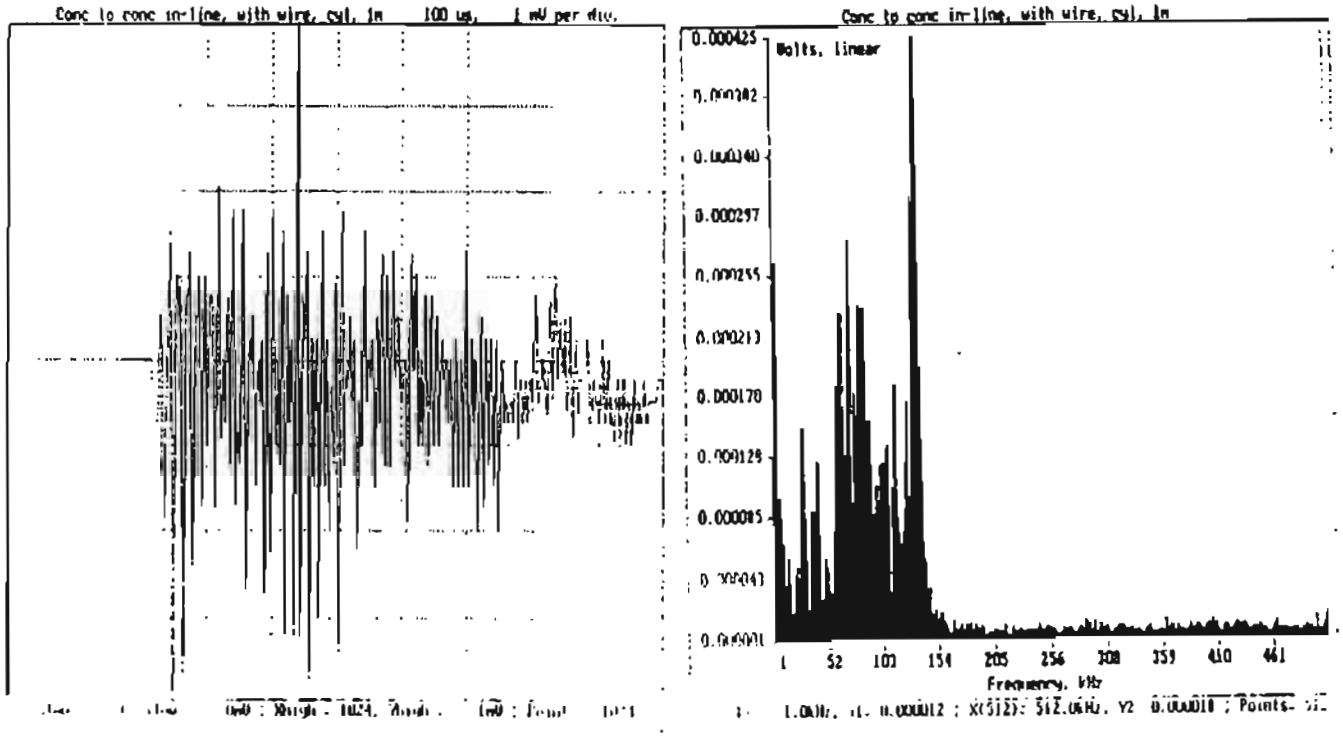

Figure 9. Signal and spectrum from pulse transmitted through concrete with adjacent wire.

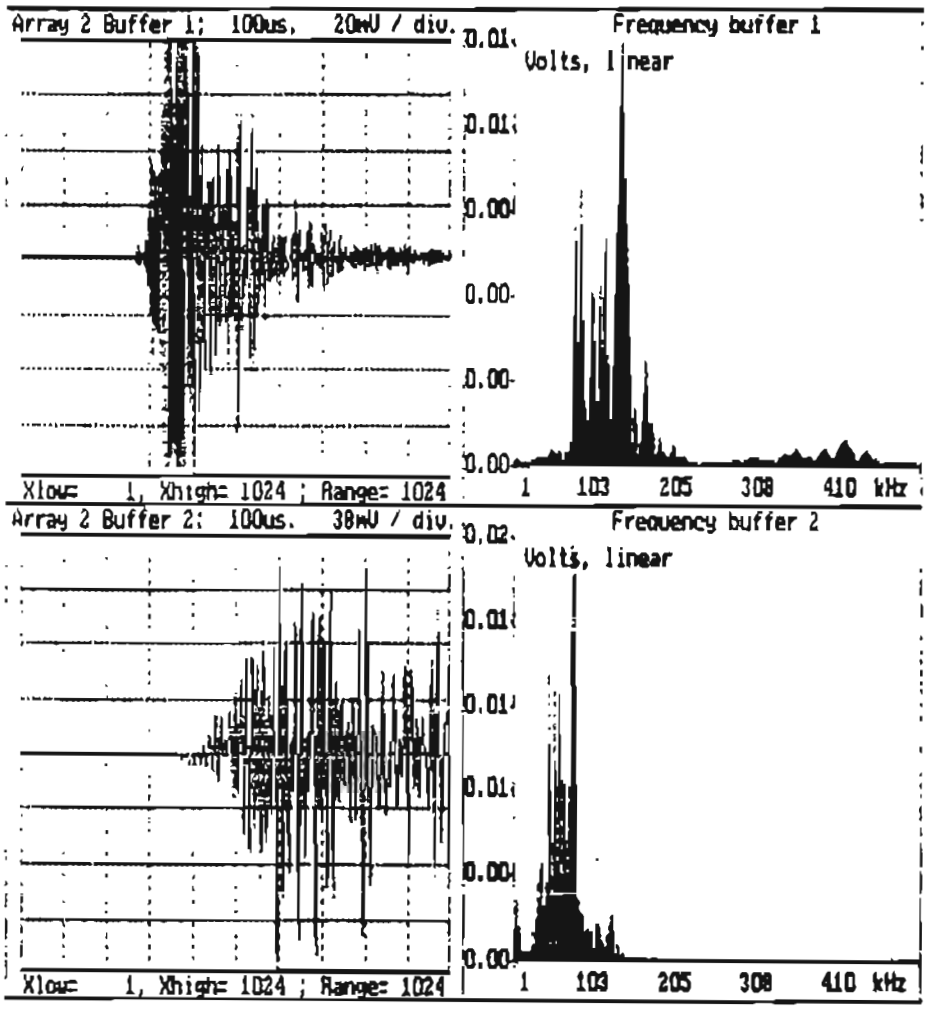

Figure 10. (a) Signal and spectrum from pulse transmitted through wire embedded in concrete.

(b) Signal and spectrum from pulse transmitted through wire embedded in concrete with chloride contaminant, taken 6 months after casting.

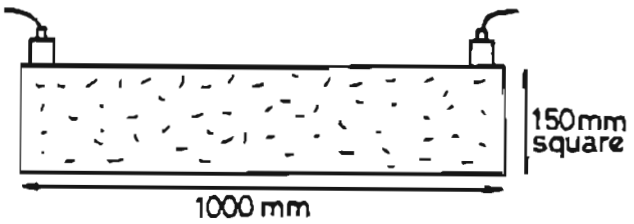

Concrete block, transverse mounting.

Figure 11.

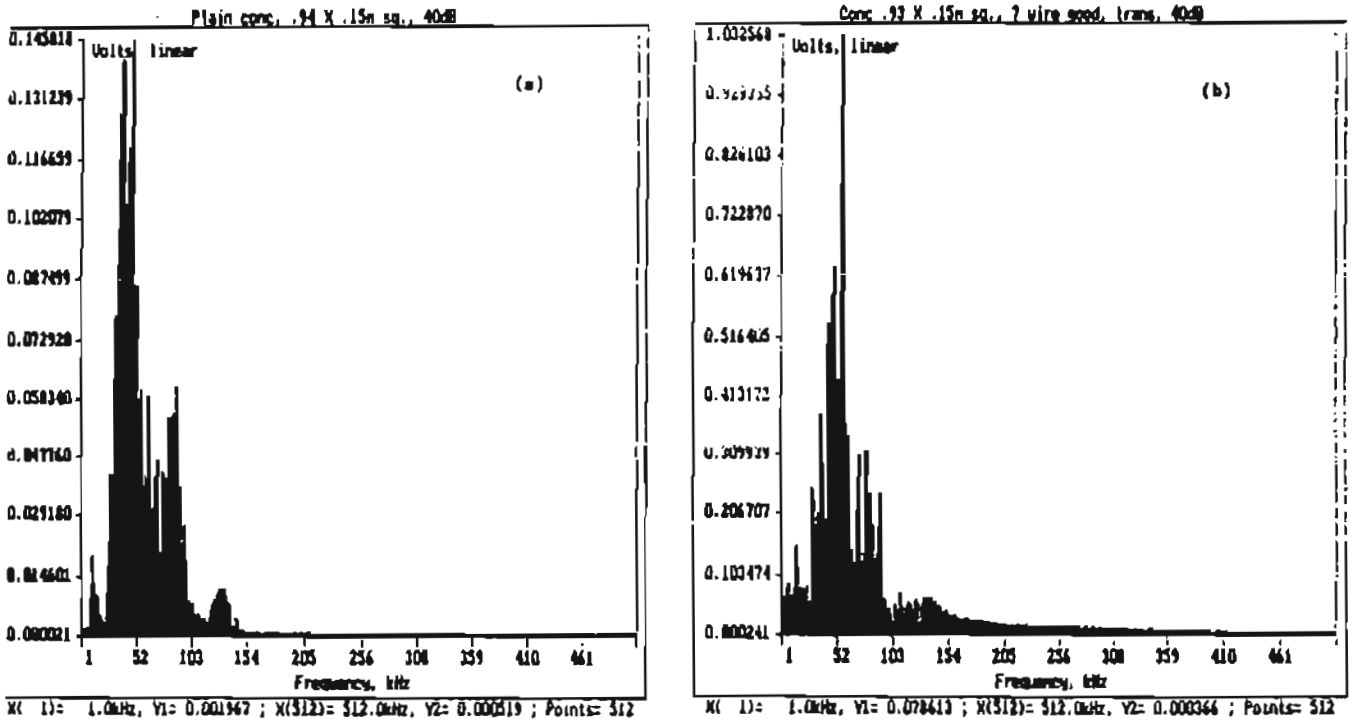

Figure 12. Spectra from pulses transmitted through (a) plain concrete block; (b) block containing 7-wire strand.

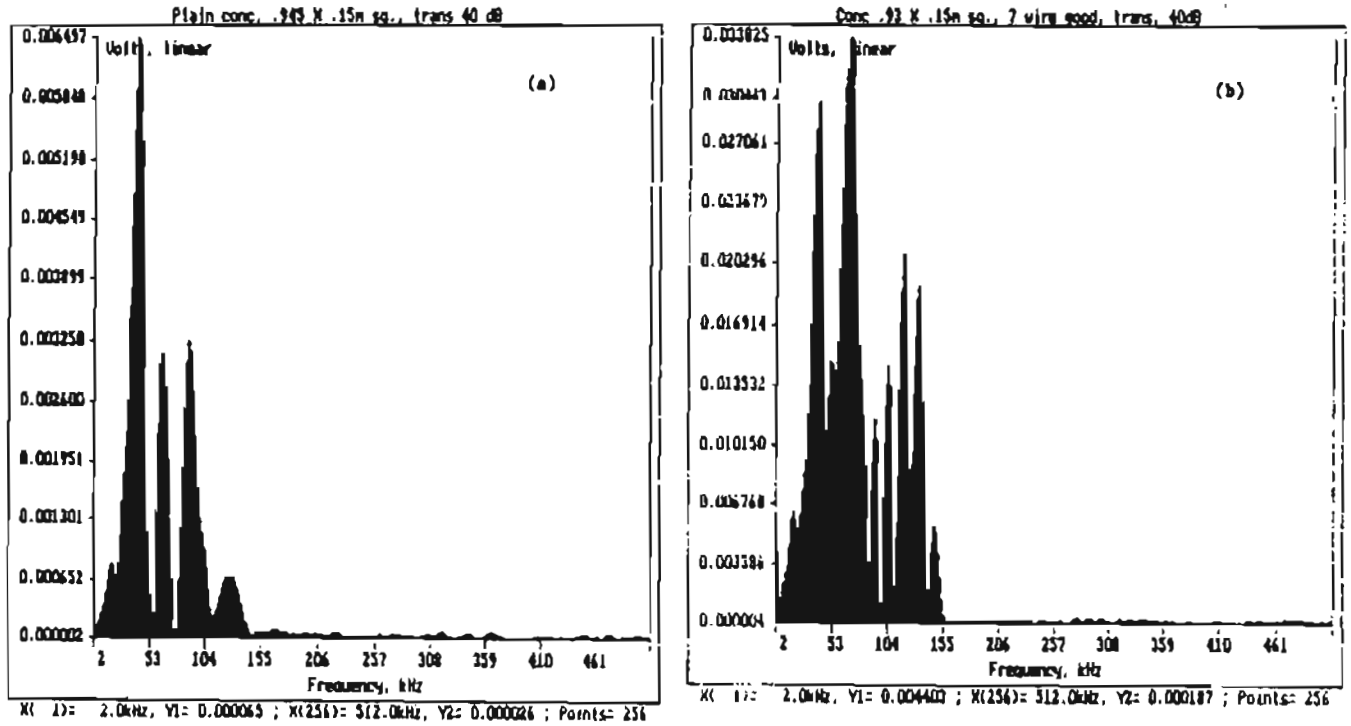

Figure 13. Pressure spectra: (a) plain concrete block. (b) block containing 7-wire strand.

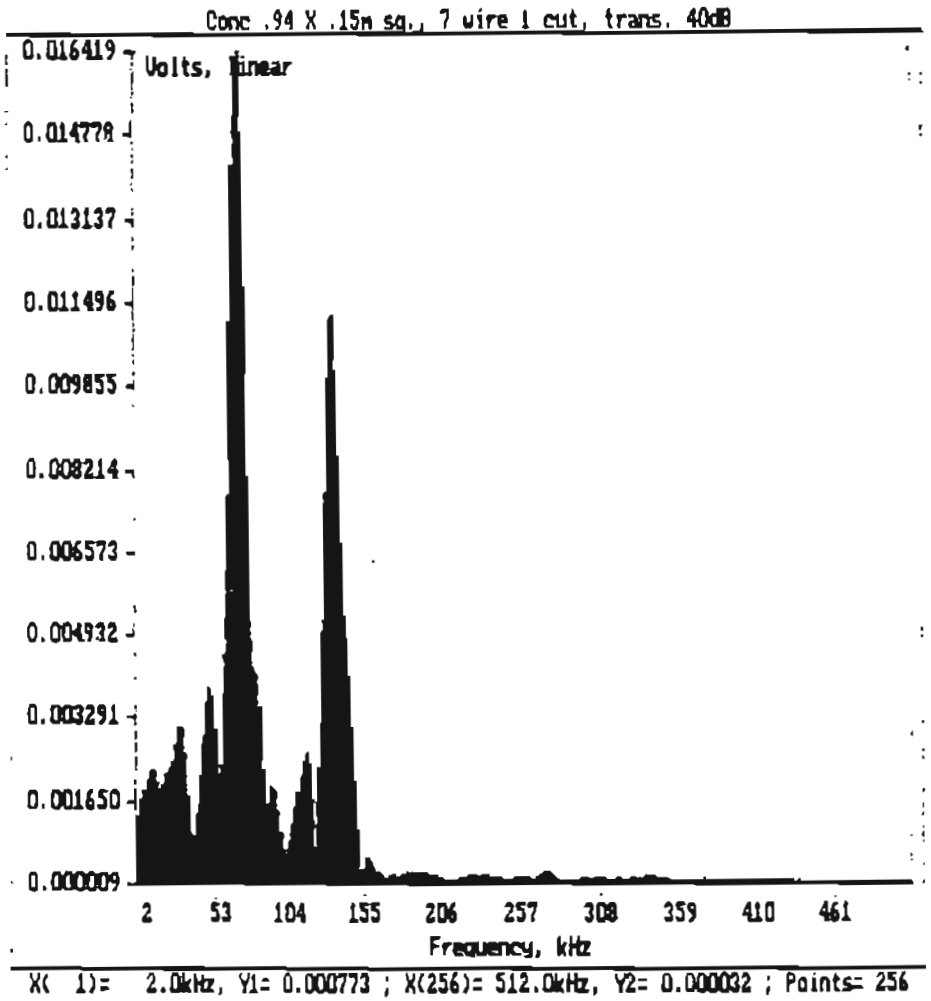

Figure 14. Prewave spectrum from signal transmitted through concrete block containing 7-wire strand with single cut wire.

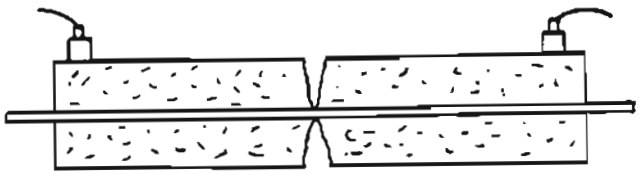

Concrete block, fractured at mid point to expose 7 strand cable.

Figure 15.

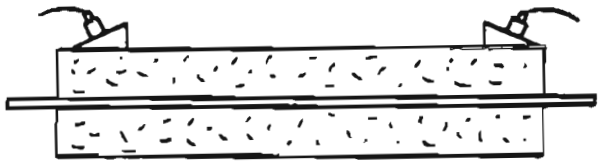

Experiment using motar wedges to facilitate h.f. propagation.

Figure 16.

Figure 17.

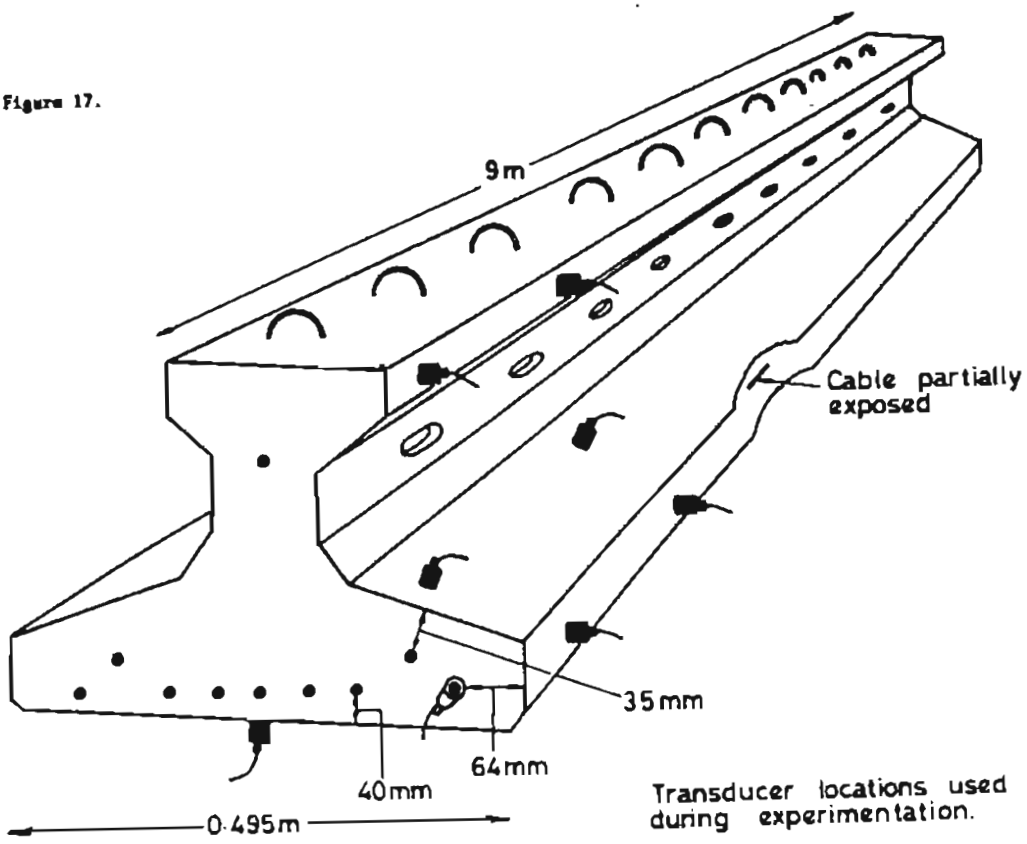

Transducer locations used during experimentation.

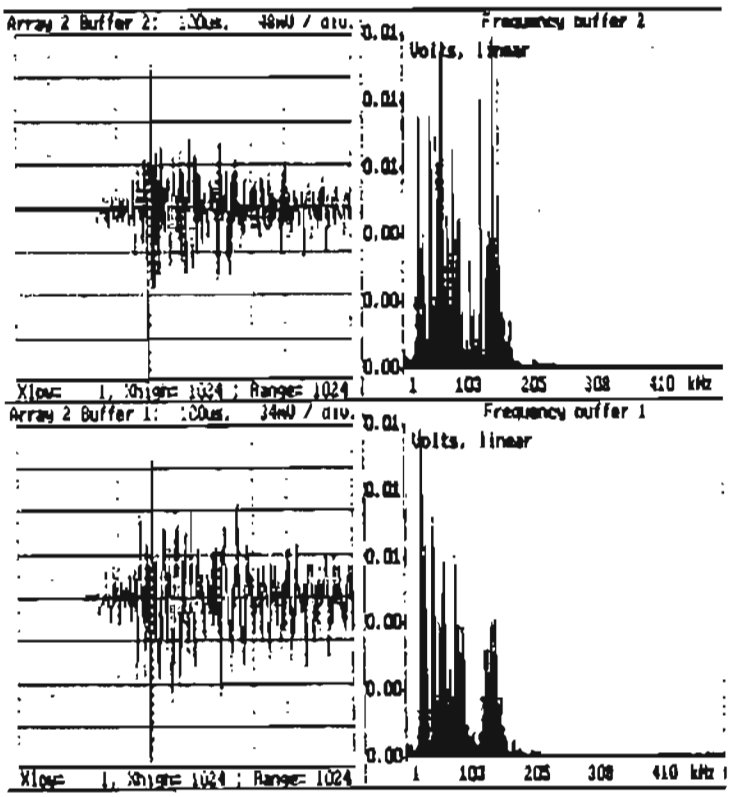

(a)

(b)

Figure 18. Signals and spectra from pulses transmitted from:
(a) steel to concrete,
(b) concrete to steel
on bridge beam, using a spacing of 1 m.

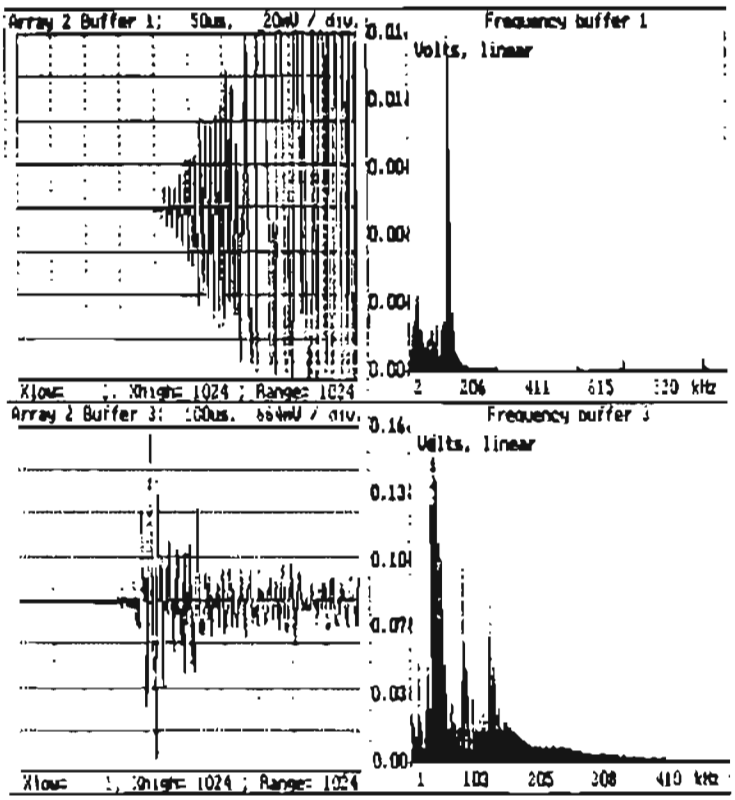

(a)

(b)

Figure 19. (a) Shearwave signal and spectrum,
(b) Main wave signal and spectrum,
taken from bridge beam with cable 64mm underlying transducers, spaced 1 m apart.

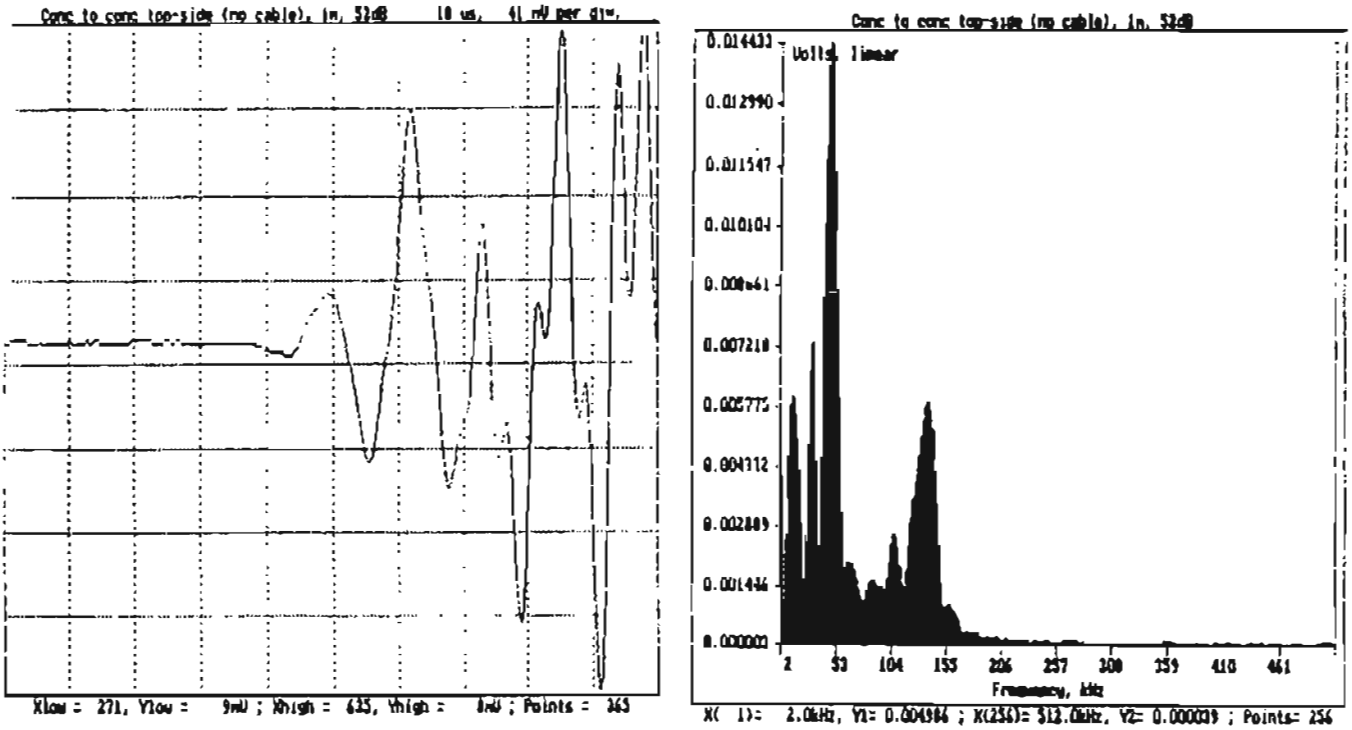

Figure 20. Pressure signal and spectrum taken from location on bridge beam with no underlying cable, with a spacing of 1 m.

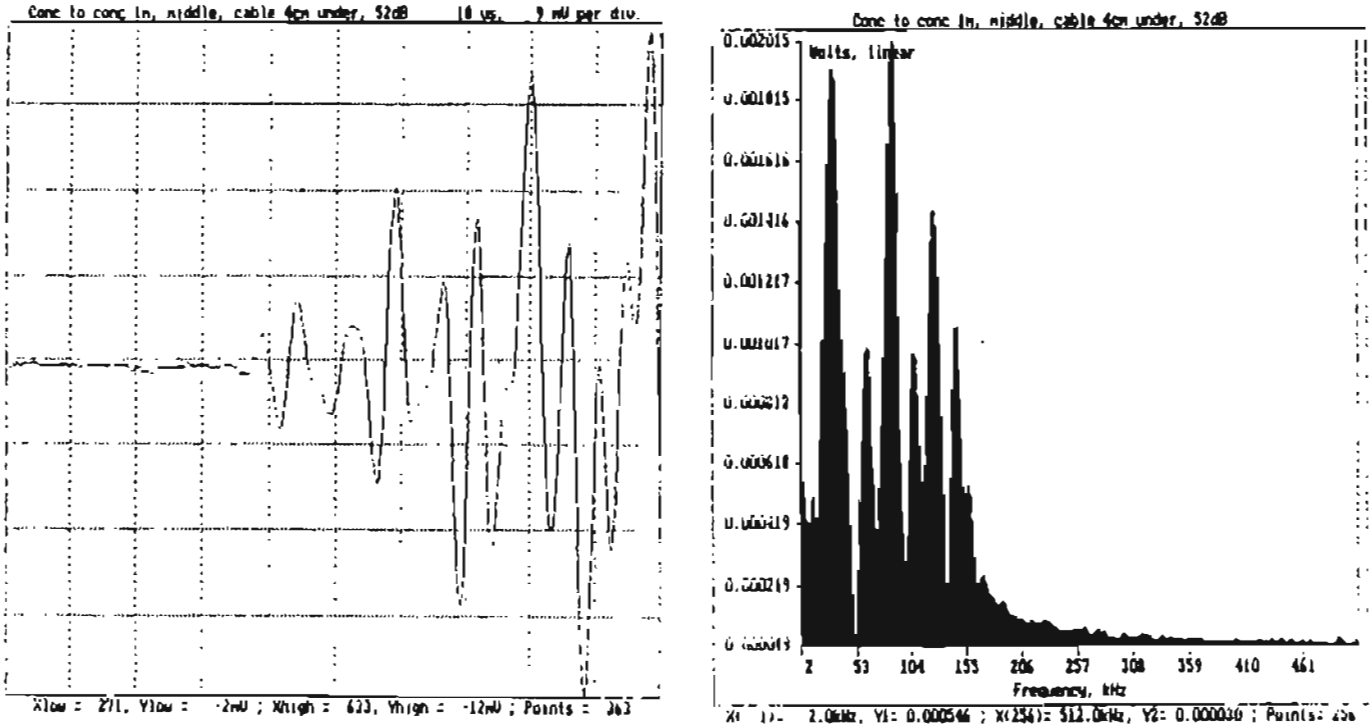

Figure 21. Pressure signal and spectrum taken from mid-point on bridge beam, with cable 40 cm underlying transducers, spaced 1 m apart.

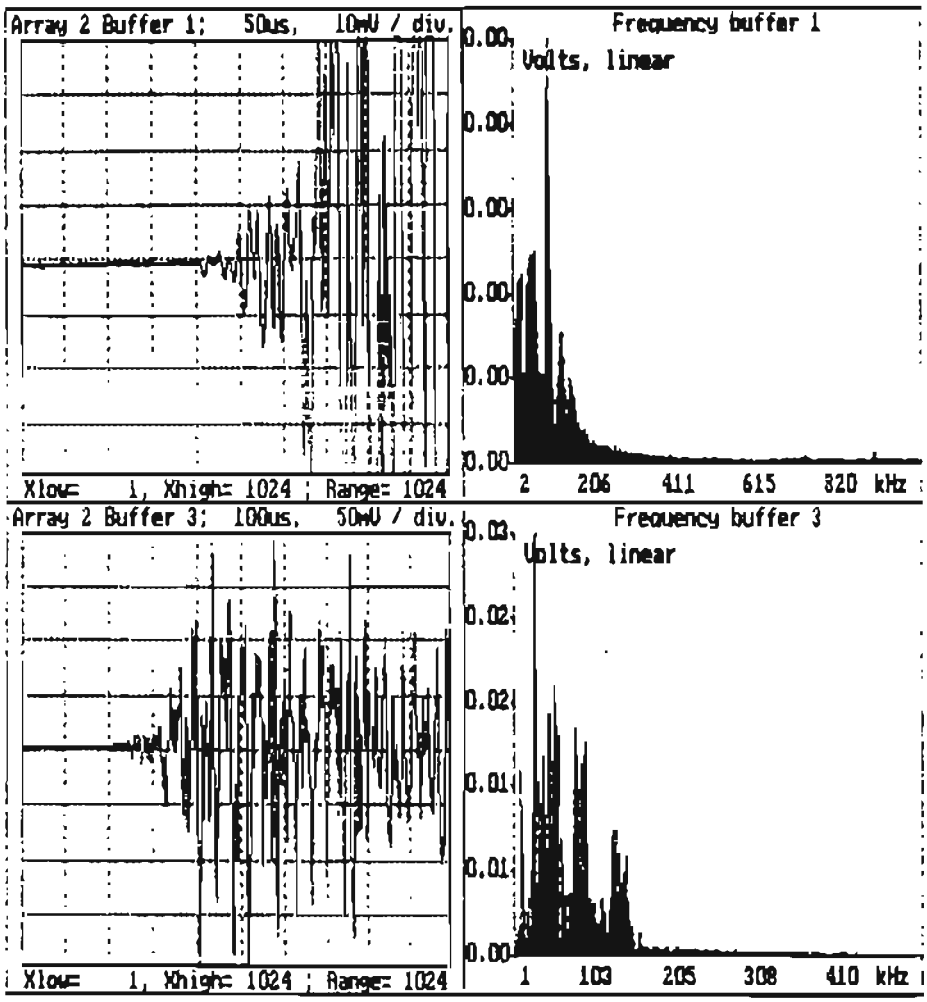

Figure 22. (a) prewave signal and spectrum,
(b) main wave signal and spectrum,
taken with transducers spanned 1 m across flaw in bridge beam.

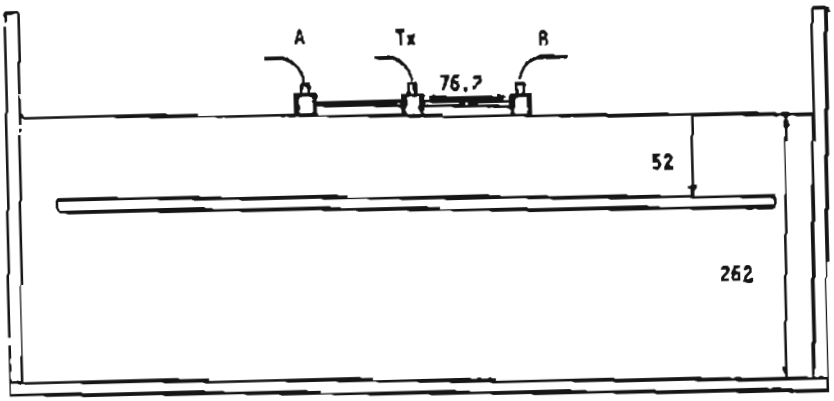

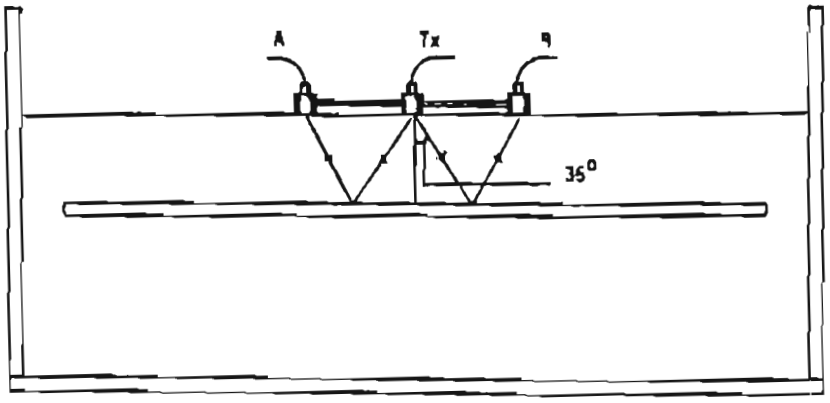

Figure 23. Linear Transducer Array System used in water showing dimensional specifications

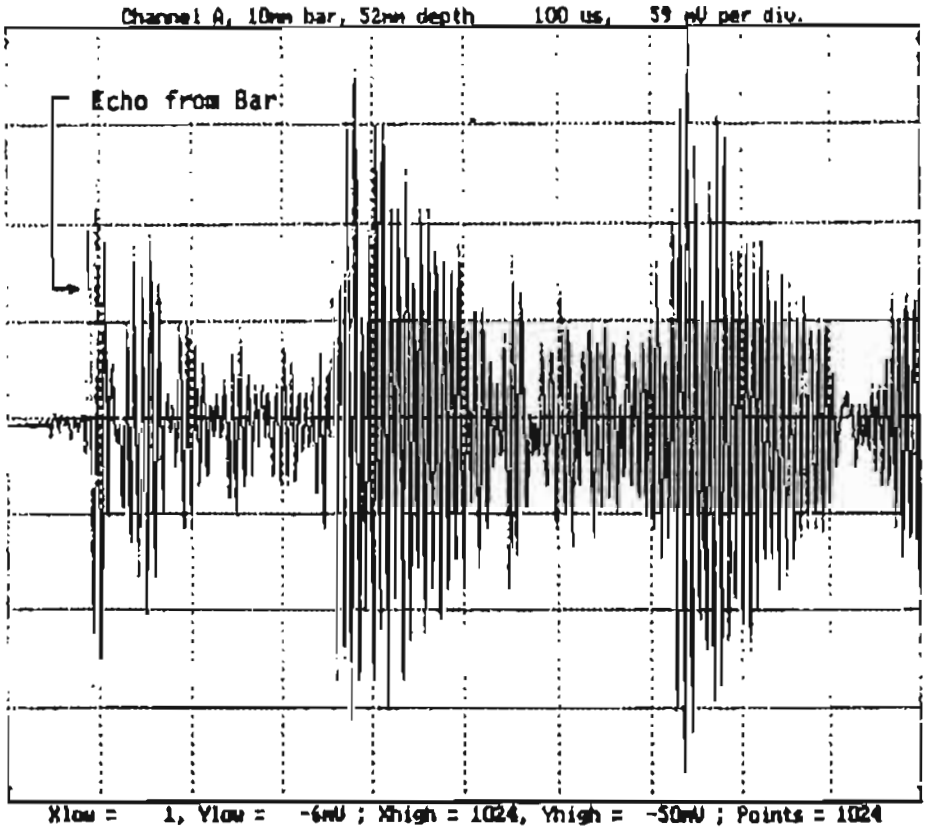

Figure
Signal trace
from Good Bar,
Channel A

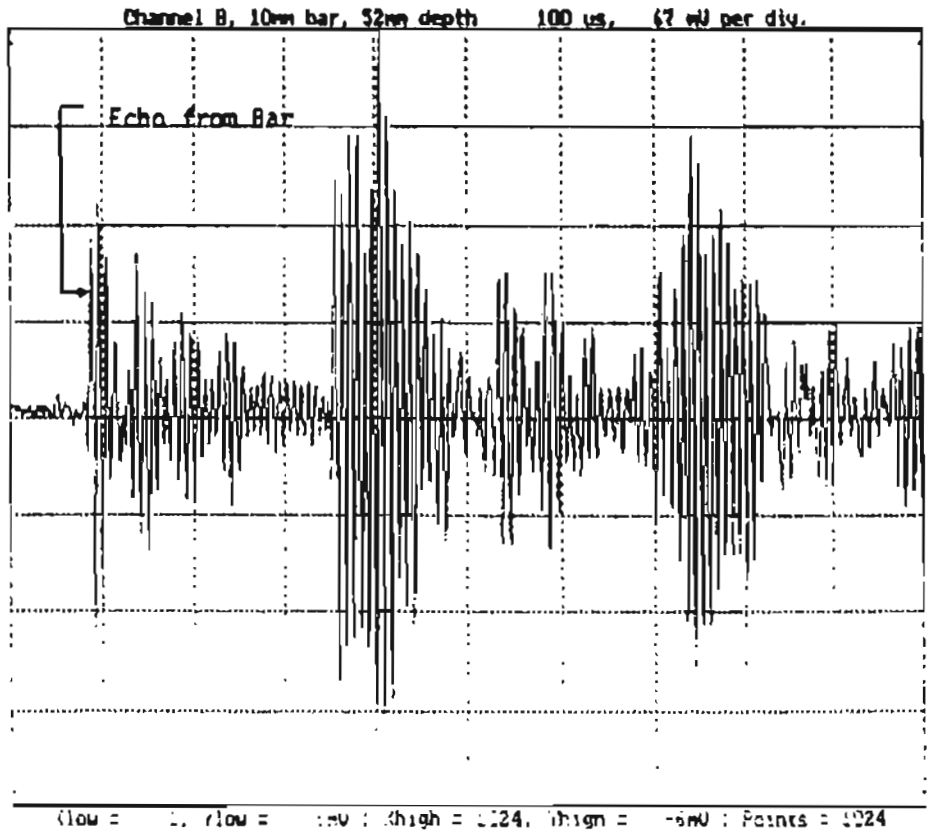

Figure
Signal trace
from Good Bar,
Channel B.

Figure 24. Typical echoes detected by transducers A and B, from good quality steel bar in water.

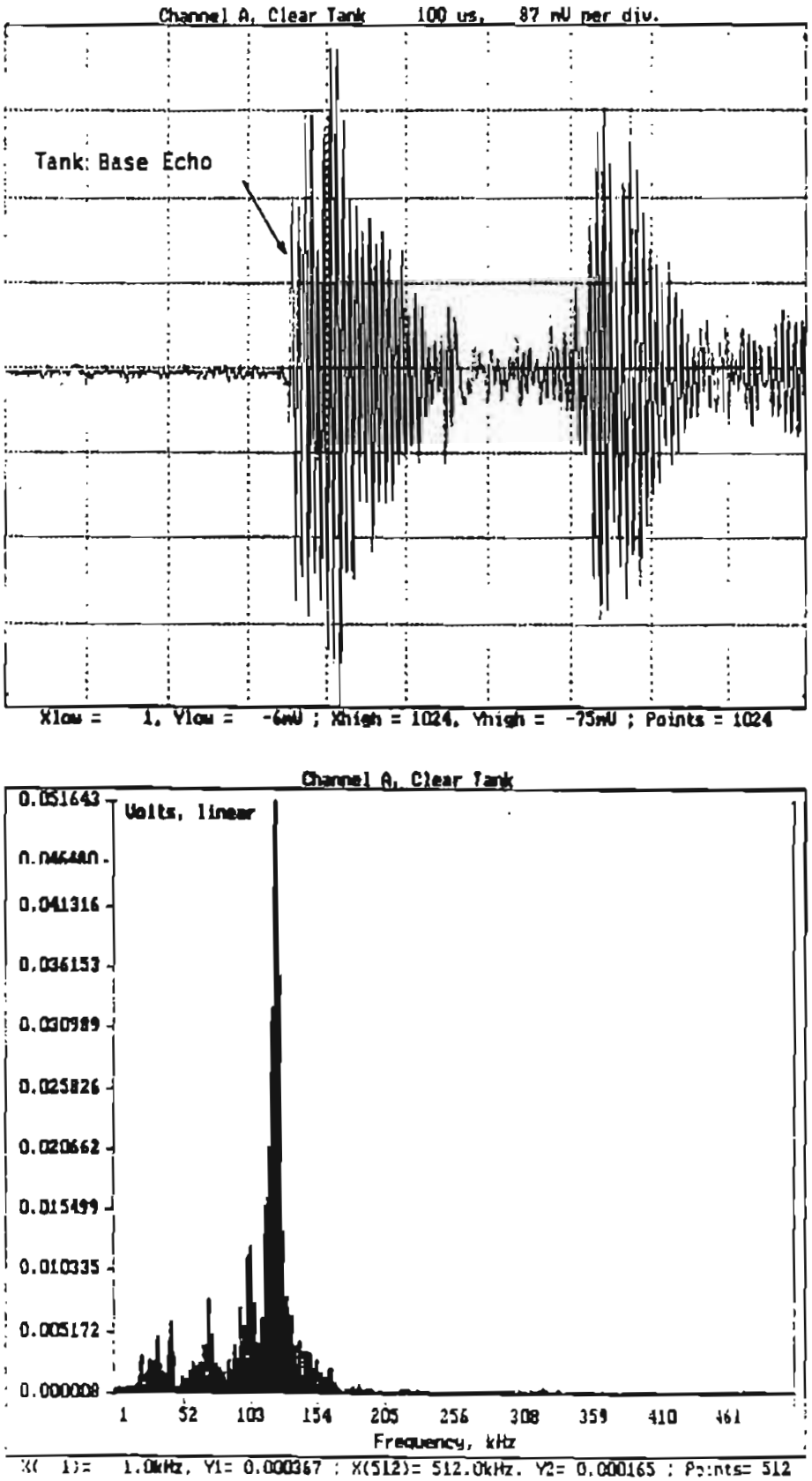

Figure 25a.Signal and Frequency Plot for Channel A in Tank containing fresh water only.

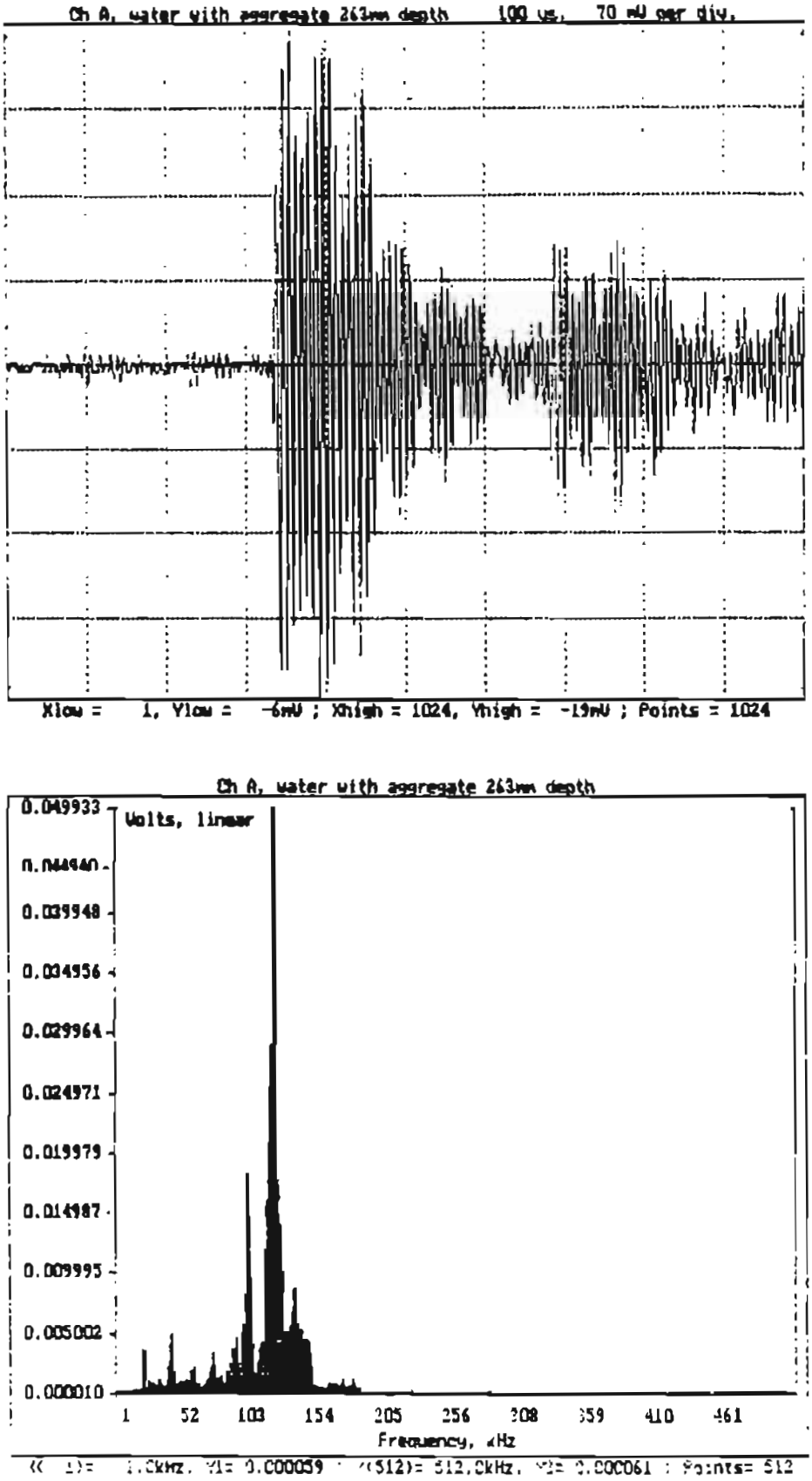

Figure 25b. Signal and Frequency plot for Channel A in Water with Simulated Aggregate.

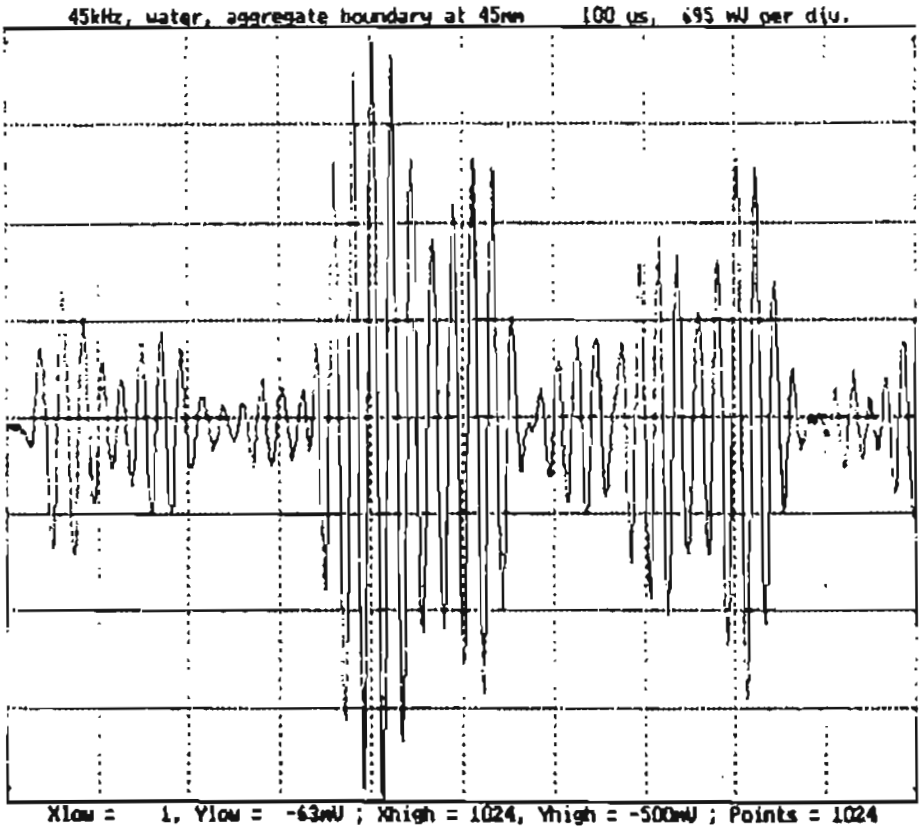

Figure 26a.
45 kHz probe in water with aggregate Note signal cross-talk in addition to tank base echo.

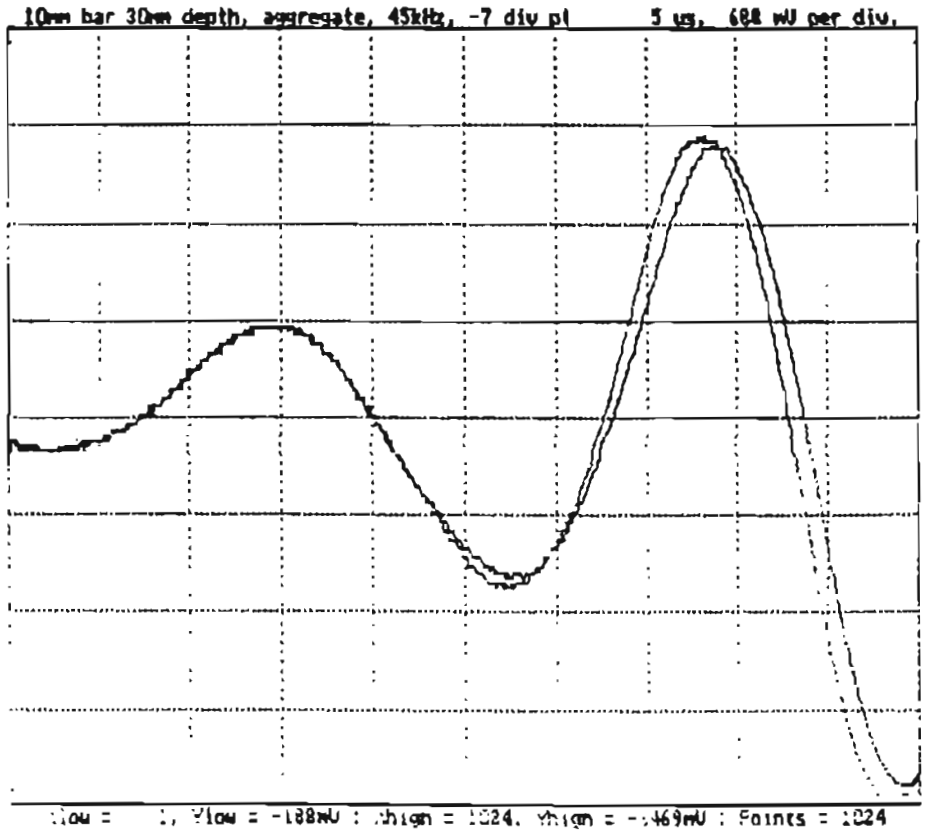

Figure 26b.
Force corrosion defect identified using phase analysis with low frequency probes.

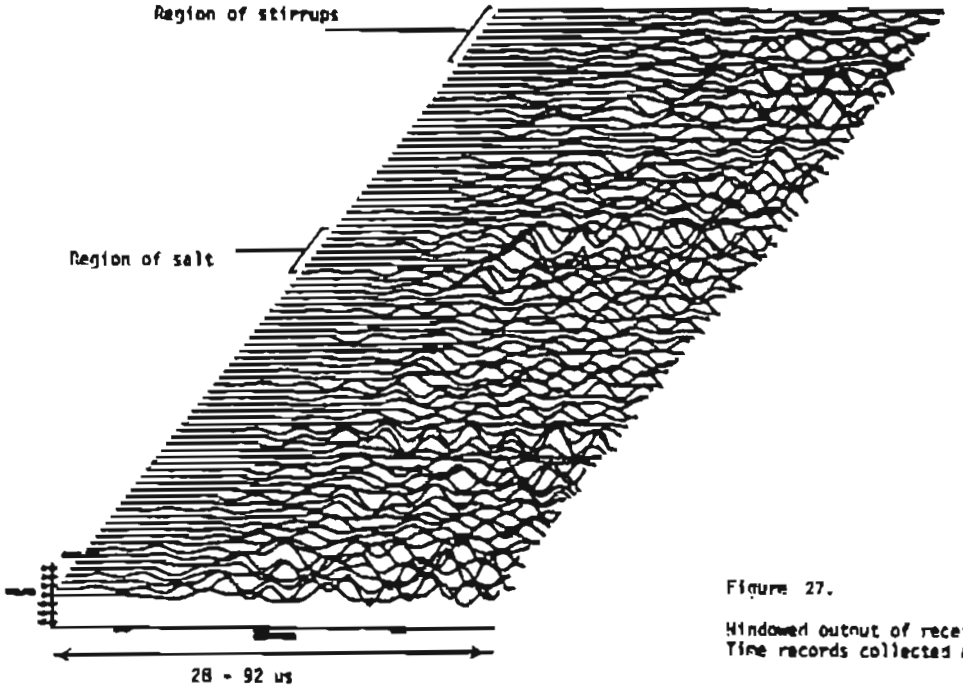

Figure 27.

Windowed output of receiver R1.
Time records collected at 50mm intervals.

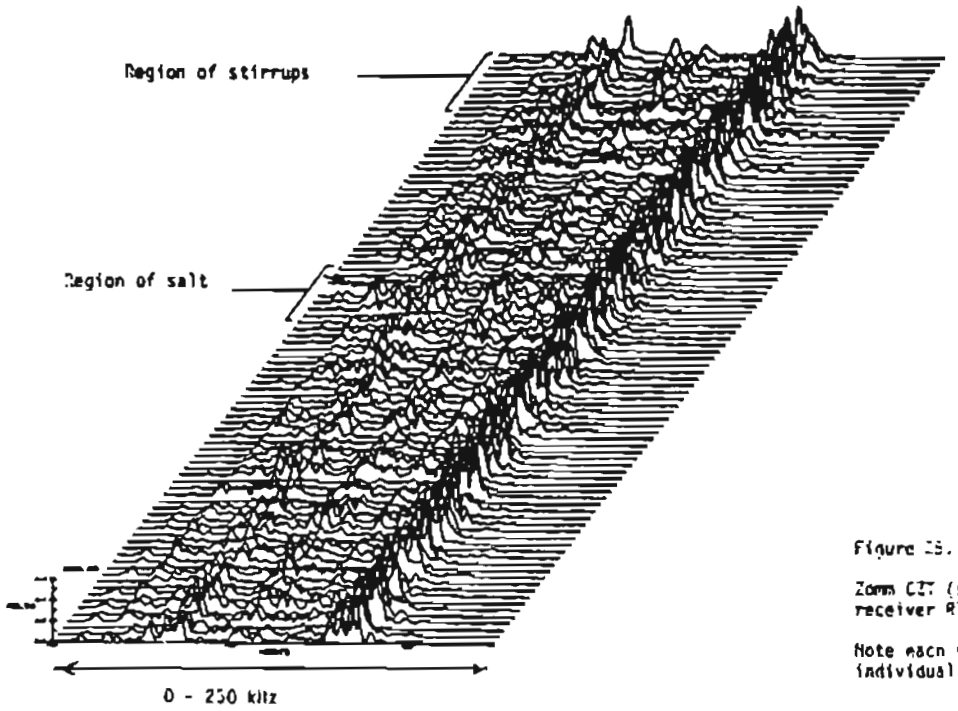

Figure 28.

Zoom CFT (spectrum) of receiver R1.

Note each spectrum has been individually auto-scaled

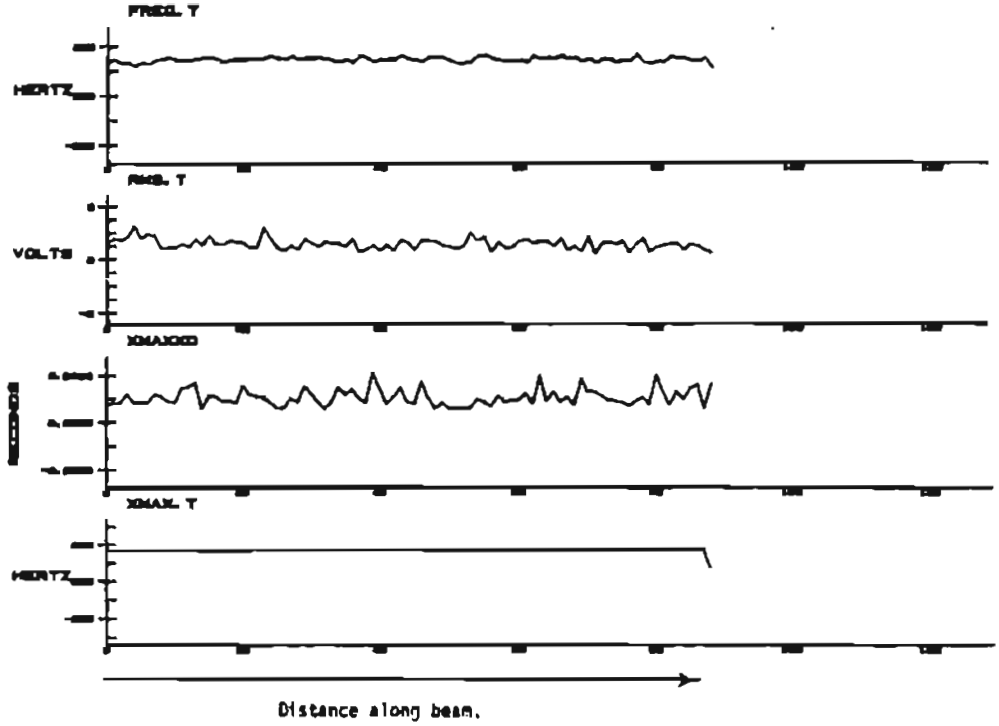

Figure 29.

Trend data, showing the following:

a. Dominant frequency, calculated in the time domain.

b. Signal RMS.

c. Point in time at which maximum signal amplitude occurs.

d. Dominant frequency, calculated in the frequency domain.

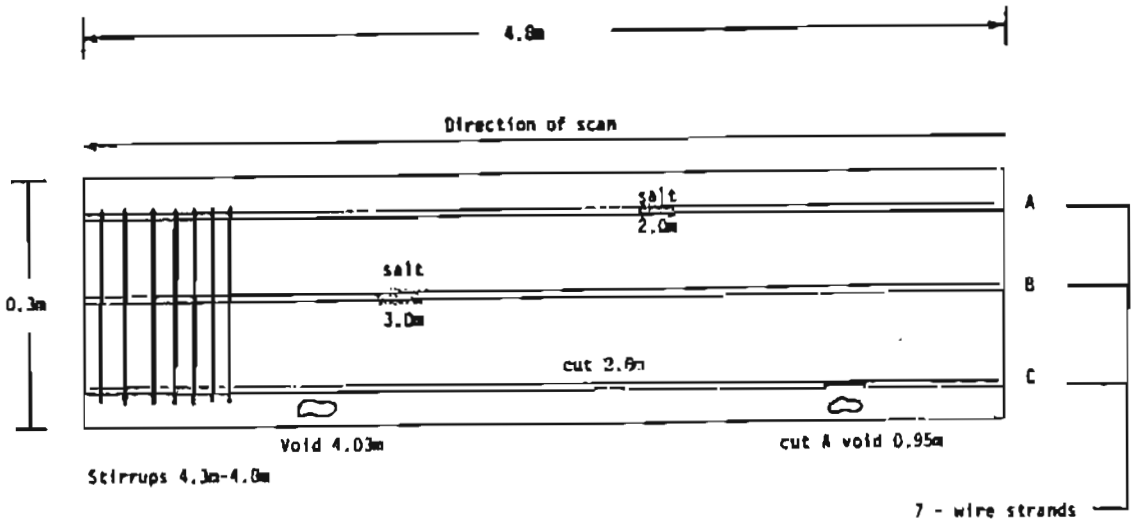

Figure 30. Upper profile of large scale test beam showing details of inclusions.

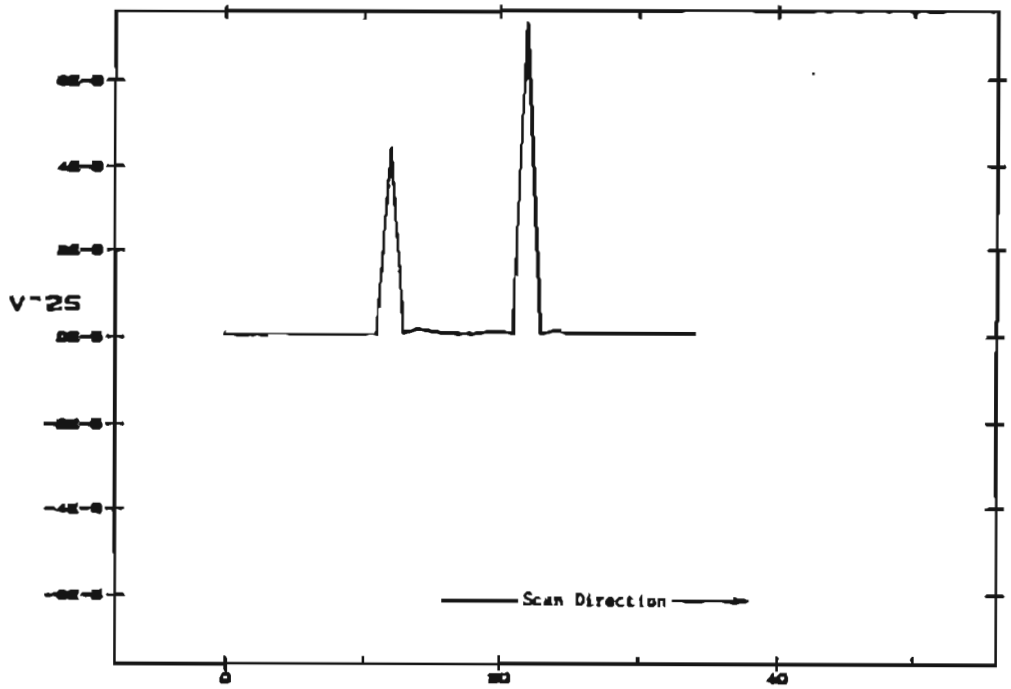

Scan of region 380 mm either side of void, along centre line of duct.

Figure 31. Energy trace of small sample scan, with void at centre of embedded duct.

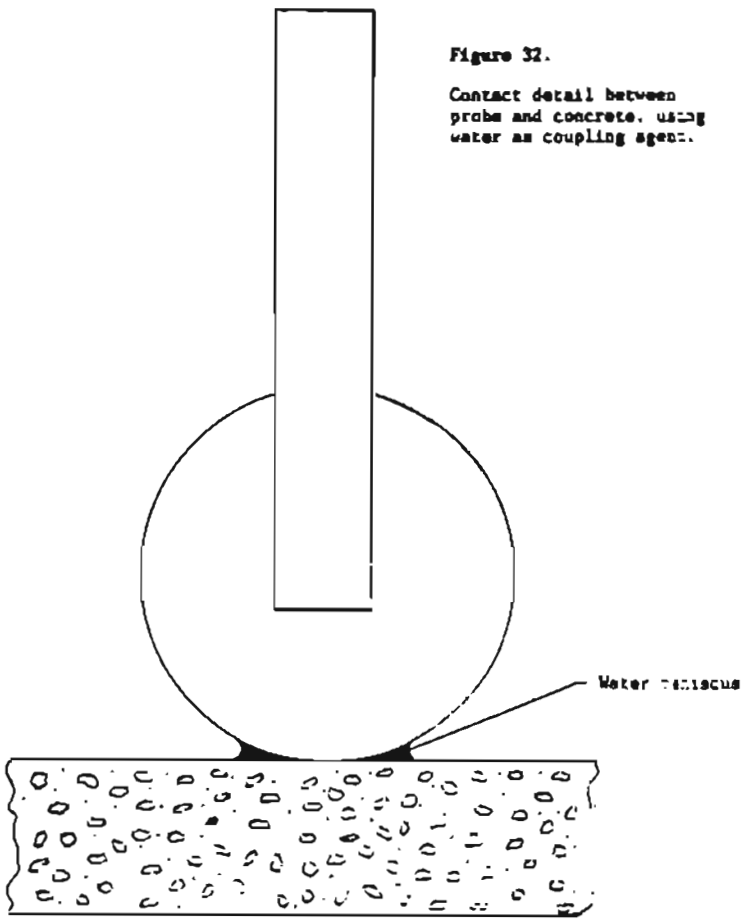

Figure 32.

Contact detail between probe and concrete, using water as coupling agent.

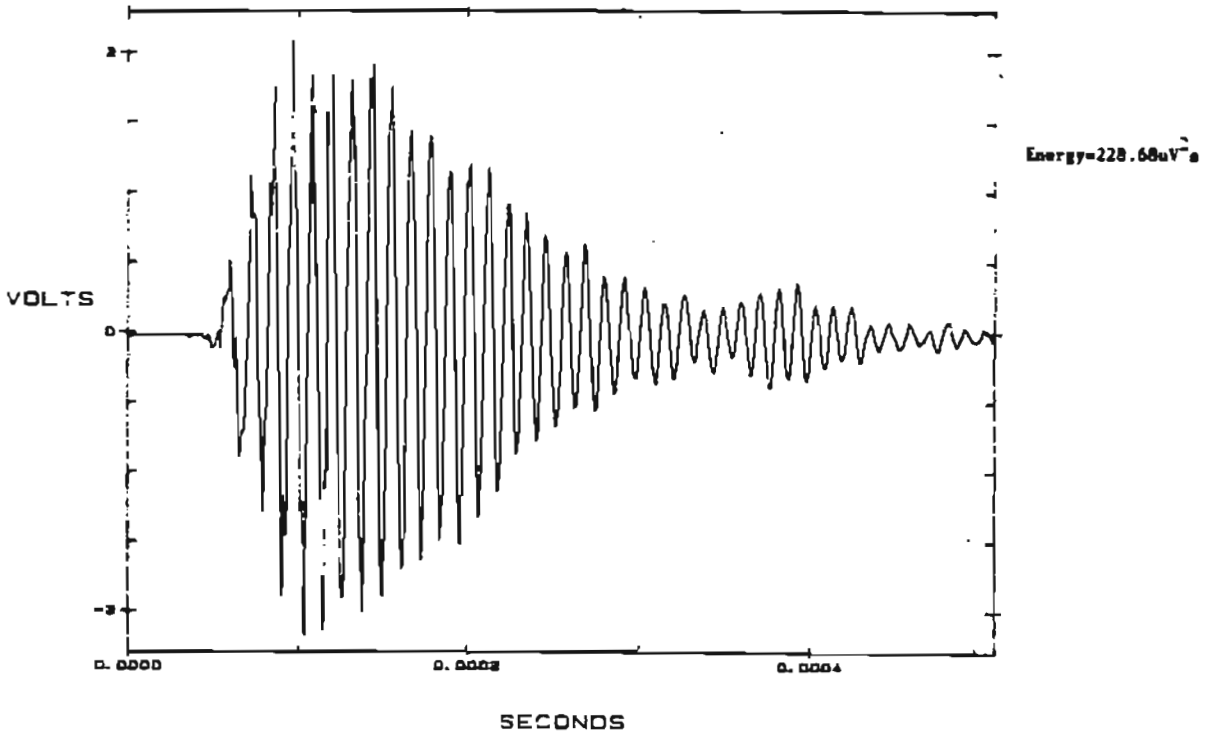

Figure 33a. Typical signal generated by rolling transducers through 70mm of concrete

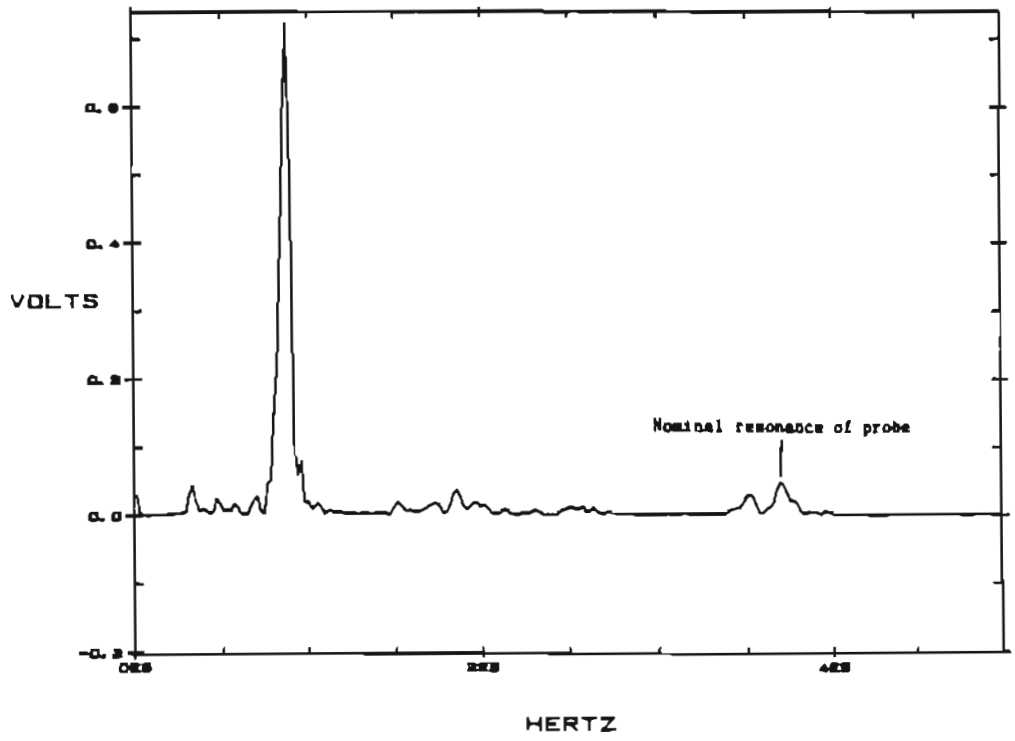

Figure 33b. Frequency spectrum of signal in Figure a. Note large amplitude low-frequency content and sharp attenuation of high-frequency resonance.

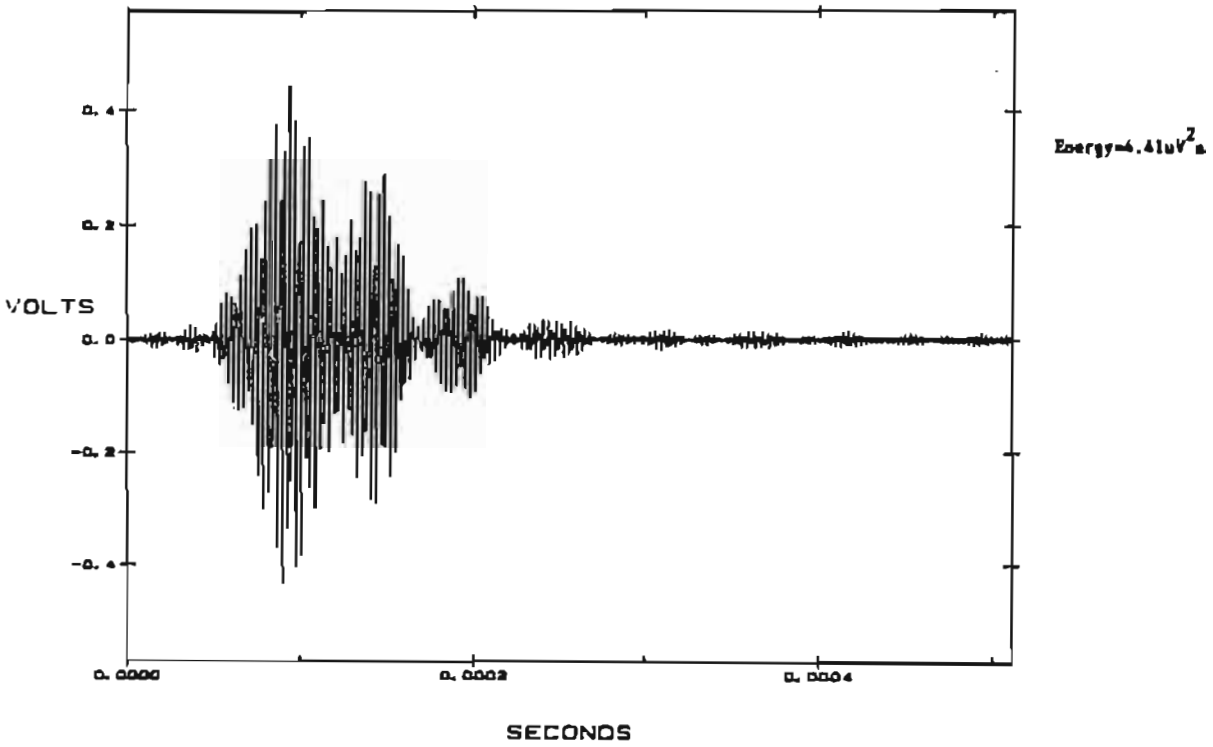

Figure 34. Signal of Figure33, filtered in the frequency domain and re-transformed to the time domain, leaving only the frequency components between 350 and 400kHz

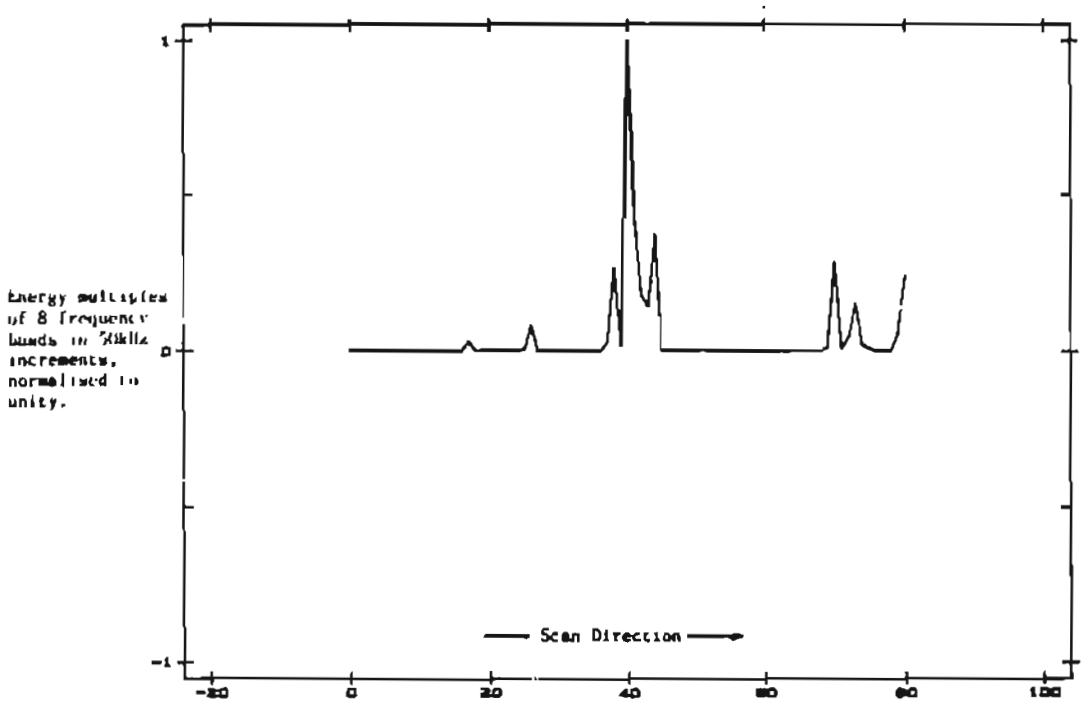

Figure 35. Trace of small sample scan, with major peak indicating region of broken and separated 7-wire strand cable.

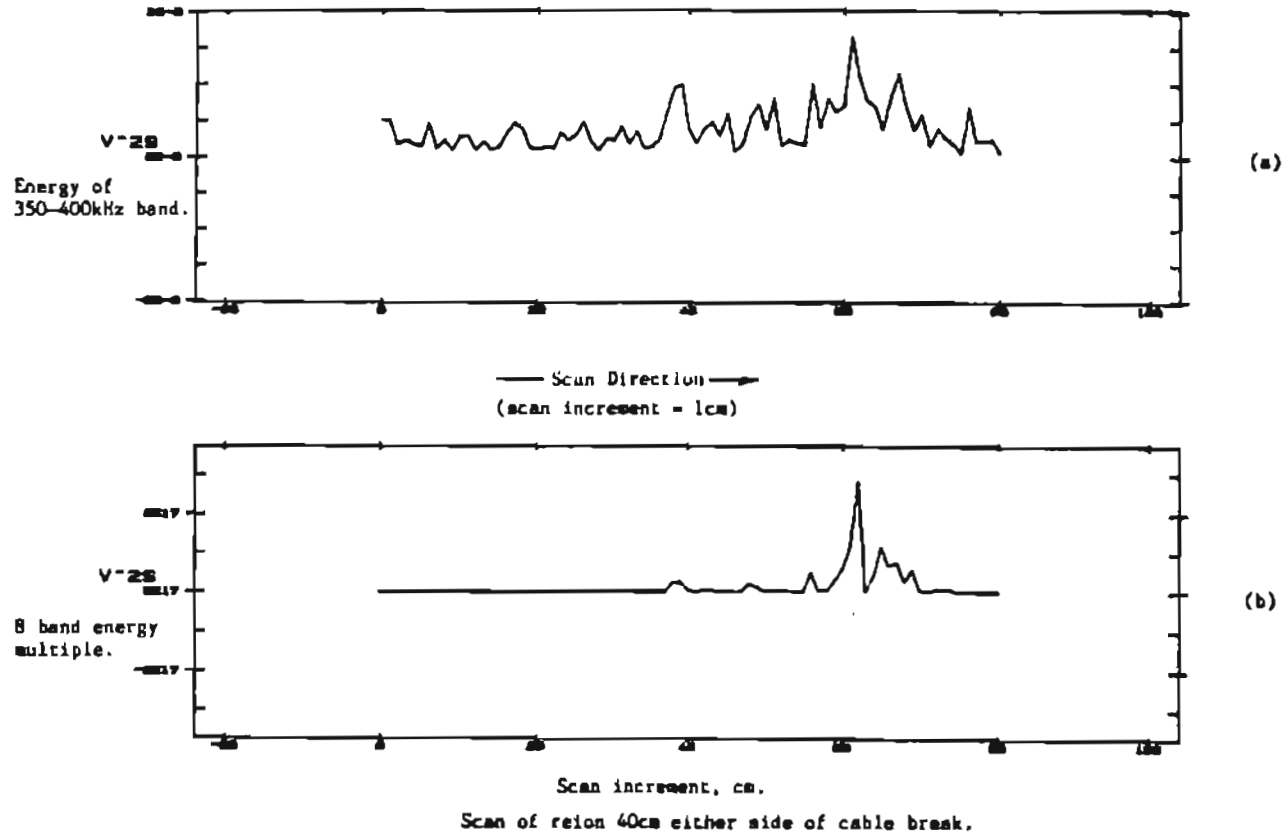

Figure 36. Trace of scan as in Figure 5, but with additional corroded region centered at scan no. 63.

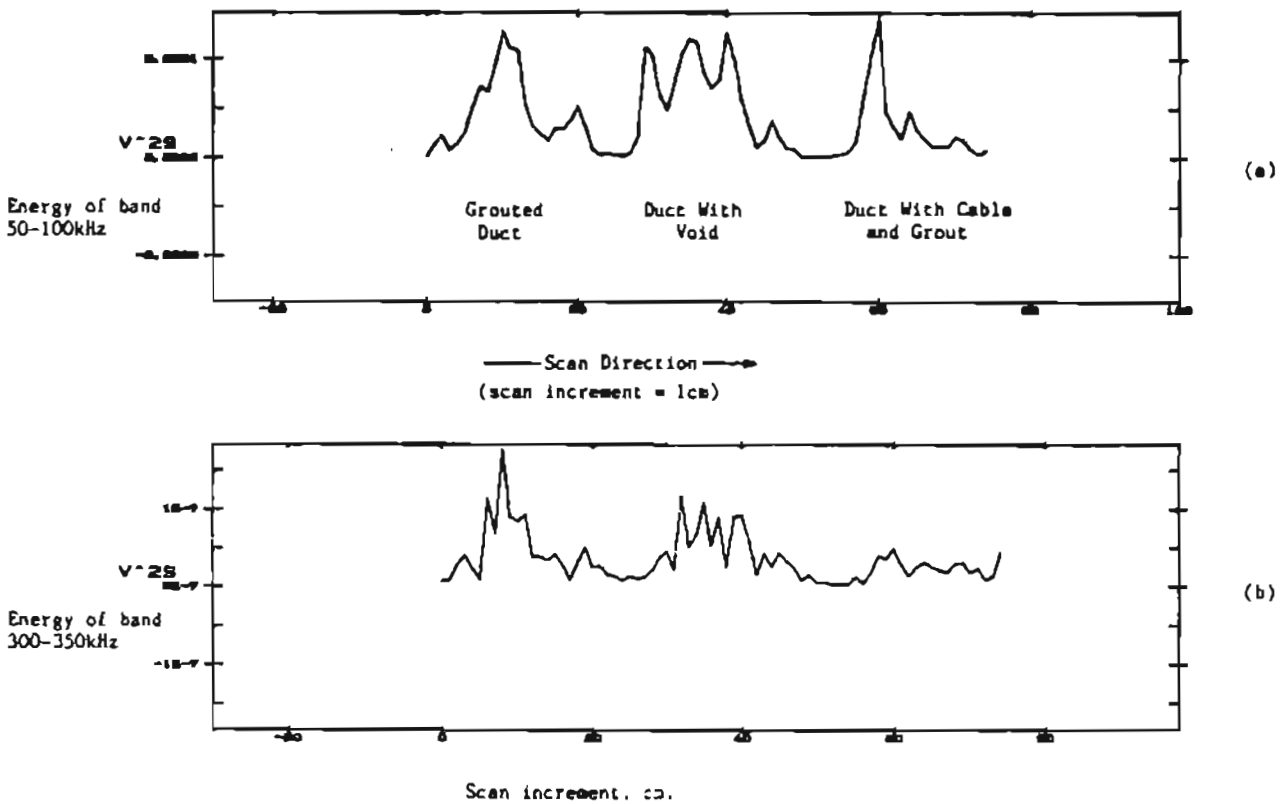

Scans of regions 12cm either side of ducts (transducers tracked 90 degrees over ducts) with duct mid-positions at scan nos. 12, 37 and 62

Figure 37. Energy traces of a transverse scan of 40mm ducted samples.

Figure 38a. Trace of scan over chloride-contaminated region of cable in large scale test

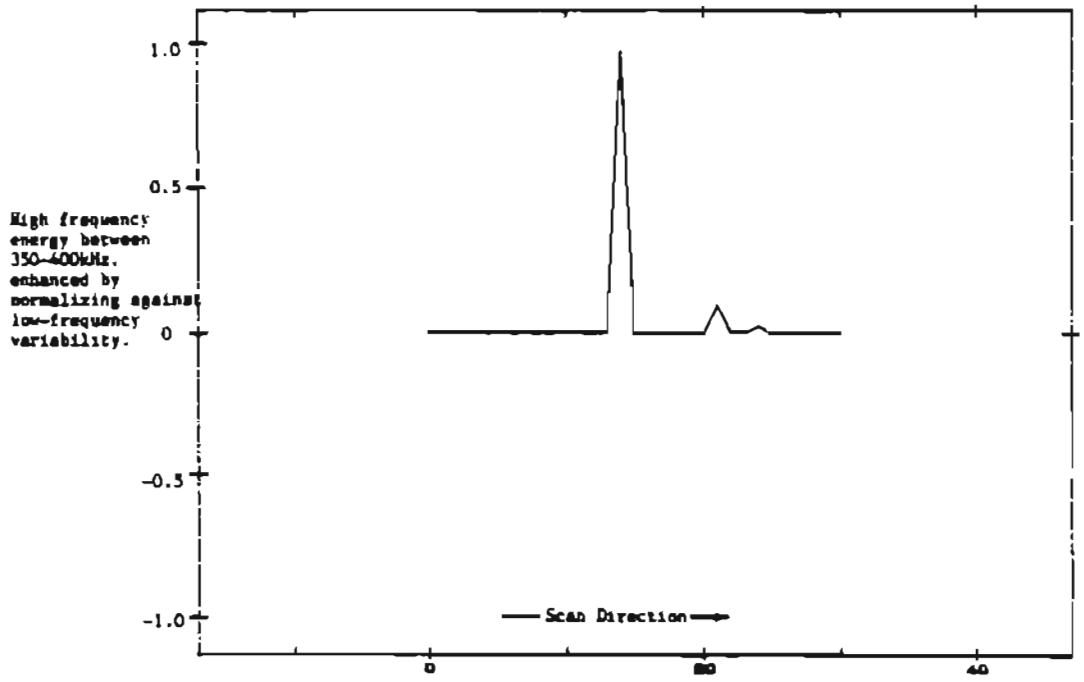

Scan of region 30 cm either side of contaminated region using a scan increment of 2 cm.

Figure 38b. Trace of scan over second chloride-contaminated region of cable

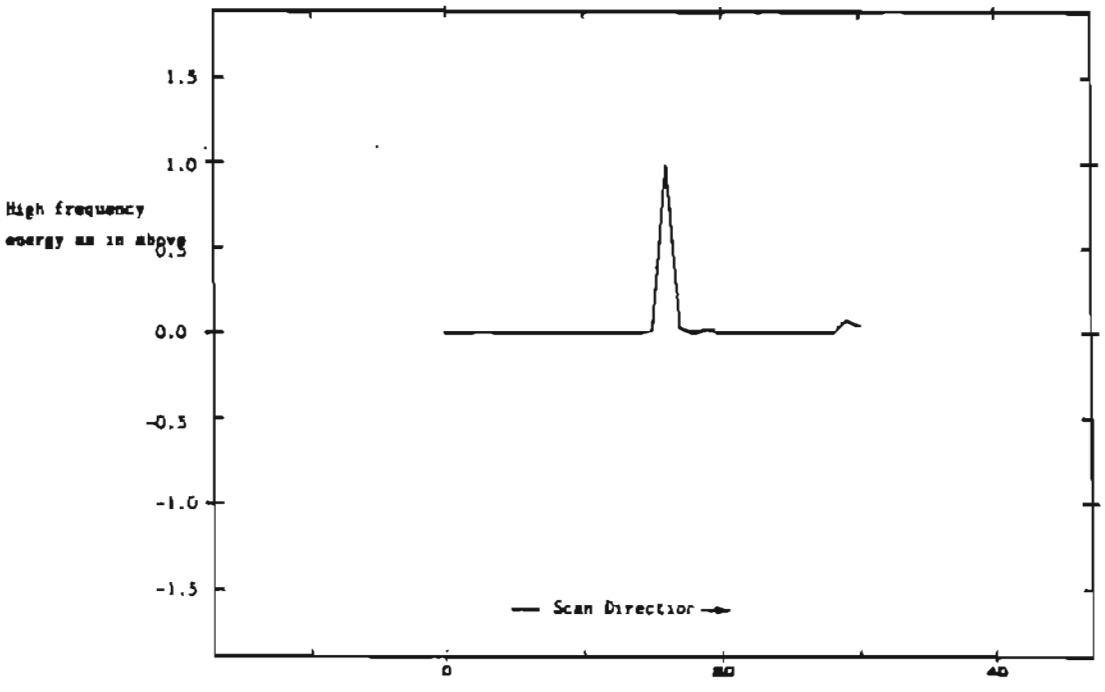

Scan of region 3[illegible] cm either side of second contaminated region using a scan increment of 2 cm.

Figure 39a. Trace of scan over region in test beam containing void.

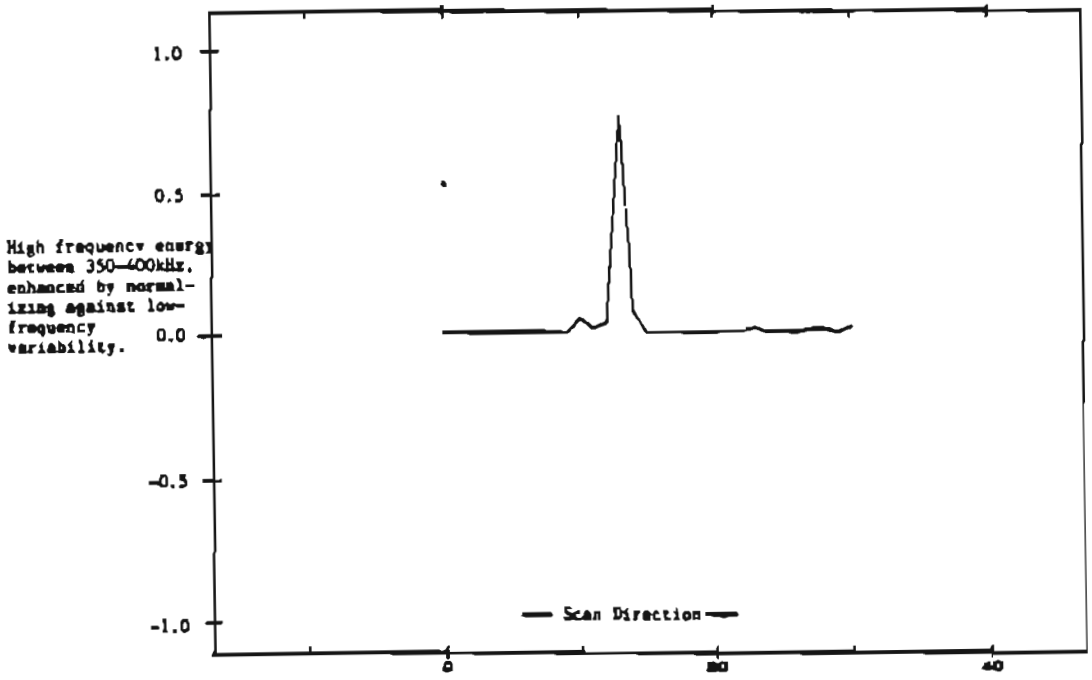

Scan of region 30cm either side of void, using a scan increment of 2 cm.

Figure 39b. Trace of scan over region in test beam containing second void

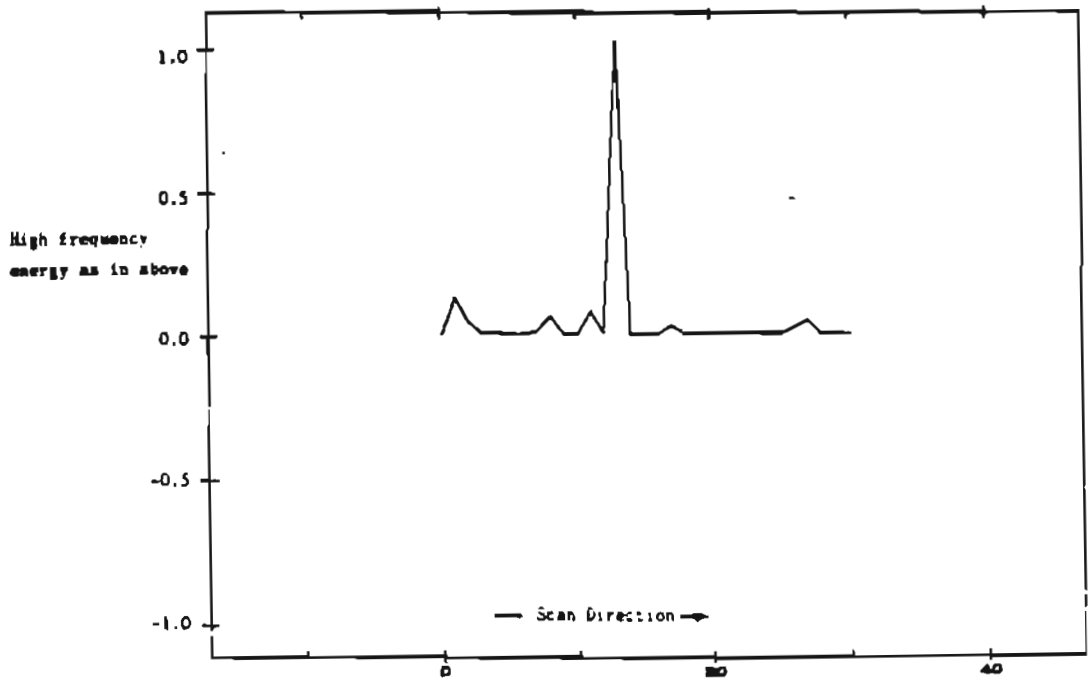

Scan of region 30cm either side of second void, using a scan increment of 2 cm.

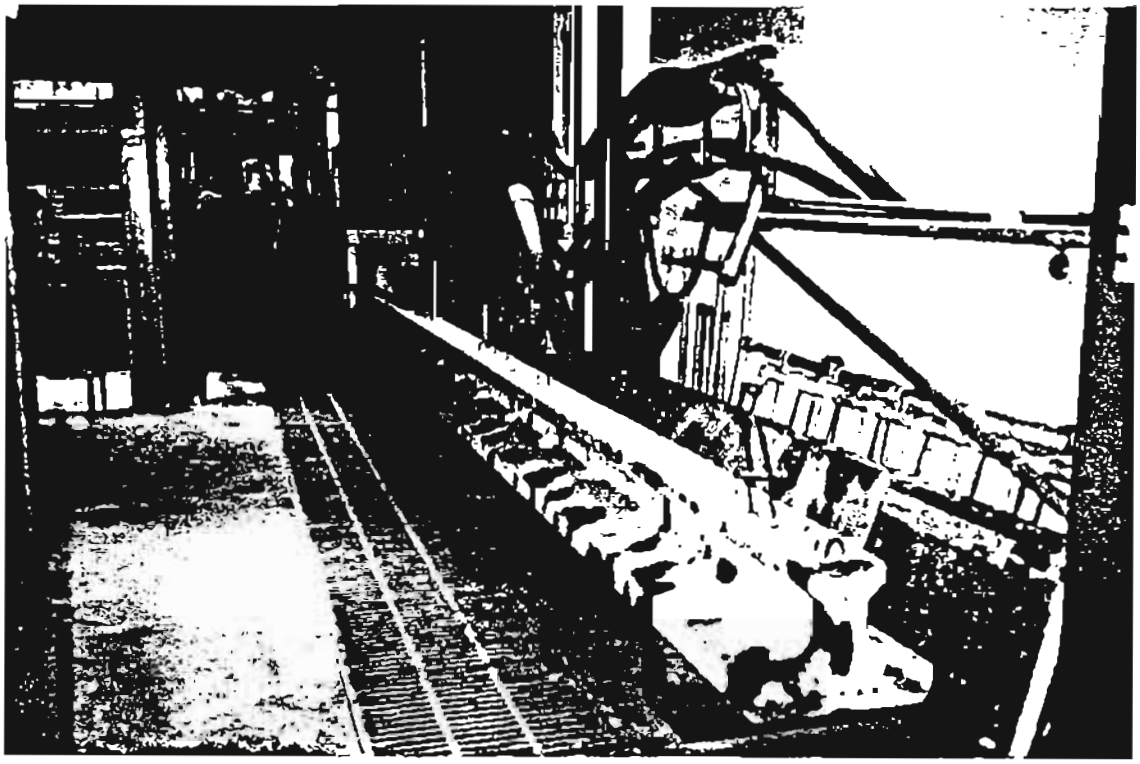

PLATE 1. The 9m Bridge Beam. Note grease stains from static tests.

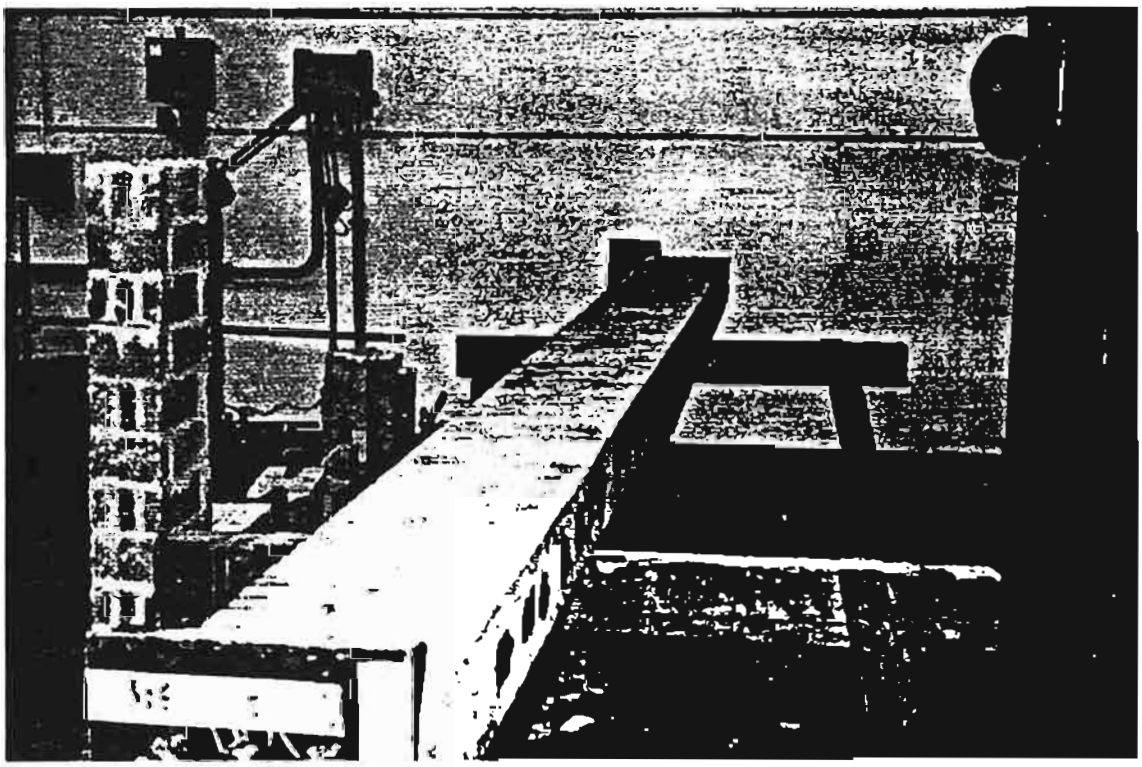

PLATE 2. The Large Scale Test Beam. Extensive tests revealed the defects.

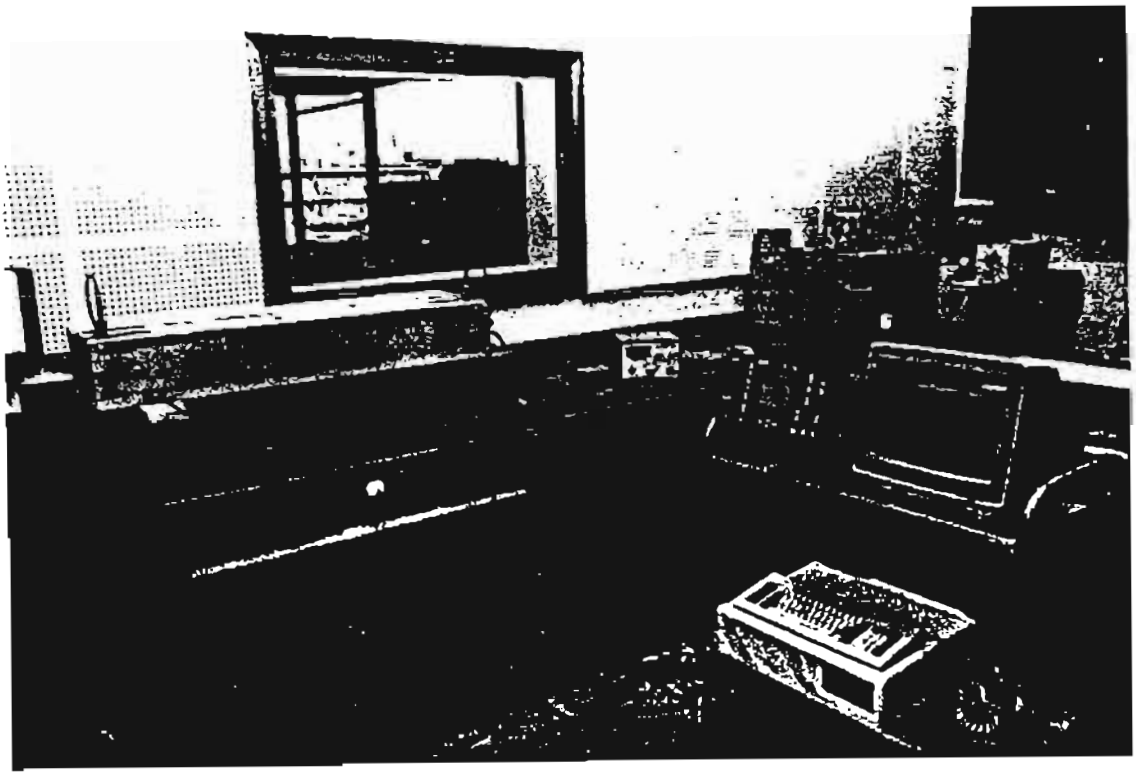

PLATE 3. Early experimental configuration.

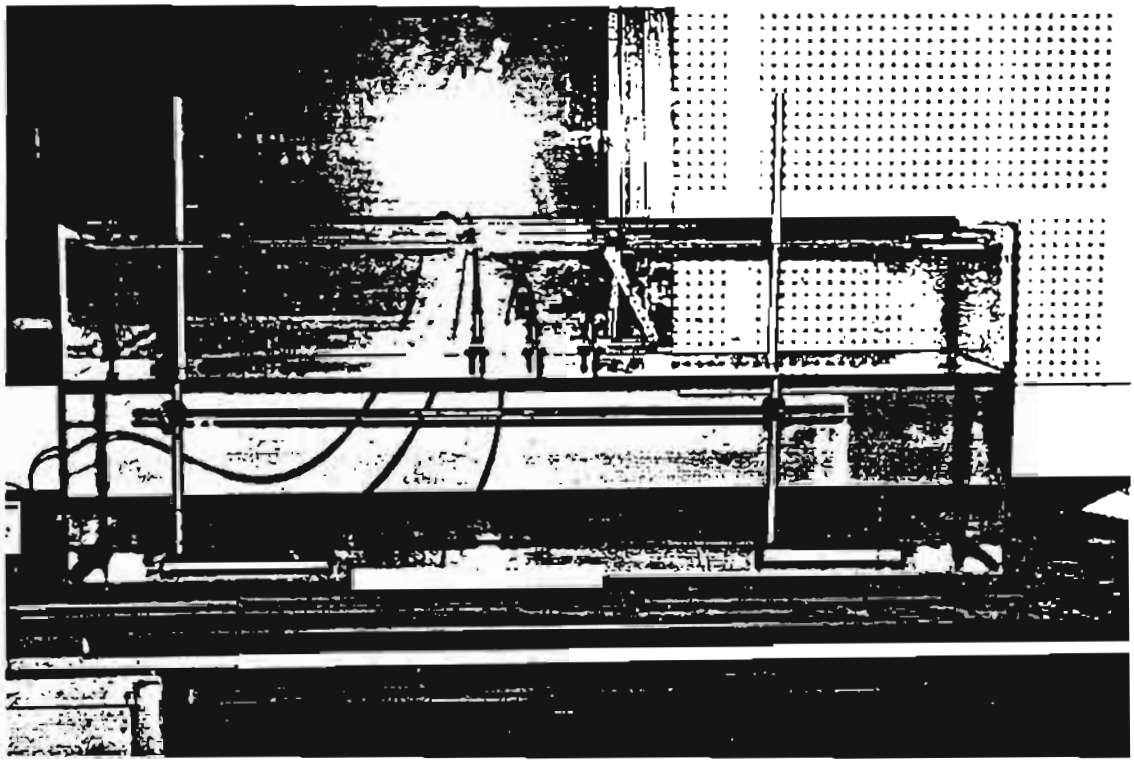

PLATE 4. Linear transducer array used in water simulation trials.

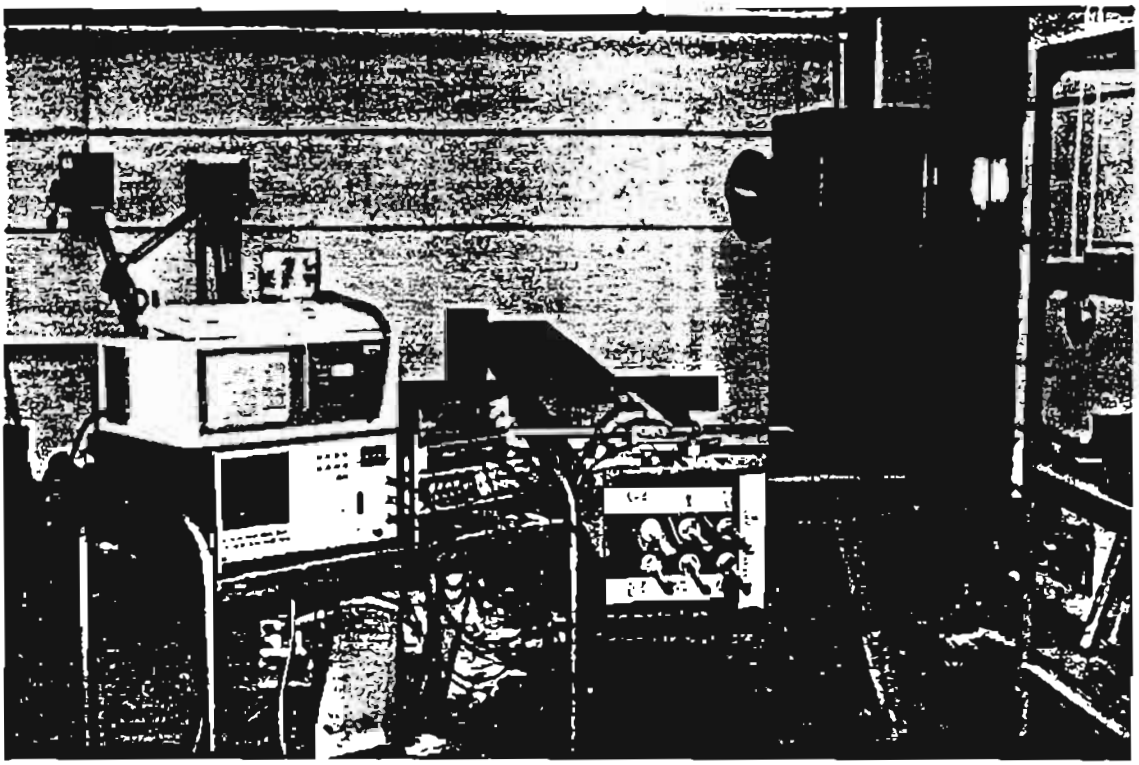

PLATE 5. The MKI CANDI system undergoing evaluation on the test beam.

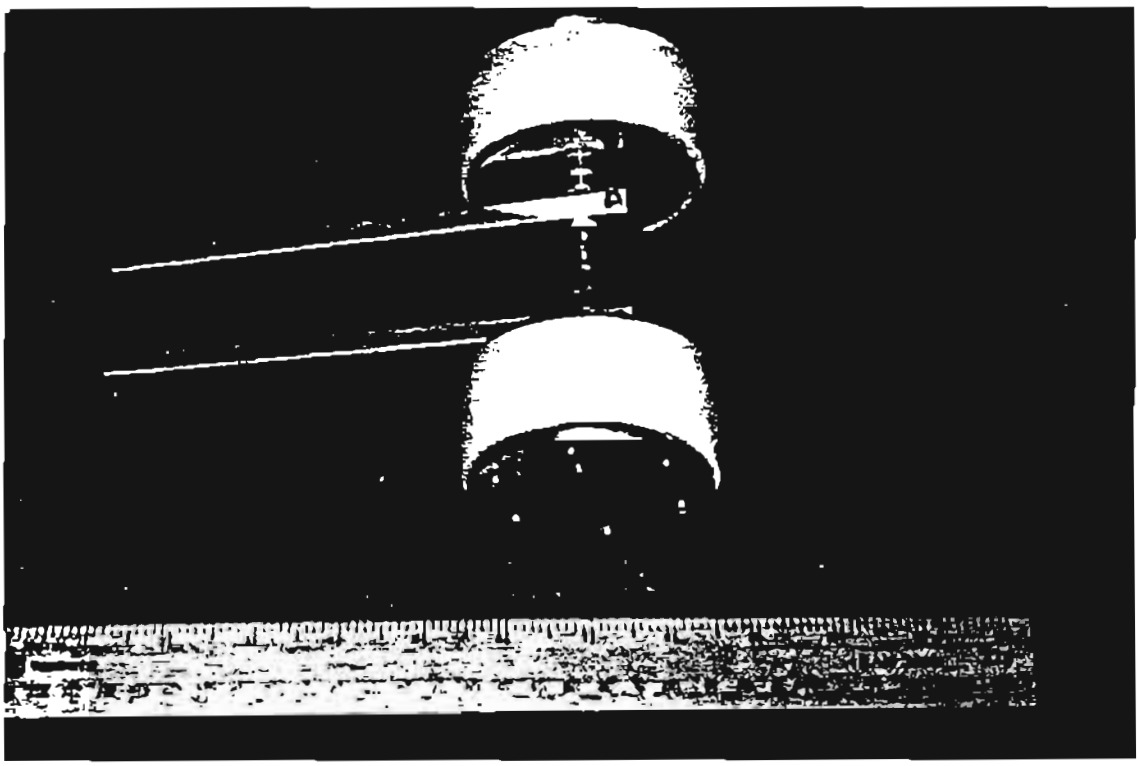

PLATE 6. The 360kHz rolling transducers, used in the current CANDI prototype.

CHAPTER 3: DISCUSSION

3.1 THE IMPORTANCE OF SPECTRAL ANALYSIS

From the very beginning of the project it was realised that methods of conventional analysis associated with ultrasonic inspection of materials were less than suitable for providing information relating to the corrosion of steel reinforcing cables embedded in concrete. These methods are almost exclusively concerned with time domain analysis, and in most of these cases, they are concerned only with measuring the time-of-flight of a signal, or the duration of the pulse-echo journey.

This opinion was held because the earliest experiments showed that pulse-echo systems were adversely affected, and in a very profound sense, by the presence of coherent signal noise in the echo data. Even if pulse-echo analysis was ultimately to be implemented in the final prototype system (and this possibility was not ruled out before considerable tests and theoretical modelling had been conducted), the amount of signal processing that would have been required to extract the valid echoes from the echoes produced by aggregate back-scatter implied that simple scalar measurements in the time domain alone would never achieve the required objective.

Before even the theoretical foundations were laid, it was intuitively felt that the key to the problem was in spectral analysis. This now seems so obvious to those involved in the project that it is taken for granted, but it is worth mentioning that virtually no commercial ultrasonic test instruments use this technique. Throughout the project, which has seen the evaluation of numerous hardware and software systems, the analysis of signals in the Fourier domain has always remained central to the methodology. It is therefore particularly gratifying to be able to state that the current prototype system, which has been successfully demonstrated to identify a range of defective conditions, employs frequency domain filtering as its fundamental operating parameter.

As in many such research projects, initial progress proceeded at an encouraging pace; it is not difficult to establish where the current limitations to a technology lie, given suitable apparatus and analysis procedures. Thus the first few months were spent formally defining the problem, and discovering that which could and could not be done.

Frequency analysis was first used in tests on cylindrical concrete samples, when attention was directed at quantifying the high frequency losses sustained by a broad band pulse as it passed through different distances in the medium. At this stage the agreement between experiment and theory was a close one, and it was possible to derive equations which provided reliable statistics relating to the amount of attenuation expected over a given distance for a specific frequency.

As the concrete cylinder experiments also showed, spectral composition changed with the proximity of buried metal components; furthermore, signals received from transducers directly coupled to embedded cables proved to be exceptionally sensitive to even small amounts of corrosion. Thus it was concluded even after the first few months that the analysis of the relative strengths of different frequency bands must play a central role in any experimental system. Emphasis was placed on comparing the relative magnitudes of high and low frequencies, rather than absolute magnitudes, as is performed now, due to variations in mean signal strength arising from coupling

inconsistencies. This problem was overcome by the introduction of the rolling transducers.

3.2 ATTEMPTS TO IMPROVE THE HIGH FREQUENCY : LOW FREQUENCY RATIO

Because of selective removal of the high frequency components, and because it was these very components that appeared to contain most of the required information, it seemed clear that the method that was most likely to produce the best results was the one that enhanced the high frequency content. High frequency enhancement was not desirable for this reason alone, but also because it was usually drowned in large amplitude, low frequency coherent noise that was initially thought to have no useful part to play in the analysis. This latter assumption proved to be not entirely accurate, and the present system, depending on the nature of the defect that it is attempting to identify, will use the energy of the low frequency harmonics, ratioed against the high frequencies, in order to correct for the background variability arising from aggregate back-scatter and the residual variability in transducer coupling.

The first attempts to improve this ratio involved pre-wave optimisation; this method worked well for geometries where the steel cable ran close to the surface of the structure, since the increased propagation velocity ensured that it was possible to discriminate between plain and reinforced concrete. It also meant that over limited distances (not more than 1 m), high frequency content was preserved in pitch-catch systems, as shown by the experiments performed on the bridge beam.

Nevertheless, pre-wave optimisation suffered certain critical disadvantages; it was not possible, by analysing the high frequency content of the pre-wave alone, to establish the presence of other defective conditions within the pitch-catch zone. Moreover a minimum transducer spacing of 1 m was required to enable the speed differential between plain and reinforced concrete to be reliably detected. This limited the accuracy of the spatial resolution and made very high frequency analysis impossible (the term very high frequency - i.e. above 300 kHz - is used here in the context of ultrasonic inspection of concrete). By contrast the CANDI prototype employs closely spaced transducers enabling the detection of these very high frequencies and providing good spatial resolution.

The second method adopted in an effort to retain the high frequencies, concentrated on propagating a defined beam into the concrete and thence the steel, thereby minimising the signal losses attributable to divergence. It was quickly discovered however that the diameter of the transducers required to give any significant advantage were prohibitively large, and even a beam that had a small divergence angle to start with would rapidly loose energy laterally due to scatter.

Closely associated with this approach were investigations into the feasibility of using pulse-echo systems. Pulse echo systems can operate well even in highly absorptive media, given suitable echo enhancement techniques such as signal averaging, cross-correlation or pseudo-random code generation. However it is important to distinguish between signal attenuation through absorption, and signal attenuation through scatter. Rayleigh scattering results in a general weakening of the signal through thermal conversion. However phase and diffusion scattering, whilst being proportional to the second and first power of the frequency respectively (Rayleigh scattering is proportional to the fourth power of the frequency), gives rise

to coherent noise at the receiving stage. This is because each scattering interface produces an echo which is as equally valid, as far as the discrimination circuitry is concerned, as the echo returned from the internal defect, itself the subject of investigation.

Coherent signal noise cannot be eliminated by the signal processing methods mentioned above; it can only be reduced by spatial averaging. Appendix B includes a discussion on the possibility of applying spatial averaging to this problem but concludes that the number of averages that are required to give useful signal-to-noise ratios would be impracticable as far as a field system is concerned.

After discovering the limitations of the pre-wave optimisation system of signal processing, and the rejection of the pulse-echo approach, some considerable effort was expended in simulation tests, theoretical work and propagation modelling, in order to maximise the information recovery process from a system that was bound always to be limited by the hardware. The water experiments strongly suggested that most of this information resided in the frequencies extending beyond 120 kHz, but with the experimental configurations used on concrete before 1990, even these moderate bandwidths could not always be reliably extracted.

The design philosophy that followed the simulation tests in water and that dictated the design of the CANDI system can be summarised in the following statement: given the highly unfavourable nature of concrete regarding the transmission of ultrasonic signals, it is pointless to attempt to generate focused or controlled beam patterns into the medium; regardless of what is attempted, the beam will be scattered; frequency optimisation must be effected through the application of software-based signal processing methods to the raw data.

By using transducers with a high natural resonant frequency spaced closely together, the current system can identify frequencies extending to 400 kHz without difficulty. This, as stated, is achieved by block-filtering the signal in the Fourier domain and inverse transforming to the time domain. Caution must nevertheless be exercised in the filtering procedure. If too little low frequency rejection is performed (i.e. low frequencies are included in the energy estimates), the trend data can become random in nature. If too high a frequency band is selected (say, in the current system, between 450 kHz and 500 kHz), the data will again have a strong random component. This is because there is virtually no energy radiated by the probes in this range and most of what will be detected is simply random thermal noise. Similarly, probes that are spaced too far apart will transmit and receive signals with high frequencies so attenuated that they are of similar magnitude to random thermal electronic noise in that range. Once again, the trend data will be incoherent.

3.3 SYSTEM SENSITIVITY

3.3.1. General

The success of this method of signal processing has been significant; the system can now detect, and with suitable signal processing can discriminate among, the following conditions:

a. Major breaks in cables, at least 15 mm in diameter involving end separation of a minimum distance of 60 mm, to a depth of 70 mm (High frequency : Low frequency band ratio measurements).

b. Voids in concrete, with a minimum diameter of 30 mm at a depth of 100 mm. Detection of smaller voids is possible at reduced depths; subsurface delamination (cross-multiplication of all energy bands).

c. Voids in steel ducts, with a minimum diameter of 40 mm at a duct depth of 70 mm (method (a) or (b) depending upon diameter).

d. Damaged or cracked concrete (generalised attenuation of all frequency bands).

e. Chloride contaminated concrete: secondary or primary effects of corrosion (see below).

One of the more unusual features of the system, which at present is only partially understood, is its sensitivity to regions in which the cable has been corroded, either by being wrapped in a paper towel saturated in salt solution prior to casting, or by passing a current through the cable via a local cathode consisting of a wire, coiled around a paper towel, saturated in salt solution and wrapped around the concrete. It cannot be stated with certainty that the system is detecting the corrosive condition directly or whether it is responding to chloride contamination of the concrete. However, attempts have been made to minimise the effects produced by localised water seepage by total immersion of the sample in water for 24 hours in order to equalise the internal moisture content of the sample.

The inconclusive results obtained from the force-corroded epoxy-coated bar tests also suggest that the system is indeed responding to changes at the concrete/steel interface and not to changes in the concrete itself. If the latter were true, then the scan data provided in these experiments would reasonably be expected to follow the pattern of the other force-corrosion tests in the region where the paper towel had been placed. This was not the case, but further work would be required to establish this beyond question.

With the provision of a track-based scanning bogie the system has the capability to be used in the field. This does not imply however, that no further improvements could be made to the hardware or software. In particular, band-switchable filter units could be included before the signals reached the amplifier. This would not eliminate the requirement for Fourier domain filtering (due to its ideal characteristics), but would improve the signal-to-noise ratio with respect to digital quantisation noise (see Appendix B). The waveform analyser could also be replaced by a dedicated FFT system which would improve the speed and significantly reduce the cost of the system.

It remains to be seen how far the filtering technique can be extended to recover the very high frequency bands. At present the limit is 400 kHz, but this is only because the transducers that are used have a resonance of 360 kHz. It is possible that useful energies could also be recovered from higher frequency probes, providing yet more detail with respect to small defects and improving the overall reliability of the analysis.

3.3.2 Improving the Processing Efficiency of the System

The attentive reader will have observed that it is not only the hardware that could be modified in the interests of speed and efficiency; at present the signal processing involves transforming the data to the frequency domain, filtering and re-transforming to the time domain to make energy calculations

on the time records. This is in fact superfluous, since it is of course entirely possible to make energy calculations in the frequency domain, without resorting to the added overhead of re-transforming to the time domain. The reason this is done is because although the energy component is the most significant of the scalar measurements, other scalar measurements were made which did require re-transformation to the time domain, such as the time at which the signal peak occurred, and the duty cycle of the record, to name but two.

All the indications are at present that a system based only on calculating the products and ratios of energies at different frequencies would provide an acceptable level of performance. Since, therefore, the necessary calculations could be restricted to the frequency domain, a speed improvement of approximately 1.6 could be effected without any modification to the current hardware configuration.

3.4 IMPLICATIONS OF THE FINDINGS

At the present time, the only established non destructive testing method capable of detecting voids or broken cables inside ducts in post-tensioned concrete construction is radiography. This technique is restricted in the total thickness which can be penetrated, and is extremely slow and tedious if carried out by conventional gamma radiography. The development of the Scorpion system in France has required very substantial capital expenditure on a single inspection unit, in which radioactive source and detector unit have to be traversed together, along the length of a bridge beam, with closure of the bridge required for safety reasons.

Whilst the present project has not reached the stage of a field prototype or commercial system, it has shown the potential for such systems to provide a means for much more economic inspection of pre-stressed concrete structures than can be achieved by radiography.

Further development of the system developed in this project could lead to track mounted bogie systems which could crawl along the length of bridge beams, with data recorded into a computer system on site, initial appraisal during scanning and final assessment after processing data at a later stage. Provision of access for installation of tracking systems would be required, but this could be carried out by available conventional equipment not requiring a dedicated machine such as the Scorpion radiographic equipment.

Although further development work is clearly essential, it is likely that scanning speeds of the order of 1 m per minute can be readily achieved, although clearly the time required to inspect a complete bridge will depend upon the size of the bridge. The weight of the equipment to be carried on the scanning assembly can be made relatively light and it would normally be possible to carry out scanning from one surface only, depending upon the geometry. One can readily see a situation in which each State Highway organization has a number of such pieces of equipment in regular and continuous use on a monitoring programme of principal inspections of bridges every five to ten years. Thus successful further development of the techniques and equipment from the present project could provide inspection capability where none was present before, with a significant contribution to safety in detecting any major deterioration in embedded pre-stressing components in concrete in time to allow remedial action to be carried out.

CHAPTER 4: CONCLUSIONS AND SUGGESTED RESEARCH

4.1 CONCLUSIONS

a. This programme of research has presented an exceedingly difficult challenge. It was recognised at an early stage that success required ultrasonic signals to be identified at much higher frequencies than used for conventional testing of concrete. Many methods were tried for this and promising successful techniques were developed at the end of the project.

b. The literature survey has shown complete general acceptance of the importance of identification of major deterioration of pre-stressing components in concrete structures to enable structural integrity to be maintained. The 'State of the Art' literature survey has shown that progress in realising this requirement has been slow and difficult, due to the involved technical problems. No existing techniques are capable of providing a simple, mobile, user friendly inspection system.

c. Whilst ultrasonic signals can be propagated along long lengths of steel rods or cables in air, once the steel is embedded in concrete, the signals become severely attenuated and it is not possible to propagate the signal for more than about one to two metres.

d. The propagation of ultrasonic signals in concrete is subject to scatter and attenuation dependent upon the relative size of aggregate to the wave length. For stochastic scattering (where the aggregate diameter is approximately the same as the wave length), signal loss is proportional to the square of the frequency, whilst for Rayleigh scattering (where the aggregate diameter is much less than the wavelength) signal loss is proportional to the fourth power of frequency. Thus high frequency signals are much more severely attenuated than low frequency signals.

e. To detect the presence of embedded steel rods/cables, for information about the condition of such steel, the wavelength of the ultrasound must be of the same order as the embedded components dimension of interest. This therefore requires information from high frequency components which have the shorter wavelength.

f. During the execution of this project, great emphasis has been placed on theoretical analysis and signal processing to be able to identify the signal content relevant to embedded components and their condition. Whilst the experimental results consistently showed differences in the first part of the ultrasonic signal received, known as the pre-wave signal, when embedded steel was present, analysis of the overall signal content in either the time domain or the frequency domain did not prove sufficiently informative.

g. Extensive experimental trials have been carried out using probes of different frequencies in the range 50-500 MHz, on single wires/rods and on 7 wire strands, with different defective conditions present, immersed in a water tank, or embedded in mortar or concrete blocks.

A prestressed concrete beam was constructed to include examples of voids, corrosion and broken wires. Concrete samples with ducts containing simulated broken wires and voids were also constructed and tested. Because of the inherent scatter and attenuation problems with ultrasonic signals in concrete, conventional ultrasonic testing methods were not successful in giving readily interpretable results about the condition of embedded components in concrete.

h. To attempt to eliminate the scatter and attenuation, an initial prototype system was constructed in which a central transmitting probe was surrounded by a quartet of receiving transducers in order that the signals received by corresponding pairs of transducers could be compared to show the difference between sound and damaged components. With conventional ultrasonic time domain analysis this prototype was not successful because signal content of interest was buried within the lower frequency higher power constituents which suffered less attenuation.

i. The next stage was to try to use discrete frequencies by transducer design. Attempts to construct transducers which restricted the ringing time to very short periods and to give a prescribed frequency response were not successful in improving the signal content. It was concluded that the high frequency signal containing the information about the condition of embedded components was becoming attenuated so much that it was always swamped by lower frequency components, and that the solution rested with signal processing techniques.

j. It was then decided to use signal processing/filtering techniques to separate out different frequency bands from signals of broad band transducers, and this technique has been very successful. An advanced signal processing technique has been developed in which the signal received at a transducer is transformed to the frequency domain to give the complete frequency spectrum. Block filtering techniques are then applied to the frequency spectrum to select the signal content lying within narrow frequency bands of say 50kHz. The signal from these restricted bands is then inversely transformed back to the time domain enabling the high frequency content material to be examined.

k. This advanced signal processing technique has been combined with the use of rolling transducers in a second prototype system for scanning concrete beams containing embedded steel components. It was initially demonstrated that the system is capable of detecting voids and defective regions in small samples. Subsequent work has shown that the present system is capable of identifying voids of the order of 30 mm diameter at depths of the order of 100 mm from the surface, and major breaks in cables involving a total separation of not less than 30 mm at a depth of approximately 70 mm. The system is also sensitive to regions affected significantly by chloride contamination over similar depths. At its present stage, the system has not been able to detect single breaks in a multi-wire strand, but this is not surprising considering the wire diameter, relative to wave lengths. Tests on fusion bonded epoxy coated steel bars have been carried out, but the system has not proved capable of detecting minor corrosion in these cases.

1. Whilst it is considered that the principal objectives of the research project have been achieved, with the development of techniques capable of locating major faults in embedded pre-stressing components, the development work has not reached the stage of a robust field prototype system or commercial version. A major breakthrough has been achieved in opening the way for ultrasonic testing systems of concrete structures to reveal the condition of embedded components.

4.2 FURTHER WORK

Further work is necessary to take the present prototype through the robust field prototype stage to commercial applications. Some optimization work is necessary on the number of transducers, their frequency and their relative positions. These studies should investigate interpretation of signals from different frequency bands, using the digital block filtering technique, and the possibility of obtaining higher resolution from higher frequency probes should be investigated. It is likely that the scanning system will include multiple receiving transducers in order to enable tracking and comparison of signals from adjacent regions to be carried out so that the central transmitting transducer with four receiving transducers should be adopted.

The potential capability of the present prototype system can be increased significantly by optimization of transducer power, frequency and signal processing. To detect voids or cable breaks of smaller dimensions than shown by the present work, it will be necessary to use higher frequency transducers of greater power. For example, 1 MHz frequency ultrasound in concrete has a wave length of about 4 mm, which would enable voids and breaks of this order of size to be detected. The scatter and attenuation of the signal at this frequency would be much greater, so to maintain the same range capability either the input transducer power or signal amplification would have to be increased. The potential limits of size of discontinuity and depth can be determined from the analysis for attenuation in the Appendices now that the fundamental principles are understood. A move to higher frequencies would have knock on effects on the signal processing equipment, but this does not preclude significant improvement to the stage reached at the end of the present project.

For a field scanning unit, the development work should investigate dedicated signal analyser and computer systems and the extent to which data should be processed in real time, and the extent to which post processing could be carried out at a later date. The cost of such a system should be explored, although it has to be recognised that commercial costs will depend upon the number of items of such equipment to be manufactured and the extent to which real time analysis of results is required.

APPENDIX A: BIBLIOGRAPHY

1. Alexander M. "Development of Procedures for Non-destructive Testing of Concrete Structures. Report & Feasibility of Impact Technique for Making Resonant Frequency Measurements". United States Army Office, Chief of Enquiries Washington D.C. 1981.

2. Ammann, W. "Reinforced and Prestressed Concrete Structures Under Shock Loading". Institut Fuer Baustatik und Konstruktion ETH Zurich, 1983.

3. Bastable, P.W. et al. "Concrete Quality and the Corrosion of Reinforcement". Report by New Zealand Department of Scientific and Industrial Research, October 1985.

4. Beal, D.B. Strength of Concrete T. Beam Bridges. American Concrete Institute, Detroit 1985.

5. Berthelot, J.M. et al. "Damage Process Characterisation in Concrete by Acoustic Emission". 2nd International Conference on Acoustic Emission, Lake Tahoe, U.S.A., November 1989.

6. Bocca, P. "Development and Present State of Non-destructive Test Methods". La Prefabbricazione (Milan) 1986, Vol. 22, No. 3.

7. Bomar, L.C. et al. "Determining Deteriorated Areas in Portland Cement Concrete Pavements Using Radar and Video Imaging". National Highway Coop. Research Programme Report No. 304, December 1989.

8. Brackett, R.L. "Underwater Inspection of Waterpoint Facilities". The Military Engineer Vol. 78, August 1986.

9. Brant, A.W. "Ultrasonic Testing of Fresh Mixes". Concrete (London 1986), Vol 11, No. 12.

10. Bungey, J.H., Malhotra, J.H. "The Influence of Reinforcement on Ultrasonic Pulse Velocity Testing". American Concrete Institute Journal, 1987.

11. Carino, N.J., et al. A Point Source-Point Receiver Pulse Echo Techniques for Flaw Detection in Concrete. ACI Journal, April 1986.

12. Cianfrone, F., Facaoaru, I. "Non-destructive Ultrasonic Impulse to Detect Failures and Deterioration Layers in Concrete Bridge Slabs". L'Industria Italiana del Cemento (1978), Vol. 48, Nos. 7 and 8.

13. Clemena, C.G., Sprinkel, M.M. and Long, R.R. "Uses of Grond Penetrating Radar for Detecting Voids Underneath a Jointed Concrete Pavement - Final Report". Viginia Highway and Transportation Research Council, Charlottesvile, Virginia, HPR-2156, May 1986.

14. Clemena, G.A. and Steele, R.R. "Measurement of Thicknass of In-place Concrete with Microwave Reflection". Virginia Transportation Research Council, April 1988.

15. Cohen, E., et al. Inspection Analysis and Restoration of Concrete in Masonry Structures. American Concrete Institute 1985.

16. Crowe, C.R. and Hasson, D.F. "Materials Trends in Marine Construction". Division of Engineering and Weapons, Naval Academy Annapolis, EW-1-90, January 1990.

17. Dahinter, K. "Inspection and Strength Evaluation of Concrete Highway Bridges in Czechoslovia". 1st International Conference on Bridge Management. University of Surrey, March 1990.

18. Demars, P. et al. "Description of Investigation Methods and Applicable Cases in the Public Sector of the Belgian Ministry of the Interior". International Conference on Long Term Observation of Concrete Structures, Budapest, September 1986.

19. Endmann, D. Condition of Grouting and Conservation of Tendons. Forschungskolloquim des Deutschen Ausschusses fuer Stahlbeton, March 1986.

20. Fedosenko, R. Ya. Operating Life and Strategy of Replacement of Supports for Transmission Lines. Elektr Stantsii (USSR) No.5 1985.

21. Francoise, D. "Fracture and Damage Mechanics of Concrete". Conference on the Application of Fracture Mechanics to Cementitious Composites. Sponsor NATO Services Committee, September 1984.

22. Garey, A. "Ultrasonic Investigation Methods Regarding Deterioration of Concrete Structures Damaged by Fire". Informes de la Construcioes, (1986), Vol. 29, No. 286.

23. Gouda (Netherlands). Acoustic Inspection and Monitoring of Prestressing Tendons and Bars in Concrete Structures. Gouda in house Publication, 1986.

24. Gylloff, K., Kopp, L. Vibration Measurements on Prestressed Concrete Bridges: A Study with Non Destructive Test Methods. Statens Provningsaustalt Boras (Sweden) 1986.

25. Hindess, S., Vondran, G. Properties of Concrete Reinforced with Fibrillated Polypropylene Fibres under Impact Loading. Chemical Concrete Research, Vol. 18 No. 1, January 1988.

26. Holt, F.B. Non Destructive Evaluation of Pavements. Concrete International Journal Vol. 9 No. 6 June 1987.

27. Horikoshi, J., et al. 1.2 GHz Band Wave Propagation Measurements in Concrete Building for Indoor Radio Communiations. IEEE Transactions Vehicle Technology, Vol. VT 35 No. 4, November 1986.

28. Janney, T.R.and Kong, K. et al. "Maintenance Repair and Demolition of Concrete Structures". Handbook of Structural Concrete, London (1983).

29. Kasai, Y. and Fuji, T. "Non-destructive Evaluation of Concrete Structure Methods and Applicability of Non-destructive Testing". Mihakai Kausai (J. #2), March 1988, pp 206-221.

30. Kneiss, H.G. "Methods of Investigation of Prestressing Members". Mittellungsablatt der Bundesanstalt fur Warserbau, 1986.

31. Kopf, R.J., Cooper, C.G. and Williams, F. "In-situ Strength Evaluation of Concrete Case Histories and Laboratory Investigations". Concrete International Design and Construction (1981), Vol. 3, No. 3.

32. Kostrancic, Z. Mathematical Evaluation of the Quality of Repairs on Concrete Specimens. Cement Concrete Aggregates Journal, Vol, 7 No. 2, Winter 1985.

33. Krauthammer, T. "Approximate Analysis of Shallow-buried Reinforced Concrete Arches Subjected to Simulated Nuclear Loads". Proceedings of the 1989 ASME International Computer in Engineering Conference, August 1989.

34. Krishon, F.J. Delamination and Remedial Repair or GFRC Cladding Panals. Texas Civil Engineering Vol. 57 No.4, April 1987.

35. Laloux, R. et al. "Acoustic Emission Techniques Applied to Civil Engineering Structures". Bulletin de Liaison des Laboratoires des Pont et Chaussees. No. 39, October 1985.

36. Lange De, et al. "Underwater Inspection of Concrete Structures". International Conference on Behaviour of Offshore Structures Delft The Netherlands, July 1985.

37. Levrero, S. and Tattoni, S. "Statistical Analysis of the Results Obtained Through Non-destructive Tests on a Reinforced Concrete Structure". L'Industria Italiana de Cemento, 1984, Vol 54, No. 11.

37(a) Lemoine L., Raharivairo, A. and Tacke, G. "Corrosion of Reinforced Concrete In Marine Environments - Methods of Inspection 8th Eur. Confr. of Corrosion, Vol 1, November 1986.

38. Lin, M.K. and Koo, T.K. "Acoustic Emission From Reinforced Concrete Beams". Nanyeng Technological Institute Singapore, Magazul Concrete Research, 41(149), 1989.

39. Lin, C.H. "Residual Strength of Reinforced Concrete Columns Exposed to Fire". National Taiwan Institute of Technology, Taipai, Taiwan. Zhougguo Gongchen Xuckau, Vol. 12, No. 5, September 1989.

40. Luo, Q. "Ultrasonic Inspection for Internal Defects of Concrete Structures with Densely Packed Parallel Steel Reinforcing Bars for Internal Defects." Nanjing Hydraulic Research Institute China Wulsun Jiance, Vol. 9, No. 2, February 1987.

41. Malhotra, V.M. "In-situ Non-destructive Testing of Concrete". American Concrete Institute Special Publication 82, out 1984.

42. Manning, D.G. "Detecting Defects and Deterioration in Highway Structures". National Research Council Transportation Research Board Publication, 1985.

43. Manning, D.G. and Mashiwi, T. "Inspection and Repair of Some Highway Bridges in Italy". 1st International Conference on Bridge Management, University of Surrey, March 1990.

44. Malhotra, M.V. "In-situ Non-destructive Testing of Concrete". American Concrete Institute Special Publication 82, 1984.

45. Makovsky, M. "Environmental Damage Caused by Lifts". Epuletgepeszeti Technika. Vol. 24, No. 4, October 1986.

46. Mani, K. "Determining the Effect of Damage Due to Fire in Concrete Structures by Ultrasound Pulse Velocity Measurements". Indian Concrete Journal, Vol. 60, No. 7, July 1986.

47. Mashani, H.N. et al. Evaluation of Fatigue Damage on the Mechanical Properties of Fibre Reinforced Concrete. Pastes Cement and Concrete Research V.15 No. 5, 1987.

48. Matti, M.A. Frozen Concrete, Concrete International Design and Construction, vol8, #4, 1986.

49. Melzer, R., The Experimental Determination of Model Dynamic Parameters. Wissenschaftliche Zeitschrift der Technischen Universitat Dresden 1988, Vol 37 No.1.

50. Mishima, T., Mitani, T., Yamamoto, T., Manufacture of Carbon Fibres with Plastics or Concrete. Japan Kokai, October 1987.

51. Nishima, T., et al. Manufacture of Composites of Carbon Fibres with Plastics or Concrete. Nippon Oil Co. Ltd. March 1986.

52. Mlaker, P.F. and Walker, R.E., et al. "Accoustic Emission Behaviour of Concrete". American Concrete Institute Special Publication 82, 1984.

53. Mueller, K.F. "Economic Use of Non-destructive Testing Demonstrated on a Reinforced Concrete Bridge Built 50 years Ago". Materialproofing Vol. 22, No. 7, (1980).

54. Muenow, R.R. "Field Proven NDT Methods for Evaluating Damage and Repair of Nuclear Facilities". Nuclear Plant Journal, Vol. 6, No. 6, December 1988.

55. Mills, R.M. "Gas and Water Permeability of Concrete for Reactor Buildings - Small Specimens". Atomic Energy Control Board Ottawa Information - 0188.

56. Mills, R.M. "Gas and Water Permeability of Concrete for Reactor Buildings - Prototype Scale Specimens". Atomic Energy Central Board Ottawa Information - 0188-2, February 1987.

57. Naus, D.J. Grouted and Non Grouted Tendons for Prestressed Concrete Pressure vessels. Oak Ridge National Laboratory Report CONF 790802-46.

58. Natke, G. & Deigent, A. "Vibration Investigation of Tunnels & Impact on the Surroundings". Univeristy of Hanover, Curt-Risch-Institute fuer Dynamik Haunover, March 1988.

59. Natke, H.G. Transient Excitations of Mechanical Vibrations in Testing Techniques. Tech. Mess. T.M. Vol. 52 No. 11, 1985.

60. Nanjokaitis, A. "Investigation of the Strength Development of Concrete During Heat Treatment - The Ultrasound Method". Baustoffindustrie Ausgabe B. Baudemente, 1976, Vol 19, No. 3.

61. Niehues, F. Radiographic Inspection of Prestressed Concrete up to 1600 mm Wall Thickness Using a 9 Mev Linear Accelerator. International Committee of Non-Destructive Testing, Columbus 1985.

62. Nymand, KK "Inspection of Prestressing Cables in Concrete Bridges". Nordsk Beton Sweden 1986

63. Naubail, M. "Methods of Diagnosis of Building Technical Fittings. Localisation of Defects in Heating Cables Embedded in Concrete". CSTC Review No. 2, June 1986.

64. Ohuma, H. "Reinforced Concrete Beam Response to Impact by Moderate Speed Gun". University of Tokyo Press, Japan, Vol. 33, 1985.

65. Onnuma, H. Impact Benaviour of Reinforced Concrete Slabs. Trans-actions of Japan Concrete Institute, Vol. 6, 1985.

66. Ohtsu, M. "Acoustic Emission Characterstics in Concrete Diagnostic Applications". Journal of Acoustic Emission, Vol. 6, No. 2, 1987.

67. Orante, K., Punakallio, E. Verification of Strength Properties of Concrete Structures by Non Destructive Methods. Espoo (Finland) in house publication, 1986.

68. Parkiss, J.A. "Steel Reinforced Concrete at Elevated Temperatures". International Journal Cem-Compos Lightweight Concrete, Vol. 6, No. 3, 1984.

69. Paul, M.J. Brandywine Shoal Lighthouse. Concrete International Journal vol 9 #6, June 1987.

70. Petrangeli, M.P. "Inspection and Repair of Some Highway Bridges in Italy." 1st International Conference on Bridge Management, University of Surrey, March 1990.

71. Pih, H, Q Bi, P.Ya. Dynamic Stress Concentration Effects on Stress Waves in Composite Models with Different Fibre-end Geometries. Experimental Mechanics, September 1985.

72. Purkiss, J.A. Some Mechanical Properties of Glass Reinforced Concrete at Elevated Temperatures. Elsevier Applied Science Published 1985.

73. Rao, P.D.S. "Some Pitfalls in Ultrasonic Pulse Velocity Method of Testing Hardened Concrete". Indian Concrete Journal, Vol. 58, No. 10, October 1984.

74. Roethig, H. and Burcharat, F. "Measuring Bow UMBO.0 for Ultrasonic Tests According to the TGL Standard". Bauinformation Wessenscheft und Technik (1990), Vol. 33, No. 1.

75. Roman, O. Pile Dynamic Analysis. A Useful Tool for the Engineer, Published by A.A. Balkema, Rotterdam 1985.

76. Rossi, P., Francois, D. Cracking of Concrete, Application of Linear Fracture Mechanics. Mechanical Rupture National Roads and Bridges (Paris) 1986.

77. Royles, R. and Morely, P.D. "Acoustic Emission and Bond Degradation in Reinforced Concrete Due to Elevated Temperatures". Materiaux et Constructions (1984), Vol. 7, No. 99.

78. Sansalone, Mary, Carino. N.J., Detecting Honeycombing, Depth of Surface Breaking Cracks. Ungrouted Ducts An Impact-Echo Method. National Bureau of Standards document 1988.

79. Sansalone, Carino, N.J. Transient Impact Response of Plates Containing Flaws. Journal of Research of the National Bureau of Standards Vol. 92 No. 6 - December 1987.

80. Sansalone, Mary, Carino, N.J. Transient Responses of Thick Circular Plates. Journal of Research of the National Bureau of Standards, December 1987.

81. Sansalone, M., et al. "Impact Echo: A Method for Flaw Detection in Concrete Using Transient Stress Waves". National Bureau of Standards (NEL) Structures, December 1986.

82. Sansalone, M and Carino, N. "Detecting Delaminations in Concrete Slabs With and Without Ovelays Using the Impact Method". American Concrete Institute Journal (1989), Vol.86, No.2.

83. Sauchez, D.R. Stress Wave Measurements on Large Raymond Type Piles. Published by A.A. Balkema, Rotterdam 1985.

84. Siuz, A.S.V., et al. "Prestress and Cracking Problems in Concrete Structural Components of Elevated Rail Transit Guideway Systems". ASCE Engineering Mechanics Division, New York, USA Publication, October 1985.

85. Silber, M. "Concrete Strength in Existing Structures". Concrete Works International (1982), Vol. No. 5.

86. Saiidi, M. and Douglas, B.M. "Effect of Design Seismic Loads on a Highway Bridge". Journal of Structural Engineering (1984), Vol. 110, No. 11.

87. Suaris, W. et al. "Ultrasonic Pulse Attenuation of a Measure of Damage Growth During Cyclic Loading of Concrete". American Concrete Journal, Vol. 84, No. 3, June 1987.

88. Suaris, W. "Detection of Crack Growth in Concrete from Ultrasonic Intensity Measurements". Material Structure, Vol. 20, No. 117, May 1987.

89. Tarasov, A.A. Vibrations of Stiffened Reinforced Shells of Revolution. Soviet Applied Mechanics, Vol. 21 No.5, May 1985.

90. Tasker, C.A. & Smith, R.L. "Ultrasonic Techniques for the Non-destructive Testing of Concrete". Proceedings of 22nd Annual Conference on Non-destructive Testing, September 1988.

91. Violette, E.J., et al. Millimeter-wave Propagation at Street Level in an Urban Environment. IEEE Transactions on Geoscience and Remote Sensing, Vol. 26 No. 3, May 1988.

92. Voiczek, G., Koenijoberg, R. and Dreicheuger, M. "The Determination of Column Concrete Strength". Materials proofing (1983), Vol. 23, Nos. 1 and 2.

93. Verhulst, K. "Acoustic Inspection of Offshore Constructions". Cement (1984), Vol. 36, No. 3.

94. Wegler, H. and Frey, H. "Supervision of the Concrete Quality of Prefabricated Elements of Reinforced Lightweight Concrete Using an Impact Test". Bton und Stahlbetonbau (1983), Vol. 23, Nos. 1 and 2.

95. Williams, M.S. "Dynamic Response of Unloaded Prestressing Tendons Cut During Demolition". American Concrete Institute Journal, Vol. 86, No. 6, December 1989.

96. Weinert, T, Langrock, S. and Guntner, U. "Ultrasonic Testing of Half-Shell Weld Joints in Reinforced Concrete". Zis Mitt pp 835-840, August 1988.

97. Wang, M.S. "Application of Acoustic Emission to the Detection of Rainforcing Steel Corrosion in Concrete". Corrosion (Houston), Vol. 38(1), 1982.

98. Yen, T. "Investigation and Analysis of Concrete Strength and Reinforcement on Old Existing Structures". National Chung-Hsing University, Taiwan. Proceedings of the 1985 Spring Conference on Experimental Mechanics, Las Vegas, Nevada, U.S.A., June 1985.

99. Yamada, K. et al. "Damping Characteristics of Acoustic Emission Propagating Through Concrete". Zairo/Journal of the Society of Material Sciences, Japan, July 1987.

100. Young, J. Francis. Properties of Concrete at Early Ages. American Concrete Institute 1986.

101. Zimmer, U. and Rumpf, W. "Possibilities of Using a Micro Ultrasound Machine in the Building Practice". Handbook of Structural Concrete, London (1983).

102. Zorn, N.F. and Reinhardt, H.W. "Concrete Structures Under High Intensity Tensile Waves". Conference on Structural Impact and Crashworklines, Vol. 2, July 1984.

103. A Finite Element Study of Transient Wave Propagation in Plates. Journal of Research of the National Bureau of Standards. Vol. 92 No. 4, August 1987.

104. Assessment of Concrete Structures Damaged by Fire. Indian Concrete Journal Vol. 61 No. 2, February 1987.

105. Building Symposium - Non-destructive Testing Methods in Civil and Structural Engineering. Bundesanstalt fuer Materialpruefing, B.A.M. Berlin, 1986.

106. Bulletin de Liaison des Laboratoires des Pont et Chaussees. No. 139, 1986.

107. Darmistadt. Concrete Annual Journal on Concrete and Concrete Structures Vol. 2 1987.

108. Finite Element Study of the Interaction of Transient Stress Waves with Planar Flaws. Journal of Research of the National Bureau of Standards V.92 n.4 July - August 1982.

109. "Inspection of Prestressing Cables in Bridges" Indian Concrete Journal vol 61 #2 Feb. 1987.

110. "Causes Evaluation and Repair of Cracks in Concrete Structures". Journal of American Concrete Institute (1984), Vol. 81, No. 3.

111. Laboratory Study of Flaw Detection in Concrete by the Pulse-Echo Method. Proceedings of the International Conference on Non-Destructive Testing of Concrete Ontario, Canada 1985.

112. Measurement of Setting Time and Strength of Concrete by the Impact-Echo Method. Journal of Research of the National Bureau of Standards V.92 n.4 July - August 1987.

113. "Non-destructive Testing Methods in Civil and Structural Engineering". Conference ZfP Bau-Simposium Zirstoeringsfr¨eie Pr¨ufing in Bauwesen, October 1985.

114. Non Destructive Testing of Concrete - Part II. CRI Technology Digest. September 1985.

115. Non Destructive Testing Methods in Civil and Structural Engineering. Bundesanstalt fuer Materialprufung (West Berlin) 1986.

116. "Acoustic Emission to Characterise Concrete Damage from Reinforcement Steel Corrosion". NACE Conference on Corrosion, Houston, 1982, Paper 38(1).

117. Principle of the Impact Echo Method. National Bureau of Standards Information Sheet.

118. Proceedings of the 28th Japan Congress on Materials Research. Japan Society of Materials Science, 1985.

119. Shimizu Construction Co. Ltd., Technical Research Bulletin No. 1, Tokyo Research Institute Annual Report, March 1982.

120. Sound waves used to Detect Flaws in Concrete, National Bureau of Standards, Washington 1987.

121. Underwater Facilities Inspections and Assessments at Naval Weapons Station, Charleston South Carolina. Childs Engineering Conference, Hadfield. Contract N62477-0-C-0102, May 1981.

APPENDIX B: THEORETICAL CONSIDERATIONS

B.1. PROPAGATION THEORY

In general terms, simple harmonic motion (SHM) may be represented by the equation

$$\frac{d^2\theta}{dt^2} + \omega^2\theta = 0 \qquad (B.1)$$

Where θ represents displacement,
t represents time, and
$\omega = 2\pi f$, or radians s^{-1}, with f in hertz.

Equation B1 is a linear second order differential equation with constant coefficients, the solution of which is

$$\theta = \xi \cos \omega t \qquad (B.2)$$

In which ξ represents the amplitude of displacement [1].

In systems possessing a natural resonance and which are excited into oscillation through the momentary application of a force, the resulting oscillations will eventually decay, at a rate which will be determined by the degree of damping inherent in the system. We will consider only light damping, in which case the active face of a transducer crystal will always generate at least ten full cycles before coming to rest, after the input of an excitation voltage spike. By analogy therefore a mass, M, suspended on a spring having a compliance C_m (the displacement per unit force) and mechanical resitance R_m, i.e. the coefficient describing the degree of damping, executes a motion described by the relationship:

$$M\frac{d^2\theta}{dt^2} + R_m\frac{d\theta}{dt} + C_m^{-1}\theta = 0 \qquad (B.3)$$

In order to simplify the algebra, the substitution $C_m M^{-1} = \omega^2$, and $R_m M^{-1} = 2\alpha$, with $\alpha > 0$ is made. The equation of motion in this case now becomes:

$$\frac{d^2\theta}{dt^2} + 2\alpha\frac{d\theta}{dt} + \omega^2\theta = 0 \qquad (B.4)$$

Since for light damping, $(\alpha^2 - \omega^2) < 0$, the roots are complex, with a general solution of:

$$\theta = \xi e^{-\alpha t}(E \cos \beta t + F \sin \beta t) \qquad (B.5)$$

and a particular solution, given the boundary conditions of $d\theta/dt = 0$ when $t = 0$, of

$$\theta = \xi e^{-\alpha t}\cos \omega t \qquad (B.6)$$

In this case, the term $\xi e^{-\alpha t}$ governs the rate at which the oscillation will decay.

As an extension to the equation of SHM, now consider a disturbance θ travelling without change (i.e. without damping) through a medium in which distance is given by x and velocity by c. At time $t = 0$, θ will be a function of x, i.e.

$$\theta = f(x) \tag{B.7}$$

After time t, the disturbance has travelled a distance ct. For a positive travelling wave, the field disturbance is described by the function

$$\theta^{+} = f(x-ct) \tag{B.8}$$

and by

$$\theta^{-} = f(x+ct) \tag{B.9}$$

for a negative travelling wave. Combining these functions and differentiating twice with respect to x whilst keeping t constant, gives:

$$\frac{\partial^2\theta}{\partial x^2} = f_1''(x-ct) + f_2''(x+ct) \tag{B.10}$$

and with respect to t, whilst keeping x constant, gives:

$$\frac{\partial^2\theta}{\partial t^2} = c^2 f_1''(x-ct) + c^2 f_2''(x+ct) \tag{B.11}$$

combining the identities given by equation B.10 and B.11 yields

$$\frac{\partial^2\theta}{\partial t^2} = c^2 \frac{\partial^2\theta}{\partial x^2} \tag{B.12}$$

Equation B.12 is the fundamental equation of wave motion in a single plane, and forms the basis for all the understanding of periodic disturbances travelling through any medium. The general solution of partial differential equations (such as the wave equation) is a subtle one, since there are is a very large number of possible ways of expressing them. The most commonly used solution is given by

$$\theta = \xi\cos(x - ct) \tag{B.13}$$

and the method by which it is solved appears in most standard texts on mathematics [2] (including two internal reports dealing with this project).

B.2. WAVE MODES

Acoustic waves travel through a medium by propagating a disturbance of particles about a mean position, with a general propagation velocity, c. As equation B.13 shows, the degree of rarefaction or compression of an adjacent

group of particles will be described by a cosine function of time at any given position, or a cosine function of position at any given time. The wavelength, λ, is described as the distance between points of identical amplitude and slope over the function. The relationship of velocity, wavelength and frequency is expressed by the identity:

$$c = f\lambda \qquad (B.14)$$

B.2.1. Infinite Solids

An unbounded medium, also known as a bulk or infinite medium, will sustain two, and only two wave modes. The first of these is the compressional or longitudinal wave, in which the direction of particles displacement occurs parallel to the direction of propagation. It is the most important mode of acoustic energy transferral in all media, and the majority of non-destructive inspection systems which use ultrasound are designed with its transmission and reception in mind. The propagation velocity [3] is given by:

$$c_\ell = \sqrt{\left(\frac{E}{\rho} \cdot \frac{1-\mu}{(1+\mu)(1-2\mu)}\right)} \qquad (B.15)$$

where E is the modulus of elasticity, in kg/ms^2
ρ is the density, in kg/m^3, and
μ is Poisson's ratio.

The longitudinal wave velocity is often used as a measure of the quality of concrete, since the strength shows a strong correlation with its modulus of elasticity, whose root is proportional to c_ℓ. Since it is difficult to make concrete to an accurate standard, c_ℓ for this material may range from typically 3.5 km/s to 4.9 km/s. In any one casting however, the velocity should not change significantly from point to point. If such changes are observed, it suggests that the strength may have been compromised in some manner, either by cracking, fire damage, insufficient compaction or chemical attack.

The second wave mode occurring in infinite media is the shear or transverse wave. In contrast to the compressional wave, in the shear wave the particle displacement takes place in a plane perpendicular to the direction of propagation. Since shear forces can only be exerted in solid media, liquids cannot in general support shear wave propagation, except under exceptional conditions such as short time durations or in liquids of high viscosity. A unique feature of shear waves is that they have no regions of refraction or compression; hence there are no localised fluctuations in density such as those which occur in all other wave modes. The velocity of shear waves is always lower than that of a compressional wave for a given medium, generally around $0.7c_L$, although the exact expression is given by

$$c_s = \sqrt{\left(\frac{E}{\rho} \cdot \frac{1}{2(1+\mu)}\right)} = \sqrt{\left(\frac{G}{\rho}\right)} \qquad (B.16)$$

where G is the shear modulus.

As will be seen in section 1.5, compressional waves incident on an interface between two solid media convert into reflected and refracted

compressional and shear components. This is significant in relation to this project, since we are interested in establishing the mechanisms of interaction at the concrete/steel interface.

B.2.2 Semi-Infinite Solids

In solids which have a boundary or a surface in contact with the air, other more complex modes of propagation may exist. The most important of these is the surface or Rayleigh wave, whose particle displacement is elliptical in nature (comprising both compressional and shear vectors) occurring, as the name suggests, along the surface of the medium and attenuating rapidly with depth. At a depth of one wavelength for instance, the amplitude is 10% that of the amplitude at the surface. Rayleigh wave velocity is given by

$$C_R = \frac{0.87 + 1.12\mu}{1 + \mu} \sqrt{\left(\frac{E}{\rho} \cdot \frac{1}{2(1+\mu)}\right)} \qquad (B.17)$$

Rayleigh waves are naturally strongly influenced by such factors as surface roughness, but an important feature of these waves is that, given an even surface, they suffer considerably less attenuation for a given linear distance than their bulk wave counterpoints, since they travel in only two dimensions.

In this project the inevitable presence of Rayleigh waves has proved both a nuisance and an advantage; most of the analysis is concerned with interpreting the information carried by the compressional waves which have travelled through the interior of the concrete. These signals are always small in amplitude and are buried in the large amplitude components of the surface waves. However, cracked and damaged concrete very rapidly attenuates Rayleigh waves, in additon to reducing their apparent velocity. Under these circumstances, they may provide valuable clues regarding the possible condition of the underlying steel.

In an unbounded plate whose thickness is comparable to the wavelength, plate or Lamb wave propagation may occur. Two types of plate mode exist. The first is the symmetrical plate wave, which travels as a longitudinal wave along the centre line of the plate causing perpendicular rarefaction and compression to occur at each face of the surface. The second type, the asymmetrical plate wave is basically a wave of plate bending, and consists of particle motion whose displacement along the centre line of the plate is transverse, and elliptical along the surface.

Finally, in media which constitute a thin layer lying on a thicker substrate, Love wave propagation is possible. In this case, the direction of displacement of the particles takes place parallel to the surface but perpendicularly to the direction of propagation.

Plate and Love waves represent special cases of propagation, their generation being strongly dependent on a geometry of media not normally encountered in this work. Although they will not be dealt with further, it is perhaps worth considering that in practical circumstances, an ultrasonic system will usually (desirably or otherwise) produce a number of wave modes whose presence makes the analysis of echoes very complicated. Under these conditions, the arrival time of signals plays an important role, since each wave mode has its own characteristic velocity.

B.2.3 Rods, $\lambda > d$

The propagation of acoustic waves in rods is of special significance to this project, since in many cases we deal with single, solid tendons. In the case of multi-wire strands however the analysis requires modification.

In rods whose diameter, d, is less than the wavelength, three types of wave can be generated: Compressional, transverse and torsional. The first type is usually referred to as a rod wave since its velocity is lower than that of compressional waves in bulk media. Its velocity is given by the relationship

$$c_{rod} = \sqrt{\left(\frac{E}{\rho}\right)} \qquad (B.18)$$

If the rod is tensioned, transverse waves may be generated. In transverse waves, the particle displacement takes place in a direction perpendicular to the direction of propagation and the central axis of the rod. These are also known as string vibrations, and the velocity is given by:

$$C = \sqrt{\left(\frac{T}{m}\right)} \qquad (B.19)$$

where T is the tension and
m is the mass per unit length

In torsional waves, displacement occurs in rotational manner about the axis, as the wave travels down the rod. In this case the torsional wave velocity is equal to the shear wave velocity in the bulk medium.

B.2.4 Rods Embedded in a Medium

A wave travelling along a rod embedded in a medium will, in general, suffer attenuation as it radiates energy into the surrounding matter. Loss-free rod wave propagation is only possible in such circumstances if the shear wave velocity of the surrounding medium exceeds that of the rod wave velocity. Similarly, loss-free torsional mode propagation can only occur if its velocity is lower than the medium's shear wave velocity. Since these conditions are never satisfied with steel cables embedded in concrete, severe attenuation results.

B.3. TRANSDUCER RELATIONSHIPS

The devices used in this research to generate the ultrasonic waves are fabricated from piezoelectric synthetic crystals. The piezoelectric effect was first demonstrated by Pierre Curie (Husband of Marie) in 1880. When a slab of this material, with its parallel faces lying normal to the axis of non-symmetry, is subjected to a mechanical stress, equal and opposite changes appear on the parallel surfaces. Similarly, the effect is reversible. When an electric field is applied to these surfaces the slab is mechanically strained, this strain being proportional to the intensity of the applied field.

Crystals cut to produce compressional waves resonate with a fundamental frequency f_0 given by:

$$f_0 = \frac{c}{2t} \qquad (B.20)$$

where c is the velocity of the compressional wave in the crystal
t is the thickness.

Higher frequencies may be generated by making use of the 2nd, 3rd or higher harmonics of the crystal.

The propagatory stress wave field generated by a circular transducer of radius r can be described using Huygen's principle, which states that the energy and phase at any given point is equivalent to the sum of the contributions from an infinite number of point sources distributed over the face of the crystal. This results in a characteristic beam pattern which comprises two distinct regions: the near field, or Fresnel region, and the far field or Fraunhofer region. In the near field, the beam shape is approximately parallel with large localised changes in intensity.

The length of the near field is given by:

$$N_0 = \frac{D^2}{4\lambda} \qquad (B.21)$$

Where D is the transducer diameter (radius r). The pressure variation along the axis [4] is given by (for both regions):

$$P_z = P_0 \sin\left(\frac{\pi}{\lambda}\left[(r^2 + z^2)^{\frac{1}{2}} - z\right]\right) \qquad (B.22)$$

where z is the distance from the transducer, and
P_0 is the pressure at source.

When the far field region is reached, the beam starts to diverge at an angle which is governed by the relationship between the crystal radius and the wavelength, i.e.

$$\theta = \sin^{-1}(0.61\lambda/r) \qquad (B.23)$$

Note that when the term in parentheses is greater than unity, the transducer will radiate omnidirectionally. In addition to the divergence angle, the pressure distribution will depend on the angle subtended to the central axis i.e.

$$P_\theta = \frac{p_0 2J_1\left\{(\pi/\lambda)D\sin\theta\right\}}{(\pi/\lambda)D\sin\theta} \qquad (B.24)$$

where p_0 is the pressure at source and
J_1 is a Bessell function of the first order.

B.4. ACOUSTIC IMPEDANCE, INTENSITY AND PRESSURE

The specific acoustic impedance of a medium, Z, is analogous to electrical impedance and can be defined as the ratio of acoustic pressure to particle velocity. It can be shown, through application of the wave equation, that Z is a product of the density and wave velocity, i.e.

$$Z = \rho c \qquad (B.25)$$

Consider now a spherical wave radiating from a point source of power P. The intensity at a distance z will depend on the spherical area at that point, i.e.

$$I = \frac{P}{4\pi z^2} \qquad (B.26)$$

The energy density, E, i.e. the energy per unit volume is proportional to I and the total amount of energy flowing through a column of unit area in unit time at velocity c is thus

$$I = cE \tag{B.27}$$

However, the energy density is also expressed as

$$E = \tfrac{1}{2}\rho\left(\frac{d\theta}{dt}\right)^2 \tag{B.28}$$

where $d\theta/dt$ represents particle (not wave) velocity. As this quantity is linearly related to pressure, and $I \propto E$, then we find that:

$$I = (2\rho c)^{-1} p^2 \tag{B.29}$$

and

$$I = \tfrac{1}{2}\rho c(2\pi f)^2\zeta^2 \tag{B.30}$$

hence

$$p = \zeta\rho c 2\pi f = (2I\rho c)^{\frac{1}{2}} \tag{B.31}$$

It is vital that the distinction between acoustic pressure and intensity be made; with a divergent beam or spherical wave, the former decreases in proportion to the linear distance from a source, whereas the latter decreases in proportion to the inverse square. Since transducers respond to pressure, not intensity, it is important to make the necessary conversions if intensity variations are being calculated if transducers are used as the monitoring devices.

B.5 Reflection and Refraction at Boundaries: Pressure Transduction

An acoustic wave passing at normal incidence from a medium of acoustic impI.edance Z_1 to a medium of acoustic impedance Z_2 will be partially reflected. The proportion of the signal reflected is given by:

$$p_r = p_0\left(\frac{\rho_1 c_1 - \rho_2 c_2}{\rho_1 c_1 + \rho_2 c_2}\right) \tag{B.32}$$

At angles other than normal incidence, up to the first critical angle, compressional and shear waves will be both reflected and refracted, their respective angles being described by Snell's law thus:

$$\frac{\sin\alpha_0}{c_1} = \frac{\sin\alpha_1}{c_1} = \frac{\sin\beta_1}{s_1} = \frac{\sin\alpha_2}{c_2} = \frac{\sin\beta_2}{s_2} \tag{B.33}$$

In which:

α_0	represents the angle of incidence of the compressional wave
α_1 and α_2	represents the angle of reflection and refraction of the compressional waves

β_1 and β_2	represents the angle of reflection and refraction of the shear waves
c_1 and c_2	represents c_ρ for each medium
s_1 and s_2	represents c_s for each medium

If the pressure of the incident wave is known, then it is also possible to calculate the pressures associated with each of the wave modes. This however is less straightforward and involves solving a set of four simultaneous equations, known as Knott's equations:

$$(A_1 - A_0)\cos\alpha_0 - B_1\sin\beta_1 + A_2\cos\alpha_2 + B_2\sin\beta_2 = 0 \qquad (B.34)$$

$$(A_1 + A_0)\sin\alpha_0 + B_1\cos\beta_1 - A_2\sin\alpha_2 + B_2\cos\beta_2 = 0 \qquad (B.35)$$

$$(A_0 + A_1)\rho_1 c\cos 2\beta_1 - B_1\rho_1 s_1 \sin 2\beta_1 - A_2\rho_2 c_2\cos 2\beta_2 - B_2\rho_2 s_2 \sin 2\beta_2 = 0 \qquad (B.36)$$

$$\rho_1 s_1^2 [c_1^{-1}(A_1 - A_0)\sin 2\alpha_0 + B_1 s_1^{-1}\cos 2\beta]_1 + \rho_2 s_2^2 [A_2 c_2^{-1}\sin 2\alpha_2 - B_2 s_2^{-1}\cos 2\beta_2] = 0 \qquad (B.37)$$

In which A_1, A_2, B_1 and B_2 represent the amplitudes of the reflected and refracted compressional and shear wave components. These relationships hold true up to the first critical angle, at which the refracted compressional wave travels along the boundary between the two media. It is given by:

$$\theta_1 = \sin^{-1}(c_1/c_2) \qquad (B.38)$$

The second critical angle, at which the shear wave travels along the boundary is given by:

$$\theta_2 = \sin^{-1}(c_1/s_2) \qquad (B.39)$$

B.6 ULTRASONIC SIGNAL ATTENUATION

Up to this point we have limited the discussion to a description of events which can essentially be defined through the application of the principles of geometrical optics. We now turn our attention to the subject of signal attenuation. This is a highly complex matter, since it includes divergence, absorption and scatter, the latter two being frequency dependent. Frequency dependency plays an important part in the nature of this research, since the spectral information returned by an orginally broadband signal will be governed by both the internal conditions of the concrete and the quality of the reinforcing steel.

B.6.1 General Loss Considerations

In a loss-free medium, the only mechanism by which an ultrasonic radiator produces a field which weakens with distance is through divergence (equation

B.22) and, if it has a directional component, through displacement from the axis of propagation (equation B.24). In practice, waves are attenuated through both absorption and scatter (in actuality all such attenuation is ultimately thermal in nature) and for a given medium at a given frequency the general function which describes pressure reduction with distance is given by:

$$P_s = P_0 e^{-\alpha x} \qquad (B.40)$$

where α is the coefficient of attenuation, and
x is the distance travelled in the medium.

Combining equations B.22 and B.40, the relationship which describes total signal loss becomes

$$P_t = P_0 e^{-\alpha x} \sin\left(\frac{\pi}{\lambda}(r^2 + z^2)^{\frac{1}{2}} - z\right) \qquad (B.41)$$

Equation B.41 is very useful for predicting the signal losses which will occur in liquids such as water, where the attenuation loss is almost exclusively dependent upon viscosity, or in fine-grain (relative to λ) isotropic homogeneous media, in which Rayleigh scattering predominates (to be discussed). In concrete however, because of the range of particle sizes a number of attenuation mechanisms operate and these are not easily described in a precise relationship.

B6.2 Signal Losses due to Scatter from Granular Inclusion

Signal scattering is a highly complex process, depending upon mean particle diameter in relation to wavelength, the number of particles per unit volume of the medium, and the acoustic properties of these particles which distinguish them from the medium.

When the diameter of the particles is small in comparison to the wavelength, Rayleigh scattering occurs whereby each particle acts as a spherical radiator. In this case, the scattered amplitude is proportional to the fourth power of the frequency, and the coefficient of attenuation becomes:

$$\alpha = 0.4\,(k\bar{D})^4\,\pi\,\bar{D}^2 N \qquad (B.42)$$

where k is the wave number, given by $2\pi/\lambda$,
$\bar{D}$ is the mean particle diameter, and
N is the number of particles per unit volume

However, in the Rayleigh region, where the scattering coefficient is proportional to f^4 the absorption coefficient increases linearly with frequency. Hence the total attenuation coefficient is given by the general relationship:

$$\alpha(f) = a_1 f + a_2 \bar{D}^3 f^4 \qquad (B.43)$$

with a_1 as the absorption coefficient and a_2 as the scattering coefficient.

In the stochastic region, in which $\lambda \approx \bar{D}$, scattering is proportional to the square of the frequency, i.e.

$$\alpha(f) = b f_1 + b \bar{D}_2 f^2 \qquad (B.44)$$

Finally, in the diffusion region where $\lambda \leq \bar{D}$, the scattering coefficient is given by

$$\alpha(f) = d_1 \bar{D}^{-1} \qquad (B.45)$$

Note that in concrete, Rayleigh, stochastic and diffusion scattering all take place since the frequencies used in the interrogation process range from 50 kHz to 400 kHz, i.e. λ ranges from approximately 80 mm down to 10 mm, with the grain size ranging from less than 1 mm up to 25 mm. It is therefore extremely difficult to determine, analytically, the effect that the individual scatters have on any received waveform after it has travelled through the concrete. It is however a simple matter to calculate, from experimental measurements, the pressure attenuation of a given frequency band over distance for a given concrete mix, and thereby establish the echo amplitude from wave reflectors in the interior of the medium.

B.6.3 Phase Losses from Rough Surfaces

Knott's equations (equations B.34 to B.37) describe the pressure amplitude of reflected and refracted wave modes at the boundary between two smooth surfaces. If the surface is rough, the two reflected waves are no longer in phase, this phase difference being given by:

$$\delta\theta = 2kh \cos \theta_1 \qquad (B.46)$$

Where θ_1 represents the angle of incidence and h is the rms of the height variability. The presence of k in this expression implies that the phase difference is directly proportional to frequency. If the phase difference is significant, the specular relection at that frequency is reduced due to interference between the two reflected waves. Effectively therefore, a rough surface acts as a low-pass filter, attenuating high frequency components whilst leaving low-frequency comparisons to be described by Knott's equation.

B.7 MODELLING OF THE SYSTEM

B.7.1 Description of the Model

Consider a signal x(t) received by a transducer positioned on the surface of a concrete beam of infinite length and finite width and height. The signal in this case is produced by a transducer mounted on the same surface which radiates at a finite angle. The signal, x(t), will therefore be a summation of the rays that have arrived at the transducer via their different paths, and this can be formally expressed as:

$$x(t) = \int_{-\infty}^{+\infty} x(\tau)\delta(t-\tau)d\tau \qquad (B.47)$$

In order to model this summation it is necessary to use the discrete angular increments for the ray paths, and equation B.47 is replaced by its discrete-time counterpart thus:

$$x(t) = \sum_{k=-\theta}^{k=+\theta} x(k)\,\delta(t-k) \qquad (B.48)$$

The model operates using the ray-tracing principle, summing the contributions of waves that have passed through the concrete and have been reflected from the sides and the steel reinforcing cables. Since the model has been developed with user-interaction in mind, it has been implemented on both mainframe and microcomputers at UMIST. The user may specify the concrete dimensions, number, condition and diameter of cable reinforcement, and the wave shape and frequency.

The equations used in the computations are those which describe ultrasonic pressure attenuation due to divergence, reflection, scatter and phase-boundary interference, i.e. equations B.21 to B.24, equations B.32 to B.39, and equation B.46. A generalized equation has been calculated to take into account losses due to absorption and scatter based on previous experimental data and is of the form:

$$\alpha = 0.1844f + 0.001f^2 \qquad (B.49)$$

with α in dB m^{-1} and f in kHz

B.7.2 Examples of Model Output

Figure B1 depicts the output produced by the model when a plain concrete beam of infinite length and cross-sectional area given by 150 mm x 150 mm is insonated with four cycles of monotonic ultrasound at 120 kHz, the receiving transducer being positioned on the same surface of the concrete at a distance of 150 mm.

By contrast, Figure B2 shows the output produced when the same configuration is used but with the addition of a single steel bar, of diameter 10 mm, running along its axis. In Figure B3 we see only the output which has been reflected from the bar, ie. the contribution from the surrounding concrete has been masked. Note that the output in Figure B2 cannot be derived by simply adding, arithmetically, the components shown in Figure B2 and Figure B3; the inclusion of a steel bar fundamentally changes the pattern of reflections within the interior of the concrete. Significantly, most of the energy reflected by the bar is confined to the early stages of the time record, a phenomenon which was confirmed experimentally early in the research project. Note also its small amplitude in comparison to the concrete signal, it is of the order of 40 dB weaker in rms pressure amplitude.

Figure B4 shows the signal reflected from the bar when the surface of the steel has been roughened from severe corrosion. At 120 kHz the losses due to phase scattering at the boundary are considerable causing a marked reduction in the signal amplitude. Figure B5 illustrates the case, again when only reflections from the steel are calculated, when the bar is fully cracked.

In a real situation, the pressure differential between the signal received from the concrete and the signal received from the steel is probably very much lower than the model predicts because the model uses a generalised attenuation coefficient, and does not take into account signal back-scatter from the aggregate or the surface travelling Rayleigh wave. It is therefore unlikely that direct evidence of corrosion will be found by simply inspecting the frequency spectrum of a time recorded signal. However, corrosion is often associated with secondary problems, such as voids and spalling, and these influence both the amplitude and frequency contents of signals in a more pronounced manner.

B.8 NOISE REDUCTION TECHNIQUES

B.8.1 General

The term "noise" when used in connection with signal transmission and receiving systems applies to any additional source of energy which in some manner interferes with obscures or degrades the wanted signal. In origin it may be, for instance, electromagnetic or thermal, and it may be random or non-random, coherent or incoherent.

The noise problems associated with the ultrasonic inspection of reinforced concrete arise from both the amplification and measuring system, and the signals scattered by the concrete which obscure the echoes reflected from the steel components, which are the only signals of interest. In the first case, the noise levels produced when high-gain amplifiers are used can virtually drown the wanted signal, but because such noise is random with time, and the echo is temporarily inconvenient, temporal signal averaging can be performed which very dramatically improves the S/N ratio. Since the noise is random, as, the number of averages approaches infinity, so too does the S/N ratio. Expressed in rms terms, this improvement is given as:

$$\frac{SNb}{SNa} = \frac{n}{2} \qquad (B.50)$$

Where SNa is S/N before averaging,
SNb is S/N after averaging, and
n is the number of averages.

Hence, a very weak signal, having an rms S/N of unity, or 0 dB, can be improved to 40 dB by taking 200 averages.

Improvements in the S/N ratio can be even more dramatic if correlation techniques to reduce the random noise. Cross-correlation involves multiplying and integrating the output pulse with the received signal. Any echoes, which will be similar in form to the output, will be enhanced by a factor approaching V^2 (where V is the voltage of the original echo) and random events will be correspondingly suppressed. The improvement in the S/N ratio is given by:

$$\frac{SNb}{SNa} = \alpha BT \qquad (B.51)$$

Where α is the on-off ratio of the pulser,
B is the transmitted bandwidth and
T is the equivalent integration time.

Both signal averaging and auto-correlation have been used to good effect to reduce the rms levels of random noise, and temporal averaging is employed as a matter of routine with regard to low-level signals.

In most cases however, signal degradation does not arise from this source, the single most important source of noise is the back-scatter produced by the aggregate. In quality this is termed coherent noise, since it is temporally invariant and is correlated with the output (interference from the mains is also non-random and temporally invariant given a fixed measuring point since it is cyclical but it is not coherent since it in no way correlates with the

shape of the ouput pulse in this case). As far as the data acquisition is concerned, it is not really noise because the echoes are just as valid so to speak, as echoes reflected from the steel. Because of its temporal invariance signal averaging (with time) will not have any effect and cross-correlation may well make matters worse.

It is however theoretically possible to reduce the effects of signal back-scatter by spatial averaging. Since the distribution of aggregate within the matrix is essentially random, and the position of the steel is constant with respect to the surface, signals taken at different points on the concrete parallel to the steel should, when averaged, provide an improvement in the ratio between the echo from the steel and the echo from the aggregate. This has in fact been attempted in the past, and whilst the random elements could be seen to diminish as the number of samples accumulated (the 5602 digital storage oscilloscope allows the user to view changes as they occur), the gross form of the signal did not and no echoes arising from the steel were identified with certainty. Three possible (and not mutually exclusive) reasons have been advanced for this:

a. Transducer ringing
b. Concrete resonance
c. Insufficient number of averages.

The problem of transducer ringing can be circumvented, if not eliminated, by placing the transducers far enough apart to ensure that the echo reaches the receiver after the oscillations have decayed to a level below that of the echo. Unfortunately, this also has due effect of reducing the strength of the echo because of divergence and attenuation losses, but an optimum position might nevertheless be found.

It is difficult in practice to determine the contribution that concrete resonance makes in lengthening the duration of the signal, and hence masking the echo. It has been observed that in air, the transducer will loose energy with each cycle, and the logarithmic decrement coefficient, δ_0 is given as

$$\exp(\delta_0) = \frac{x(t-1)}{x(t)} \qquad \text{(B.52)}$$

Where $x(t-1)$ is the amplitude at time t-1 and
$x(t)$ is the amplitude at time t.

When coupled to concrete, the decay coefficent δ_c is greater than δ_0, i.e. the decay is quicker because of the damping applied to the transmitting face of the transducer. However, for another transducer acting as a receiver, $\delta_0 > \delta_c$, effectively, because of the dispersion effect of the medium. Now if δ_c tends towards δ_0 as n, (the number of spatial averages) tends to infinity, it can be deduced that back-scatter, and not resonance, is the major contributory factor to the reduction in damping.

Experiments have revealed that the pulse length received does indeed shorten with spatial averaging, but in these tests $n=32$ which was not enough to reveal the presence of a coherent echo; neither did these tests indicate whether the duration of the pulse would continue to shorten with further averaging, and hence indicate that the contribution from resonance (including side wall reflection) could be ignored. Clearly this is an area where more investigation is required.

B.8.2 Echo Amplitude Optimisation

Recent experiments, not formally documented here, show that the echo amplitude detected from the base of a sample 150 mm^2 in section was 20 dB weaker than the signal which had reached the receiver by other routes and 36.5 dB weaker than the output, which is about 1 V, rms. This experiment was conducted by placing the transducers on either side of a cut 140 mm in length, i.e. leaving only 10 mm joined at the base. Any signal reaching the receiver could only travel there by returning from the base. The attenuation predicted by the theoretical model under these circumstances was -90 dB. The real figure was surprisingly high, that is, it was thought the attenuation would be much greater. Using a second model it was possible to estimate the number of spatial readings required to provide a useful signal-to-noise ratio with respect to the steel cable. The input parameters were as follows:

Velocity:	3900 m/s
Density:	2700 kg/m^3
Ultrasonic resonant frequency:	200 kHz
Transducer radius:	20 mm
Cable diameter:	17 mm
Cable depth:	60 mm
Transducer spacing:	150 mm

Under these circumstances, the attenuation is computed to be 54 dB, which is 37.5 dB weaker than the signal that reached the receiver directly. Since the peak-to-peak signal amplitude will be of the order of 200 mV, the oscilloscope sensitivity will be set at 50 mV/division. At this sensitivity, the analog to digital converter can resolve to a precision of 1.5625 mV. Now 1 V (the rms output of the transducer) attenuated by 54 dB is 2.00 mV. In other words, 1 to 2 bits of 256 will change as a result of the cable echo. Not only is 2 bits unresolvable by eye, it is also quite impossible to analyse computationally.

Assuming, for the moment, the extraneous signal is spatially variant and can be reduced by spatial averaging and assuming a workable S/N ratio (echo to back scatter) to be +30dB, it is possible to calculate the number of averages that are required to produce a signal which can be processed numerically.

Hence the current S/N ratio, given by SNa, is -34.1 dB or 0.0197. To improve this to +30dB, or 31.6, given by SNb, we transform equation (B.50) to:

$$n = \frac{2(SNb)}{SNa} \qquad (B.53)$$

This gives n to be 3208. To produce a S/N ratio of 0 dB, where both echo and back-scatter are of equal magnitude, n would be 102.

As stated above, this possible improvement could only be realised if the predominant noise is from base-scatter and not say, from surface travelling waves.

B.9 DESCRIPTION OF CANDI SIGNAL PROCESSING

CANDI identifies changes in the internal composition of a concrete specimen (small or actual bridge beam) by insonating the medium with a broad band ultrasonic signal, discretising the received signal into frequency bands by filtering in the Fourier domain, and comparing the ratio of energies of those bands in the time domain once they have been re-transformed.

Eight bands are used, from 0 to 400 kHz and 50 kHz in width. The manner in which the bands are compared or combined depends on the kind of defect that is being sought; it can take the form of cross-multiplication, in which all energy bands are simply multiplied together (an operation not dissimilar to cross-correlation), and this has been particularly successful in locating moderate to large sized voids when increased reflectance of all wavelengths is to be expected. In other cases involving corrosion, small regions of delamination or complete breakage and separation of a cable, the higher frequency components only tend to display changes in energy beyond the limits normally attributable to random variability. The low frequencies, because of their longer wavelength, remain relatively unaffected. In these instances, the ratio is taken of the high frequency to low frequency energy, using the low frequencies to correct for background variability.

The manner in which the energies of the frequency bands varies according to the internal state of the concrete, and the random contributions of the aggregate and coupling variability, have been numerically simulated using computer programs written as recently as May 1990. The various methods of signal processing were then applied to these simulated data and were shown to be effective at recovering signals that would otherwise have remained buried in noise. The discussion below details three particular methods of analysis that have been used to locate defects in the beams and samples used in this work.

B9.1. Case 1: Random Noise with Weighting Coefficient

Consider a function $y = f(t,\omega)$, in which y is a discrete time variable, changing randomly with both time and frequency. For a given frequency or wavelength, then:

$$y = f(t) \tag{B.54}$$

Where t ranges from 1 to n and for a given time:

$$y = f(\omega) \tag{B.55}$$

Where ω ranges from 1 to m.

In matrix notation, the complete discrete-time data-set may be written as:

$$\underline{Y} = \begin{vmatrix} y_{11} & y_{12} & y_{1n} \\ y_{21} & y_{22} & y_{2n} \\ y_{m1} & y_{m2} & y_{mn} \end{vmatrix} \tag{B.56}$$

In the above notation, each row of the matrix represents a signal that varies randomly with time for a particular frequency.

Consider further, at a given time at some point when $1 < t < n$, say $t = g$, the y variable is weighted by a coefficient b, where $b > 1$, for all values of ω.

Hence:

$$\underline{Y}_1 = \begin{vmatrix} y_{11} & by_{1g} & y_{1n} \\ y_{21} & by_{2g} & y_{2n} \\ y_{m1} & by_{mg} & y_{mn} \end{vmatrix} \qquad (B.57)$$

If y lies within the range $0 < y < 1$, and the coefficient b is arbitrarily assigned a value of, say, 1.8, this value representing an increase in energy at that point, then a typical signal trace (i.e. one row of $\underline{Y}_1$) for a given frequency will appear as the trace shown in Figure B5.a. In this example, n = 400, and the weighting coefficient has been applied to $y_{1,200}$. In many cases, the weighted signal will not lie above the noise threshold because of the random nature of the noise magnitude.

In order to recover the signal of interest, a new function, z, is derived, ranging from 0 to n, in which each point is a multiple of a given column of $\underline{Y}_1$, i.e. for any given point in time, a multiple is derived of each frequency reading.

Hence:

$$Z_t = \prod_{\omega=1}^{\omega=n} y_{\omega,t} \quad \text{(for } t = 1 \text{ to } m\text{)} \qquad (B.58)$$

This operation will under most circumstances greatly enhance the magnitude of Z_g over the noise threshold, as shown in Figure A1.b. This method is in fact closely analogous to the cross-correlation function, which assumes that within the data-set, there is a series of values which resembles the correlation operator.

In practical terms, as the transducer receives a signal from each scan position, because of the random nature of the aggregate profile, the signal strength will vary randomly, and each frequency band will also show a random variation. If a large defect (such as a void) is encountered, which reflects all frequency bands, the random signals will now be weighted with a coefficient greater than unity. Thus, in order to detect such defects, the best strategy of signal processing to adopt is a simple multiplication of the energy bands as described here.

B9.2. Case 2: Partially-Correlated Noise with Weighting Coefficient

In practice it is never the case that the discrete-time variable is random both with position and frequency. Although the signal strength varies more or less arbitrarily from point to point on a concrete surface (above a certain level) it is clear that the strength of a given frequency band will bear some relation to that of an adjacent frequency band.

In order to simulate this condition, an initial random function is generated, $y = f(t)$, with t ranging from 1 to 400 and a weighting coefficient is applied to point 200, with a value of 1.7, see Figure B6.a. The remaining frequency bands are generated by partially correlating them to the first, i.e:

$$Y_{\omega,t} = Y_{1,t} + R \qquad (B.59)$$

Where: ω ranges from 2 to 10,
t ranges from 1 to 400
R is a random coefficient lying in the range $0 < R < 0.25$.

The final function, Z_t, is derived by application of Equation B58. Figure B6.b shows how once more the signal of interest is raised clear of the noise threshold. Again, this method of signal processing favours the identification of voids or regions of delamination, when it is reasonable to assume that all frequency bands will show an increase in energy over the region of interest.

B9.3. Case 3: Partially-Correlated Noise with Weighting and Normalisation Function

Certain internal conditions of the concrete should, in theory, result in the attenuation of certain frequency bands whilst leaving others unaffected. In particular, an interface which is roughened over a region will reduce the intensity of the reflected high frequency components without attenuating the lower bandwidths. If the discontinuity is such that only a single band remains unaltered, signal recovery is possible using the operation:

$$Z_t = \frac{Y_{1,t}}{\prod_{\omega=2}^{\omega=n} Y_{\omega,t}} \qquad \text{B.60}$$

for $t = 1$ to m, with $Y_{1,1}$ to $Y_{1,t}$ representing the unaffected frequency band. The frequency bands $Y_{2,t}$ to $Y_{\omega,t}$ are generated using the method given by Equation B.59, and the attenuation for these same bands, is achieved by applying a weighting coefficient b, at point $n = 200$, where b is in the range $0 < b < 1$. Figure B7 shows how this method can be successful in recovering signals that have been severely attenuated as a result of selective scatter or absorption.

References to Appendix B

1. Blitz. "Ultrasonics".

2. Spencer, A.J.M. et al. "Engineering Mathematics". Van Nostrand Reinhold (U.K.) Co. Ltd., 1977.

3. Kraukramer. "The Krautkramer Booklet". Krautkramer GMBH.

4. Woodcock, J.P. "Ultrasonics". Adam Hilger Ltd., 1979.

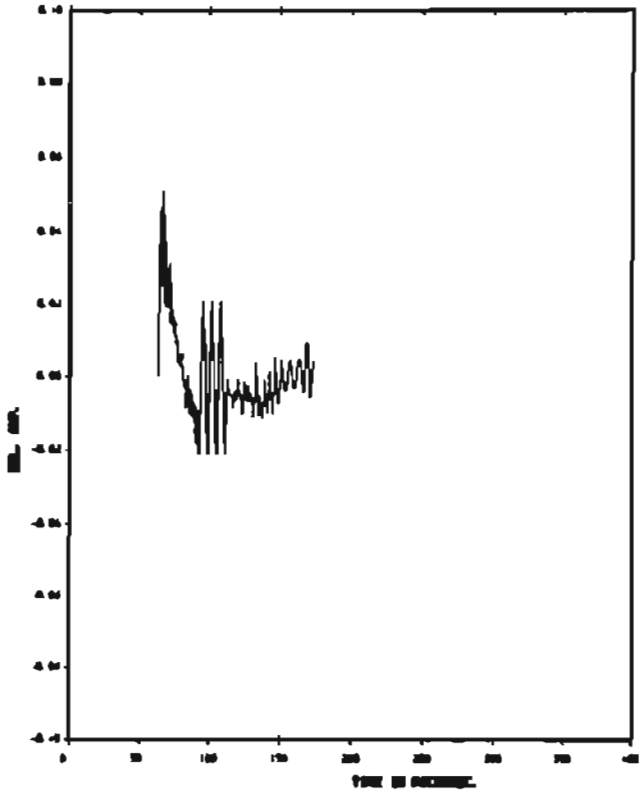

CONCRETE

Figure B1.

Predicted output of ultrasonic system in plain concrete, at 150kHz

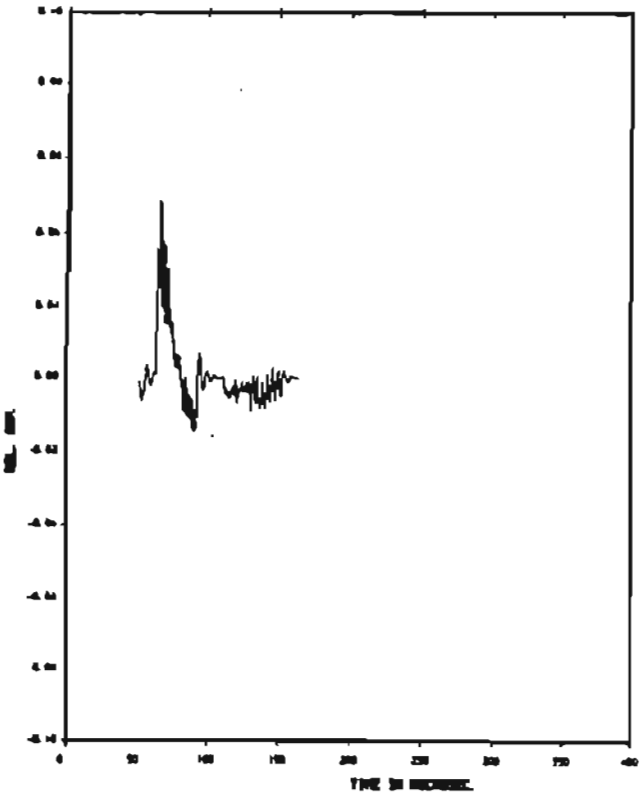

CONCRETE WITH WIRE THROUGH

Figure B2.

Predicted output of ultrasonic system in concrete with a single steel bar

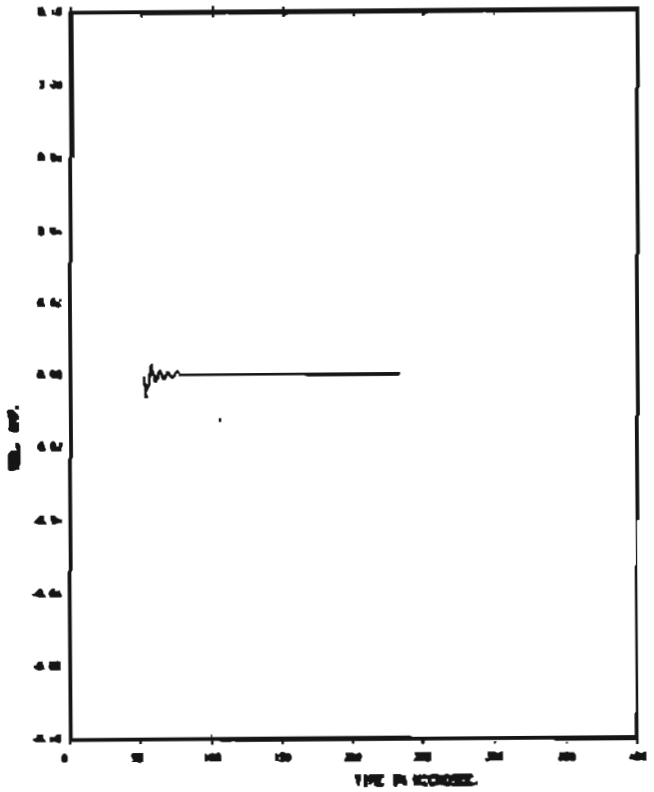

CONTRIBUTION OF THE WIRE ONLY.

Figure B3.

Predicted output of ultrasonic system considering only the signal contribution from good quality steel

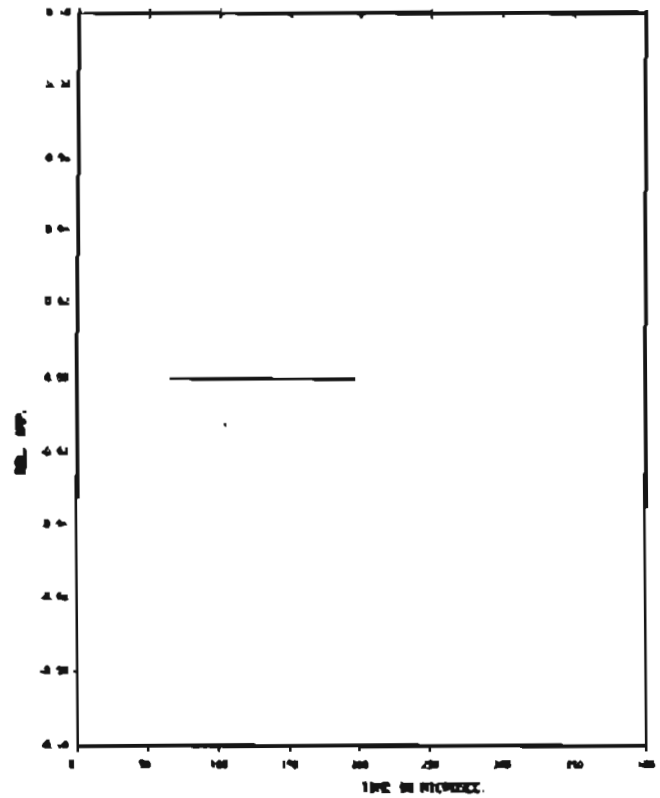

CONTRIBUTION OF THE WIRE ONLY.

Figure B4.

Predicted output of ultrasonic system considering only the signal contribution from a corroded steel bar in concrete

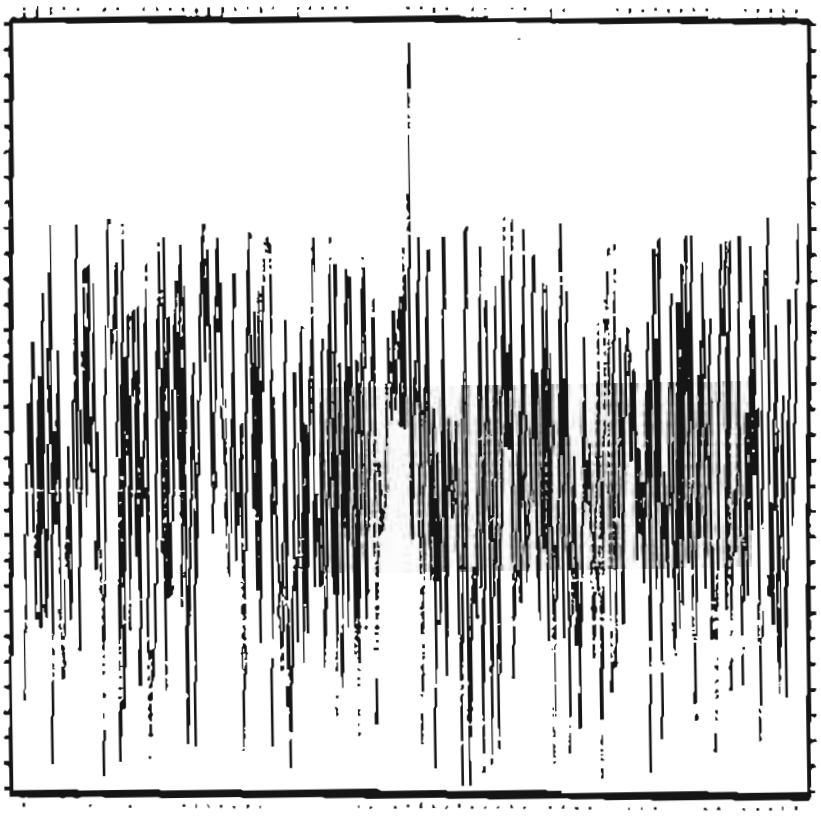

Figure 15.a

Typical random noise signal with central weighting coefficient of 1.8

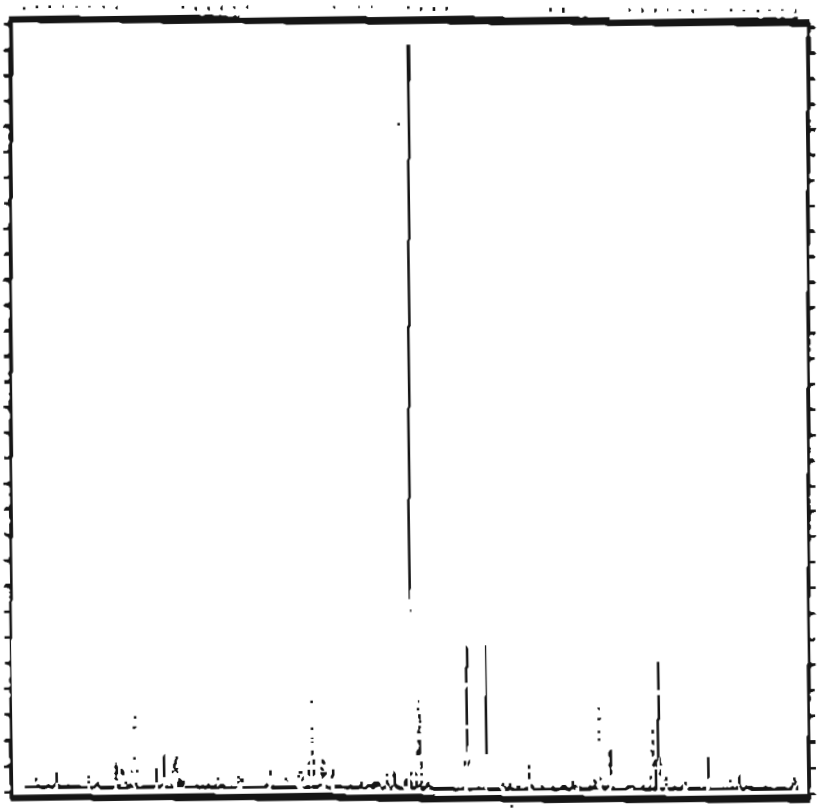

Figure B5.b

Signal obtained after successive multiplication of 10 traces, each unique but similar to above.

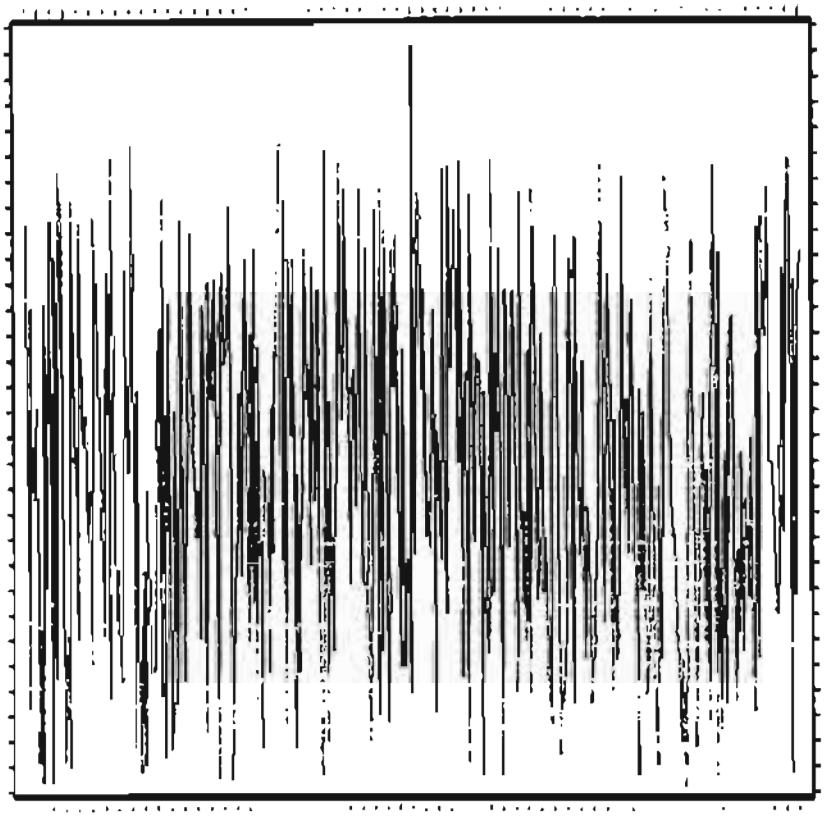

Figure B6.a

Typical random noise signal with central weighting coefficient of 1.7

% Relative Energy

No. of Readings (400)

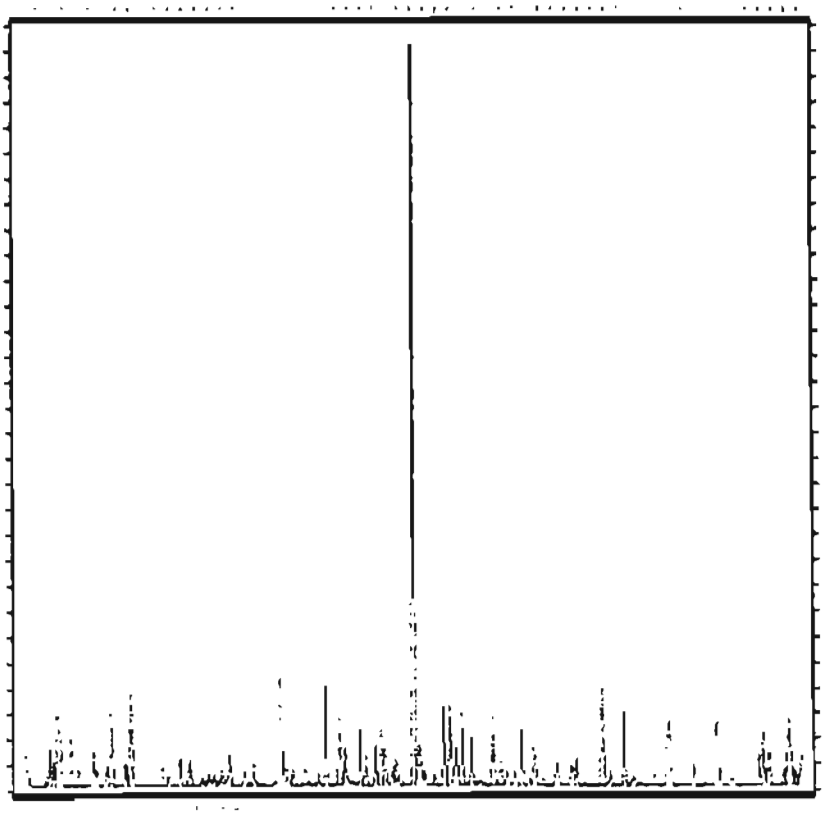

Figure B6.b

Signal obtained after successive multiplication of 10 partially correlated traces, convolved with a random weighting coefficient.

% Relative Energy

Figure B7

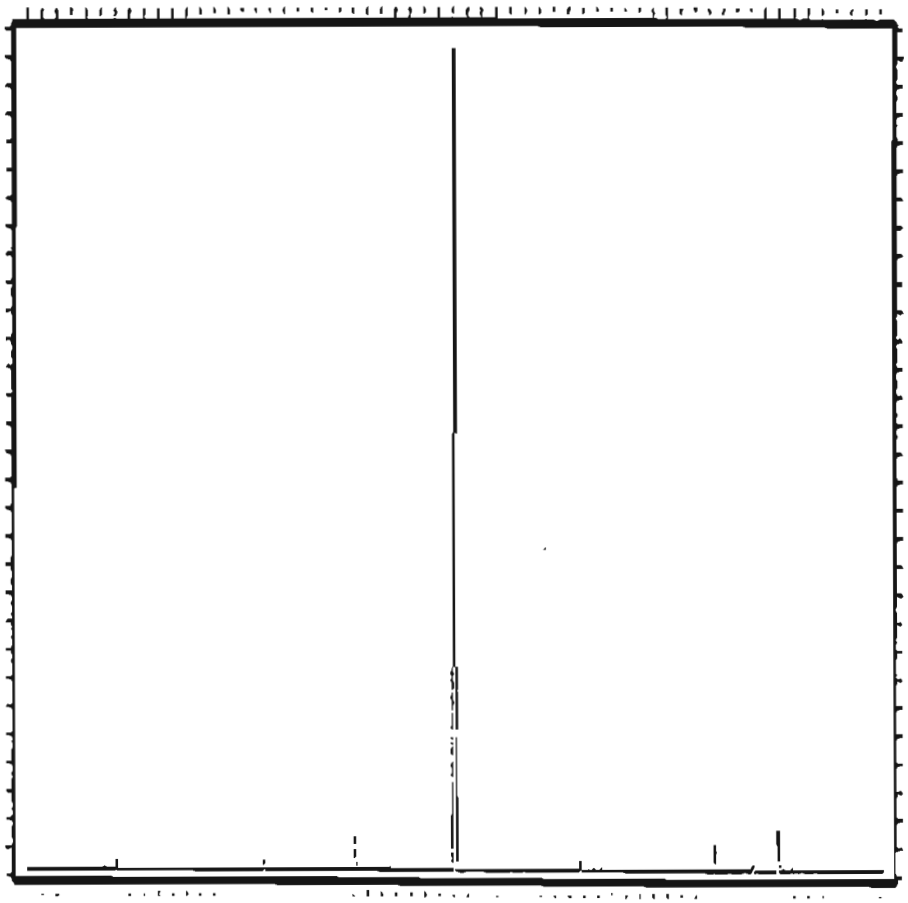

Signal obtained after successive division of a single trace by partially correlated, randomly weighted traces, with a central weighting coefficient of 0.26. Nine traces used as the denominators.

APPENDIX C: A THEORETICAL JUSTIFICATION FOR THE REJECTION OF THE PULSE-ECHO APPROACH

The following example illustrates why, given the nature of concrete and the restrictions placed on the frequencies that can be realistically applied in these circumstances, pulse-echo systems are unlikely to be successful in returning echoes above the level of noise arising from aggregate back-scatter.

A transducer diameter 0.025 m and resonance 150 kHz radiates with an intensity I_o of 5 Wm^{2}. Estimate the echo amplitude, expressed in $kgm^{-1}s^{-2}$ (Pascals) of a signal reflected from a void of the same area as the transducer face, buried 0.1 m below the surface of a concrete slab, assuming c = 4000 m/s and $\rho = 2700\ kgm^{-3}$.

The initial sound pressure, P_o, is given by:

$$P_0 = \sqrt{(2I_0\rho c)} = 1.03923 \times 10^{4}\ kgm^{-1}s^{-2} \qquad (C.1)$$

The wavelength, λ, is given by:

$$\lambda = c/f = 0.02667 \qquad (C.2)$$

The half-angle of divergence, θ, is calculated using the identity:

$$\theta = \sin^{-1}\ [0.6(\lambda/a)] \qquad (C.3)$$

where a is the radius of the transducer face. However, in this case $[0.6(\lambda/a)]>1$, so the transducer radiates with an approximately hemispherical wavefront. At a depth of 0.1 m, the intensity, I_1, which is governed by the inverse square law, becomes:

$$I_1 = \frac{I_0 a^2}{2a^2} = 0.0390625\ Wm^{-2} \qquad (C.4)$$

where r is the depth of the void. The ultrasonic intensity of the echo at the surface, I_2, is therefore given by:

$$I_2 = \frac{I_2 a^2}{2a^2} = 3.05176 \times 10^{-4}\ Wm^{-2} \qquad (C.5)$$

The echo amplitude is thus:

$$P_1 = \sqrt{(2I_2\rho c)} = 81.1899\ kgm^{-1}s^{-2} \qquad (C.6)$$

Equation (6) converts the acoustic intensity to a pressure, since the transducers respond to the latter. Hence the total divergence loss, V_d, expressed as a ratio of pressures, is given by:

$$V_d = 20\ \text{Log}\ \left(\frac{P_1}{P_0}\right) = -42.24\ dB \qquad (C.7)$$

We must now consider the attenuation losses due to scatter and absorption, V_s. The detailed experimental work described in Appendix D, dealing with

attenuation of broad-band signals in concrete, established V_s for f = 150 kHz at approximately 10 dB per 100 mm. Therefore in this case, the attenuation loss is -20 dB.

The total signal loss the for combined outward and return path, taking into account both divergence, scatter and absorption is given by:

$$V_t = V_d + V_s = -62.14 \text{ dB} \qquad (C.8)$$

This example assumes perfect coupling and no losses elsewhere in the system. In practical terms, it implies that if a transducer outputs a signal with a perceived strength of 5.0 V rms (a typical figure), the perceived echo amplitude would be 3.9 mV. At maximum sensitivity, the analyser A/D is capable of resolving to 0.488 mV,i.e. when it is configured to a sensitivity of +0.125 mV, operating with a 9-bit resolution.

However, given the amplitude of the signal back-scatter, which is many times greater than the echo amplitude, it would not be possible to configure the acquisition system to maximum sensitivity because it would simply saturate. Although an echo signal of 3.9 mV rms can easily be amplified, since it is inextricably mixed with coherent noise, the signal-to-noise ratio is not improved.

Although spatial averaging could theoretically eliminate the problem of signal back-scatter, it is important to realise that if the echo amplitude is below the minimum resolving power of the acquisition system, no amount of signal averaging will improve the situation.

The example used in this case involved a void with a flat surface, but in practice the cables have a curved surface, which reflect at best 62% of the signal at normal incidence, with dimensions close to the wavelengths of the interrogating frequencies. The implications with respect to p_2 are therefore obvious.

APPENDIX D: FOUNDATION EXPERIMENTATION

D.1 ATTENUATION ANALYSIS

D.1.1 Introduction

Ultrasonic inspection systems used on homogeneous materials, such as steel or human tissue (here homogeneous is used in the sense that any inclusions within the matrix proper, having an acoustic impedance Z, significantly different to that of the matrix, Zo, have a mean radius r where $r \leq 0.5\ \lambda$, λ being the interrogating wavelength) are invariably configured as pulse-echo systems in order to acquire information relating to the internal structure of the material under test.

It has long been considered that pulse-echo systems are not well suited for use on concrete-like media due to the highly inhomogeneous nature of their internal structure. Moreover, because of the severe attenuation at high ultrasonic frequencies (greater than 500kHz), ultrasonic inspection is generally conducted in pitch-catch mode at frequencies not extending beyond 60kHz, where λ, (depending upon the propagation velocity of the concrete), is approximately 65 mm. Internal imaging in the conventional sense is not possible at this frequency - because of the coarse resolving power of the wavelength - and this low frequency, pitch catch method is usually restricted to establishing the strength of the concrete.

This project is concerned with deriving information on embedded steel within concrete, and one technique which has recently been under evaluation is pulse-echo. There are two attendant problems with this approach. One is signal attenuation and the other is echo-noise arising from signal reflection from the aggregate. If it could be shown that a sizeable echo is returned from any internal steelwork (say, above -60 dB), then the remaining problem - that of coherent signal noise - could be eliminated by the application of suitable signal processing techniques.

Note: the term "Coherent Signal Noise" is considered as a separate, and unfortunately, more thorny problem then "Incoherent Signal Noise". See Appendix B.

This group of experiments was performed on a number of concrete mixes and sample lengths in order to quantify the effects of signal scattering and attenuation at different frequency levels. In the past attenuation has always been applied in a loose sense but here some attempt has been made to identify the effects of Rayleigh, phase and diffusion scattering.

D.1.2 Method

Figure D1 depicts the configuration used in these experiments. Two wide-band transducers with a nominal centre frequency of 500 kHz were coupled to either face of a solid concrete cylinder using a medium grade grease. One transducer was excited to resonance by a 600V spike and the other, acting as the receiver, was connected directly to the input of the Solartron digital storage oscilloscope. No amplification was used. After the data were acquired they were transferred to computer and subsequently analysed using ULTRAMATH 1.5.

The cylinders were 500mm in diameter and ranged in length from 100mm to 500mm, in 100mm increments. Three mixes were investigated: Mix 1 contained

no aggregate but was composed entirely of sand and cement. Mix 2 contained aggregate with a mean diameter ≤ 10mm, and Mix 3 contained aggregate with a mean diameter ≤ 20mm.

D.1.3 **Analysis**

Table D1 contains information relating to the first 512 μs of the received signal. In the time-domain this information includes the propagation velocity (this is assumed to be of the compressional wave), the signal rms value and the signal energy. The last was calculated using the identity $tV_{rms}^2 \times 10^6$, assuming a 1 Ω load, and is expressed in Volt -microseconds, a unit which is commonly applied in these circumstances.

In the frequency domain the signal strength at various frequency bands has been calculated, using absolute voltage amplitude from the linear spectra. Frequency bands (always 25kHz in width) have been used rather than single harmonics since the latter give rise to gross statistical error due to random fluctuations in the estimated spectra. These frequency bands were calculated by integrating the amplitudes over the shown limits thus:

$$\int A = \int_a^b x(\omega)d\omega \approx \sum_{n=a}^{b} x(\omega) \qquad (D.1)$$

where b = a + 25 kHz, and n in 1 kHz increments.

Table D2 contains the equations that have been calculated, together with their associated correlation coefficients, r, when the relationship

$$\text{Log } (\int A) = a_0 + a_1 \text{ (distance)} \qquad (D.2)$$

is assumed to be linear. Strictly speaking this relationship should only be used when there is neglible loss from divergence and when a single frequency, rather than a frequency band is employed as the dependent variable. Divergence losses were kept to a minimum in these experiments by the use of small diameter cylinders, and the frequency bands were kept as narrow as possible whilst still, hopefully, eliminating the effects of random variability. Also included in Table D2 is the attenuation, expressed in dB per 100mm, for each frequency band in each of the three concrete mixes.

In mix 1, the total signal energy does not decrease steadily with increasing length but reaches a maximum at 300 mm. This is probably not a genuine effect arising from, for instance, signal channeling but is probably due to variations in the concrete quality from sample to sample, the possible presence of voids or coupling variation. Whilst mixes 2 and 3 do not always show a steady drop in signal energy with distance, the pattern of mix 1 is not repeated.

Generally speaking the signal strength declines not only with length of sample, but also with increase in frequency. Moreover, the weakest signals are also shown to be associated with the samples containing the largest mean aggregate size, mix 3. However, Tables D2a-D2c would suggest that the situation is not as simple as might first be supposed. Table D2a clearly indicates that the attenuation, expressed in dB per 100 mm, increases in severity with increasing frequency. However, for mix 1 (no aggregate), in the 25 kHz to 50 kHz, the drop in ultrasonic pressure is calculated to be 2 times for every 100mm. Between 125 kHz to 150 kHz it is 3 times, between 225 kHz-250 kHz it is 3.9 times, and between 325 kHz to 350 kHz it is 2.5 times.

Note: Ideally, the last attenuation figure should be greater than the three preceding it. Similarly, this should also be the case for those columns in Tables D2b and D2c which balk the underlying trend. The reason that they do not is because their absolute magnitudes, given in column 8 of Tables D1a to D1c, are so small that they do not correspond to their true value but to the noise characteristics of the measuring system. The oscilloscope can resolve any signal to a maximum resolution of 0.00390625 (1/256), or 48.2 dB. In some cases the signal amplitudes given in column 8 of Table 1a to 1c are less than 1/256 times the total signal rms value, which is given in column three. The higher frequency harmonics will always be slightly greater than their true value by a constant factor, which will contribute to a corresponding larger percentage of the total as the real value declines. Signal digitisation essentially involves quantisation into a series of step functions, and the Fourier spectrum of a step function has harmonics extending to infinity whilst decreasing logarithmically.

In Table D2b, the attenuation is generally more severe than for Table D2a, although it does not increase as rapidly with frequency and in Table D2c, with the exception of the last frequency band, the attenuation is more or less constant across the spectrum.

D.1.4 Discussion

These attenuation experiments quantitatively demonstrate what has been known infinitively, with regard to its possible impact on any system design or data interpretation software. It is Rayleigh Scattering, in which the mean particle diameter is much smaller than the wavelength, which affects the higher frequency components most severely. Hence mix 1, which contained only sand and cement, with particles less than 1 mm in diameter, gave rise to the most severe attenuation in relation to frequency. The smallest wavelengths, at 325 kHz - 350 kHz lay between 11 mm and 16 mm, and so it may be concluded that Rayleigh Scattering was the only scattering mode of significance in these experiments. In this mode, each particle scatters a fraction of the energy incident upon it given by

$$7/9\ (ka)^4 \qquad (D.3)$$

where a is the particle diameter, and $k = 2\pi f/c$

To derive the attenuation coefficient per unit distance, the change in intensity over an incremental distance is given by

$$dp = -7/9\ (ka)^4 PN\pi a^2 dx \qquad (D.4)$$

where N is the number of particles over distance. Writing

$$2a = 7/9\ (ka)^4 \pi a^2 N \qquad (D.5)$$

then

$$\frac{dp}{d} = -2\alpha\ dx \qquad (D.6)$$

This is a differential equation of the form $dQ/dt = kQ$ in which the general solution is $Q = Ae^{kt}$.

Hence the pressure drop is given by:

$$\int \frac{dp}{p} = \int -2\alpha dx = p_s = p_o e^{-2\alpha x} \qquad (D.7)$$

Thus the energy of the signal declines in proportion to the fourth power of the frequency.

In mix 2, where the mean aggregate size was roughly equal to the wavelengths of the higher frequency components, phase scattering occurred in addition to Rayleigh Scattering. This is less severe than Rayleigh Scattering, being proportional to f . However, for the longer wavelengths, this aggregate would also be a source of Rayleigh Scattering. Correspondingly therefore, the attenuation gradient is slightly less steep for mix 2 than it is for mix 1, i.e. 6.6 dB per 100 mm - 11.8 dB per 100 mm in comparison to 5.7 dB per 100 mm - 11.8 dB 100 mm for mix 1 (ignoring the last frequency bands). The absolute attenuation figures are higher, because the second mix is a source both of Rayleigh and phase Scattering.

This pattern is continued in mix 3, in which diffusion scattering (when $r>\lambda$) has begun to affect the high frequency components. The attenuation figures shown are approximately equal for the first three frequency bands, although, as has been mentioned earlier, the reliability of these data are limited by the resolution of the measuring system. In all probability the attenuation should still increase with increasing frequency but not as markedly as it does in Table D1a.

These findings have important implications for any final interrogation system, be it pulse-echo or pitch-catch. Furthermore, it is now necessary to differentiate between signal attenuation through absorption, and signal attenuation through scatter. Rayleigh scattering results in a general weakening of the signal through thermal conversion, but phase and diffusion scattering, whilst less severe, give rise to coherent noise at the receiving stage because even scattering interface produces an echo which is as equally valid as the echo produced by the internal object which is the subject of investigation.

These experiments would suggest that as far as signal strength is concerned, the presence of aggregate is not the major contributory factor. It therefore follows that if a method could be found to obviate the effects of coherent signal noise, which does affect the shorter wavelengths much more than the long ones, a high frequency inspection system might be feasible.

In order that these experiments provided reliable attenuation loss statistics, the effects of divergence loss were minimised by the appropriate choice of sample dimensions. Unlike attenuation loss, divergence loss operates independently of frequency and is related solely to the beam-spread function of the transducer/medium combination. It must be taken into account when considering the signal-to-noise characteristics of a system, and the total signal loss, V_t in dBs, is given simply by

$$V_t = V_s + V_d \qquad (D.8)$$

Where V_s is the attenuation loss and V_d is the divergence loss.

Assuming an attenuation loss of 12dB per 100 mm (a factor of 6) and assuming the beam spread to be spherical (this is justified given the effects of signal scatter, frequency used and transducer diameter commonly employed in

this work; it is also supported by experimental evidence discussed in Section 2, dealing with propagation made analysis), then the divergence loss from a 20 mm transducer at a concrete depth of 100 mm would be 28dB. Hence the pulse-echo attenuation would be:

$$V_t = 2(V_s + V_d) = 2(12 + 28) = 80 \text{ dB} \qquad (D.9)$$

This figure corresponds within a few dBs to purely theoretical work that was carried out in February 1989. It also agrees with calculations performed independently within the Civil Engineering Department, UMIST. Thus these calculations have been both devised theoretically and confirmed experimentally.

80 dB is not an encouraging number, it represents a reduction in signal strength of 10^4 with a concrete cover of 100 mm. Although this would be improved to approximately 60dB at a depth of 70 mm, and, by the use of existing pre-amplifiers the echo could be restored to its original amplitude, this would not eliminate from the signal the contribution of coherent noise, which will always be many hundreds of times stronger than that proportion of the signal corresponding to the pertinent echo.

The conclusion that must be drawn from these data is that pulse-echo systems are unlikely to operate successfully on this medium unless the effects of signal back-scatter can be overcome. Failing that, one alternative is to examine the total change in the signal (rather than isolating a part of it) received by a transit-time system. The mathematical justification for accepting or rejecting this line of enquiry will be dealt with in the following section.

D.2 PROPAGATION MODE ANALYSIS

D.2.1 Introduction

The purposes of this group of experiments, entitled propagation mode analysis, were five-fold:

a) The identification of wave modes, other than compressional, such as shear and Rayleigh (surface) waves, and their contributions to signals detected by transit-time systems.

b) Beam divergence in relation to frequency.

c) The effects on signal strength, transit-time and frequency of surface cracks in relation to transit-time systems.

d) The effects on signal strength, onset time and frequency of multiple surface cracks and steel reinforcement close to the concrete surface in relation to transit-time systems.

e) The identification of high-frequency components within the total signal, and the estimation of their rates of decay in comparison to the low-frequency components.

In the past it has been assumed that the most significant contribution to the signals propagated and received (in all the experiments) was made by the compressional wave. Certainly, the transducers are designed to generate only

these waves but this ignores the fact that mode conversion occurs at material boundaries and that Rayleigh or surface wave can be generated from compressional forces acting on the surface of the sample. If some of the signals detected in transit-time systems are indeed from Rayleigh type emissions, this has important implications for systems which seek to inspect conditions well below those at the surface.

D.2.2 Direct and Indirect Transmission Systems

D.2.2.1 Method

This experiment sought to identify the differences which existed between signals which had been transmitted through a sample, and those which had been transmitted along its surface. Figure D2 shows the arrangements. A plain concrete slab of dimensions 700 mm x 700 mm x 150 mm was mounted on wooden trestles and two wide-band transducers with a nominal centre frequency of 500 kHz were coupled to each face with a medium grade grease, care having been taken to ensure that the transducers were directly in line with one another. A single shot was recorded, and the transducers were repositioned on one face of the slab, 150 mm apart over the centre of the sample. A second reading was then taken.

D.2.2.2 Analysis

Table D3 contains a summary of the time domain and frequency domain statistics calculated for these experiments. Figure D3a shows the corresponding time records and frequency spectra. The first significant observation is that whilst there does not appear to be a major difference between the rms values of the two traces - the direct transmission data are 1.4 times the amplitude of the indirect set, the estimated acoustic velocity, which is constant for a given wave mode, is markedly different, 4411.8 in comparison to 2941.2. If the signals had been very different in strength the differences in velocity could not be determined with any confidence since a low amplitude signal would give an apparent lower velocity. The spectra also indicate that, for the surface-mounted transducers, much more of the energy is concentrated towards the low frequency end of the spectrum.

Figure D3b provides a more detailed picture of the onset of the signals in both cases. The difference in velocity is clearly evident, and much higher frequency components are associated with the direct transmission system. Table D4 gives the statistics and these suggest that components of different frequency arrive at the receiver at different times.

This hypothesis is given further credibility by Figures D4a and D4b. In Figure D4a, the original data have been selectively low-pass filtered in the frequency domain and then inverse-transformed to produce time records which contain only those frequency components lying below 100 kHz. Under these circumstances, both signals commence at approximately the same time. In Figure D4b, the original data have been selectively high-pass filtered, leaving only those harmonics which extend beyond 100 kHz. Now the difference in velocity is clearly evident.

The filtered signals shown in Figures D4a and D4b serve to highlight another phenomenon which had hitherto remained hidden: the high frequency components of the signal decay much more rapidly than their low frequency counterparts. Furthermore, the high frequency components associated with the direct-transmission experiment decay more rapidly than those associated with

the indirect-transmission equivalent. A possible mechanism for this feature of signal attenuation will be given below.

D.2.2.3 Discussion

The difference in velocity of the waves associated with the direct and indirect transducer configurations appears to indicate that Rayleigh waves are involved with signal propagation in the latter case. Rayleigh waves travel at a speed close to that of shear waves, which is given by:

$$C_s = \sqrt{(\frac{G}{\rho})} \qquad (D.10)$$

Where G is the modulus of rigidity and ρ is the density.

Depending upon the medium, the velocity of shear waves lies between 0.4 and 0.7 that of compressional waves. The Rayleigh wave vector has two components, one longitudinal and the other transverse, acting at right angles to the surface.

There remain, however, certain difficulties with the Rayleigh wave hypothesis. Since the transducers are intended to generate compressional waves, the greatest proportion of the acoustic energy delivered into the concrete will propagate in this mode. Why then, are the rms values for the two measured signals different by only a factor of 1.4? The answer, possibly, lies in the fact that surface waves do not penetrate appreciably into the interior of the solid, most of their energy is contained within a single wavelength of the surface and there is an exponential decrease of intensity with depth. Since they propagate only in two dimensions therefore, surface waves retain the unique characteristic of suffering very low attenuation. Hence, although the compressional wave signal started with much greater energy, by the time it reached the base of the sample it had been attenuated to the point that its rms value was similar to that of the surface travelling wave.

This also would appear to explain why the high frequency components are less rapidly filtered out in the direct-transmission case from in the indirect transmission case.

The above paragraphs do not imply that no echoes from greater than one wavelength into the concrete reach the surface mounted transducers. They do suggest, however, that in comparison to the surface wave components their contribution may be smaller than was previously thought.

As a final corollary to this aspect of the research, the direct-transmission data allows us to cross-check the attenuation calculations of the preceding section. The signal received in this case has experienced both attenuation loss and divergence loss, and having travelled through 150mm of concrete, the figures become

$$V_t = V_s + V_d = 18dB + 17.5dB = 35.5\ dB \qquad (D.11)$$

(Divergence loss is calculated using a transducer diameter of 20 mm).

The rms output of these transducers has been measured at 0.921 V. Table D3 shows that after 150 mm of concrete this has fallen to 0.015.

$$\text{Hence } 20 \text{ Log } \{\frac{0.921}{0.015}\} = 35.7dB \qquad (D.12)$$

The answers given by equations (D.11) and (D.12) could not be much closer.

D.2.3 Beam Divergence Estimation

D.2.3.1 Method

Two wide-band transducers with a nominal centre frequency of 500 kHz were coupled to a plain concrete sample as shown in Figure D5. The sample was 1 m in length and 0.15 m^2 in section. The shortest distance between the transducers, as indicated by the dotted line, was 600 mm. Two sets of readings were taken. In the first case, the transducer on the top of the sample acted as the transmitter and the transducer on the side as the receiver. Figure D6a shows the onset of the signal detected in this case, together with its spectrum. Figure D7a shows that same signal extended to 1024 μs, again with its spectrum. In the second case, the transducer on the side acted as the transmitter and the one mounted on the top as the receiver. The corresponding signal and frequency traces are shown in Figures D6b and D7b.

D.2.3.2 Analysis

It has been demonstrated many times in the past that with the transducers used, and the frequencies at which they resonate, it is not possible to launch a well defined acoustic beam pattern into the concrete. In homogeneous media the beam divergence angle is governed by the relationship between the crystal diameter and the wavelength, i.e.

$$\theta = \sin^{-1} 1.2\ (\lambda/D) \qquad (D.13)$$

Where θ is the half-angle of divergence.

Even at 250 kHz, with transducers having a diameter of 20 mm, θ is 74° (assuming c_2 to be 4000 m/s). However, in homogeneous media in which the beam radiates omni-directionally, this does not imply that there is no axial pressure variation. This variation is governed by the expression.

$$P_\alpha = P_0 \left\{ \frac{2J_1\left(\frac{2D \sin \alpha}{\lambda}\right)}{\frac{2D \sin \alpha}{\lambda}} \right\} \qquad (D.14)$$

Where α is the angle subtended to the acoustic axis,
P_0 is the pressure at the axis, and
J_1 is a Bessel function of the first order.

Using this expression, it can be shown that for a 150 kHz signal propagating in a homogeneous medium, the pressure when α =76.5° is 0.7 that of the pressure when α = 13.5°.

Whilst Table D5 indicates that the first 100μ s of the signal (shown in Figure D6a) propagated to an oblique angle is weaker than when propagated close to the acoustic axis, this is not borne out in Table D6, which contains statistics relating to the first 1024μs. In the latter case, the oblique pressure is actually stronger.

D2.3.3 Discussion

One of the interesting features of this experiment is the way in which a close similarity can be observed between the two sets of signals, especially during signal onset. A quantitative assessment of this similarity can be performed by plotting the first trace, Figure D6a, as a function of the second, in Figure D6b. The resulting x-y plot is depicted in Figure D8. This is termed coherence analysis and, in this case, returns a correlation coefficient of 0.8770.

Note: Coherence analysis is only valid when no phase displacement exists between the two signals. If this is not the case, the cross-correlation function should be applied in its place.

It is not difficult to understand why the signals should appear so similar; the velocities given Table D6 suggest that the signals have travelled by the shortest route possible, and hence both would have travelled through the same aggregate profile, albeit from opposite directions. What is more significant is the apparent absence of any pressure difference between the two sets of figures; this is almost certainly due to the scattering effect of the aggregate, and implies that little benefit can be derived from the use of either large diameter or focused probes. For this reason, this experiment also gives limited support to the hypothesis that with single surface transit-time systems, some of the wave energy is derived from a surface travelling wave.

D.2.4 Single Surface Groove Effects

D.2.4.1 Method

A plain concrete sample, of dimensions 1 m x 0.15 m^2, was cut across the width of one face to a depth of 15mm and a width of 5 mm. Transducers were mounted as shown in Figure D9, positioned 200 mm apart the first test and 500mm apart in the second, with the cut lying at the midpoint between the transducers. The readings that were taken were compared to those which had been taken in the absence of any surface discontinuity.

D.2.4.2 Analysis

Figure D10a shows the trace and spectrum obtained from an intact sample and a transducer spacing of 200 mm, and Figure D10b shows the data captured when the surface has been cut, as described above. The spectra indicates that most of the signal energy is concentrated in the band below 100 kHz. Indeed, Table D7 shows that, for the unscored sample, the mean frequency lies at 66.3 kHz with a peak at 23 kHz, and for the scored sample the mean frequency is 62.9 kHz with a peak at 12 kHz. The approximate wavelengths (within 5%, since it is difficult to know for certain the true velocity) are 51.1 mm and 53.9 mm respectively.

Since the groove only extends to a depth of 0.3λ, it is not to be expected that there will be a radical change in the signal energies detected between the first and second readings. There should, however, be some noticeable changes to the wave packet as the aggregate profile through which the second signal must travel changes. As a corollary to this, the apparent velocity in the second case should be lower - this is borne out by Table D7. Furthermore, it is lower by 14.5%, which implies that the wave travelled around the face of the discontinuity, which is the action of a Rayleigh-type wave.

Figure D11 depicts in more detail the differences that exist between the two signals when considering the first 200 μs. It is reasonable to suppose that these differences would become steadily more apparent as the depth of the cut was increased.

Figure D12a shows the data obtained with transducers spaced at 500 mm on an intact sample, and Figure D12b provides the data obtained when the same sample was cut as described. In this instance, major discrepancies between the traces and spectra are virtually non-existent. The coherence analysis, shown in Figure D13, indicates a close similarity between the traces, the correlation coefficient of which is 0.6782.

D.2.4.3 Discussion

The data referring to the last experiment revealed a puzzling aspect of this kind of propagation; although the velocities, as evidenced by Table D8, would suggest that the dominant mode of propagation is via the surface wave (the measured velocities are even lower than those given in Table D7, where the transducers were spaced at 200 mm), there appears to be little disruption to the signal when the sample includes the surface cut. The time domain and frequency domain statistics all lie within a few percent of each other.

It is however possible, that at this distance the effect of the cut on the waves given the bulk of the sample, is considerably reduced. At a depth of 20 mm the surface wave would still retain some 50% of its energy, which might explain why there is no noticeable difference in the velocities. Unfortunately, this line of reasoning would contradict the evidence of the velocity figures for the first experiment. More work is required on this aspect of propagation for a fuller knowledge of the mechanisms involved.

D.2.4.4 Multiple Surface Crack Investigation

This experiment involved the examination of a reinforced sample using transducers placed in six different locations. Figure D14 shows the sample that was used, with the transducer positions (in transit-time configuration) indicated by a, b, c, d, e and f. Once again wide-band 500 kHz transducer were employed. The sample was reinforced by two steel bars of 17 mm diameter lying 20 mm below the top surface (measured from their outer surface), and two 5 mm diameter steel rods running parallel, close to the lower surface of the concrete. In addition, stirrups were present at intervals of 50 mm.

D.2.4.5 Analysis

Figure D15a contains the signal and frequency spectrum obtained with the transducer positioned at location (A). This region of the sample, on its wide face, was free of any discernable faults. By comparison, Figure D15b shows the signal and spectrum obtained from position (B), an area rich in cracks extending well below one surface of the material. Table D9 provides the time domain and frequency domain statistics.

In accordance with the surface wave hypothesis, the apparent velocity across the cracked region is 79% that of the velocity across the intact region. Neither velocities are of the order usually associated with compressional waves in concrete (between 3900 m/s and 4500 m/s). The signal rms is lower in the cracked case by 14dB, and the wave packet has lost some of the high frequency components associated with the signal of Figure D15a. In the second set of readings, for positions c and d (referenced to Figure D16a, D16b and Table D10 respectively), a similar pattern emerges, but with the

addition of some unexpected results. Position d includes a fault in which some of the concrete cover has been lost, exposing the underlying steel bar reinforcement. The velocity is lower than at position c, but only by 7%. The signal trace is markedly dissimilar however, having lost nearly all of the high frequency components associated with the c-trace. Furthermore the envelope of the wave packet is completely altered, indicating that that signal has taken a different route to reach the receiver. What is completely unexpected however, is that the energy associated with the d-trace is 6.3 times greater than the energy of the c-trace (rms higher by 2.5 times).

Further apparent anomalies arise when considering traces (e) and (f), represented by Figures D17a and D17b and Table D11. Both traces are rich in high frequency harmonics-extending beyond 200kHz in the case of (e) a crack-free zone (unlike (f) in which cracks appear at a depth showing at 30mm below the surface) - but the velocity of the signal in trace (f) is estimated at 4067-4068 m/s, far higher than any velocity measured previously on this sample and almost too high for the wave to be considered as travelling in a Rayleigh mode.

D.2.4.6 Discussion

Assuming that with indirect transit-time some of the energy appearing at the receiver is in the form of a surface wave, it is almost certain that the extent and depth of the cracks related to position (C) would have partially disrupted this mode of propagation. Moreover, the compressional wave signal which did reach the receiver arrived through multiple internal reflection and as a consequence suffered severe attenuation as the statistics of Table D9 appear to indicate. This reasoning however, whilst consistent with earlier results, cannot explain why the energy associated with trace (D) is greater than that associated with (C). Since the surface had been damaged to the point of reinforcement exposure at (D), the signal at first sight appears to have travelled through the steel to reach the receiver. Normally (and this has been verified on earlier experiments) such a path facilitates the retention of high frequency components, but this has clearly not happened as the spectrum of Figure D16b testifies. Furthermore the velocity is far too low for this to be considered a likely possibility. Since both the velocity and frequency content are inconsistent with the notion that the majority of the signal passed through the steel (at least a small fraction of it must have), it follows that the wave front travelled by reflecting off the side walls. It is also possible that the internal cracks reduced the dissipation of the energy to the surrounding concrete, thereby increasing its rms value above that of the (d) trace.

With regard to the traces shown in Figures D17a and D17b, the similarity between the shapes of the envelopes indicates a surface wave contribution. There are differences in the spectra, since the spectra associated with position (E) appears to contain higher amplitude high frequency components. However, it is not clean whether there are genuine differences merely random statistical variations. On the basis of previous evidence, it does not seem likely that cracks well below the surface could affect the gross spectrum in such a manner, particularly since the trace taken at position (c), again an area of relatively intact concrete, does not bear any striking resemblance to the spectra of positions (e) or (f) (Figures D16a, D17a and D17b respectively).

The Propagation Mode Analysis sections dealing with;

- direct and indirect transmission systems,
- beam divergence,
- single surface groove effects and
- multiple surface cracks

has not answered all of the questions associated with indirect transit-time propagation, but most of the evidence points to the fact that the surface wave is a factor in any estimation of signal energy contributions. Whilst it is certainly not true that sub-surface components do not play a role in this scheme of events, only careful signal processing will extract those components that are affected by the internal conditions.

D.3 Frequency Sweep Analysis

Prior to the introduction of moderately high frequency probes combined with Fourier domain filtering, various techniques were used in an attempt to improve the high frequency content of the signals generated by the transducers.

One of these techniques involved exciting the transducers not with a simple voltage spike - a method analogous to striking a bell with a hammer and allowing it to resonate at its own natural frequency - but with a single, controlled sine wave of predetermined frequency. The circuit used to generate this wave shape is described in detail in Appendix G. Because of the low impedance of the output stage (connecting to the transducer), it was hoped that the crystal would be forced to undergo a controlled period of expansion and compression in phase with the energising sine wave.

However, spectral analysis revealed that it was virtually impossible to alter the frequency characteristics from those given by their impulse response (i.e. after shock excitation). Although the transducers normally produced a broad band signal, the centre frequencies were very much stronger than the side bands. This was because the degree of damping for most of the devices was fairly light - high damping reduces the sensitivity considerably, a severe limitation when interrogating heterogeneous media.

From this it was concluded that high frequency enhancement could only be realised through the use of suitable probes and signal processing methods, although it was not until some time later that this assumption proved to be correct.

ATTENUATION ANALYSIS

TABLE D1

a. MIX 1, NO AGGREGATE

LENGTH mm	VELOCITY m/s	RMS V	ENERGY Vs	INTEGRATED - FREQUENCY - AMPLITUDE kHz 25-50 (144-72)	kHz 125-150 (29-24)	kHz 225-250 (16-14)	kHz 325-350 (11-10)
100	3846.1	0.1399	10.0242	0.2443	0.1680	0.1704	0.0433
200	3636.3	0.2183	24.4103	0.2071	0.1628	0.3547	0.0290
300	3571.4	0.2577	34.0134	0.1181	0.0461	0.0349	0.0047
400	3478.8	0.1911	18.7046	0.1342	0.0147	0.0106	0.0032
500	3496.5	0.0623	1.9879	0.0114	0.0022	0.0014	0.0012

b. MIX 2, AGGREGATE < 10mm

				(160-80)	(32-27)	(18-16)	(12-11)
100	4347.8	0.2515	32.3827	0.1956	0.1142	0.1332	0.0191
200	4545.5	0.2198	24.7256	0.1875	0.0871	0.0866	0.0073
300	4225.4	0.1402	10.0601	0.2051	0.0465	0.0079	0.0019
400	3669.7	0.1518	11.7938	0.1764	0.0047	0.0036	0.0035
500	3311.3	0.0159	0.1294	0.0044	0.0011	0.0007	0.0006

c. MIX 3, AGGREGATE < 20mm

				(156-78)	(31.26)	(17.16)	(12.11)
100	4166.7	0.1544	12.2055	0.2180	0.0437	0.0303	0.0039
200	4651.2	0.2454	30.8373	0.1279	0.0173	0.0041	0.0027
300	3947.4	0.0408	0.8535	0.0364	0.0022	0.0008	0.0008
400	3333.3	0.0608	0.8913	0.0129	0.0030	0.0018	0.0016
500	3472.2	0.0246	0.3090	0.0040	0.0004	0.0003	0.00003

NOTES:

1. Figures in brackets denote λ at those frequencies.

2. All calculations based on 1st 512 µs after onset of signal.

TABLE D2

a. MIX 1, NO AGGREGATE

FREQUENCY (kHz)	a_0	a_1	r	Attenuation dB/100mm
25-50	-0.1535	-0.2847	0.8367	5.7
125-150	-0.0318	-0.4826	0.9602	9.7
225-250	0.3088	-0.5909	0.9158	11.8
325-350	-0.9109	-0.4056	0.9771	8.1

b. MIX 1, AGGREGATE ≤10MM

FREQUENCY (kHz)	a_0	a_1	r	Attenuation dB/100mm
25-50	-0.0572	-0.3305	0.7141	6.6
125-150	-0.1289	-0.5327	0.9526	10.7
225-250	-0.1524	-0.5907	0.9818	11.8
325-350	-1.4441	-0.3371	0.9209	6.7

c. MIX 1, AGGREGATE ≤20MM

FREQUENCY kHz	a_0	a_1	r	Attenuation dB/100mm
25-50	-0.1158	-0.4467	0.9935	8.9
125-150	-0.9063	-0.4747	0.9589	9.5
225-250	-1.3514	-0.4322	0.9072	8.6
325-350	-2.1418	-0.2465	0.8752	4.9

TABLE D3

	Transducer - Direct	Coupling Indirect
Velocity	4411.8	2941.2
Rms	0.0153	0.0109
Energy	0.2395	0.1223
fmean	105.7	81.8
f s.d.	104.0	90.8
$\int f$	0.1529	0.1362
fmax	14.0	14.0

TABLE D4

	Transducer - Direct	Coupling Indirect
Velocity	4411.8	2941.2
Rms	0.0762	0.0148
Energy	0.0882	0.0437
fmean	109.6	89.2
f s.d.	102.6	94.8
$\int f$	0.1382	0.0990
fmax	13.0	44.0

TABLE D5

	Transducer - Tx on Top	Coupling Tx on Side
Rms	0.003	0.006
Energy	0.001	0.003
fmean	50.1	79.5
f s.d.	68.7	108.9
$\int f$	2.3456	4.8536
fmax	10.0	10.0

Coherence Analysis: r = 0.8770

TABLE D6

	Transducer - Tx on Top	Coupling Tx on Side
Velocity	3896.1	3973.5
Rms	0.0208	0.0142
Energy	0.4416	0.2073
fmean	52.0	50.8
f s.d.	89.5	78.1
$\int f$	0.1793	0.1319
fmax	6.0	24.0

TABLE D7

	200mm - Unscored	Spacing Scored
Velocity	3389.8	2898.6
Rms	0.0113	0.0143
Energy	0.1310	0.2112
fmean	66.3	62.9
f s.d.	84.5	92.2
$\int f$	0.1258	0.1461
fmax	23.0	12.0

Coherence Analysis: r = 0.6555 (50 µs - 250 µs)
r = 0.2052 (251 µs - 450µs)

TABLE D8

	500mm - Unscored	Spacing Scored
Velocity	2873.6	2976.2
Rms	0.0129	0.0120
Energy	0.3385	0.2971
fmean	32.4	33.5
f s.d.	38.8	37.2
$\int f$	0.1270	0.1349
fmax	15.5	15.5

Coherence Analysis: r = 0.6781

TABLE D9

	Wide - Uncracked	Face Cracked
Velocity	3038.0	2400.0
Rms	0.01984	0.004
Energy	0.4029	0.0162
fmean	65.6	67.3
f s.d.	74.4	97.1
$\int f$	0.2226	0.0428
fmax	12.0	12.0

TABLE D10

	Narrow Face, Uncracked	Damaged Cracked
Velocity	1983.5	1846.2
Rms	0.0196	0.0491
Energy	0.3928	2.4681
fmean	68.1	65.4
f s.d.	111.4	107.9
$\int f$	0.1768	0.3090
fmax	9.0	13.0

TABLE D11

	Narrow Face, Uncracked	Intact Depth-Cracked
Velocity	1983.5	4067.8
Rms	0.0071	0.0062
Energy	0.0534	0.0393
fmean	95.6	77.2
f s.d.	96.1	93.4
$\int f$	0.1042	0.0718
fmax	6.0	9.0

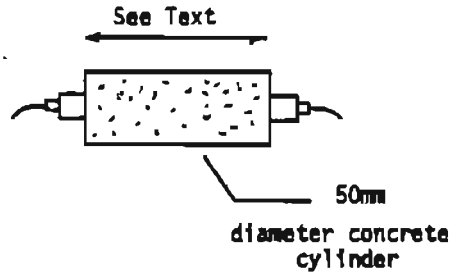

Figure D1

Attenuation System

Figure D2.a

Direct Transmission

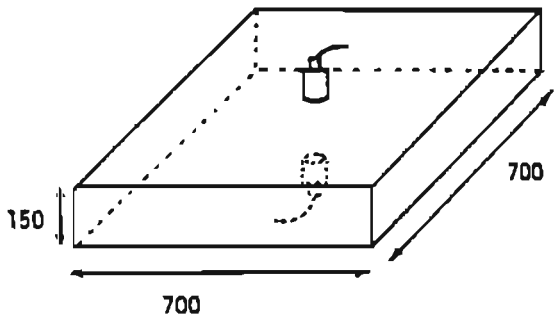

Figure D2.b

Indirect Transmission

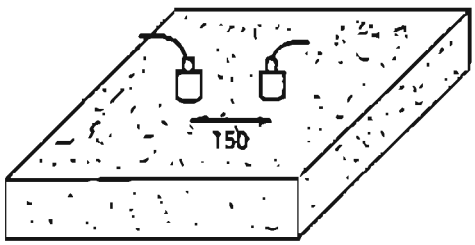

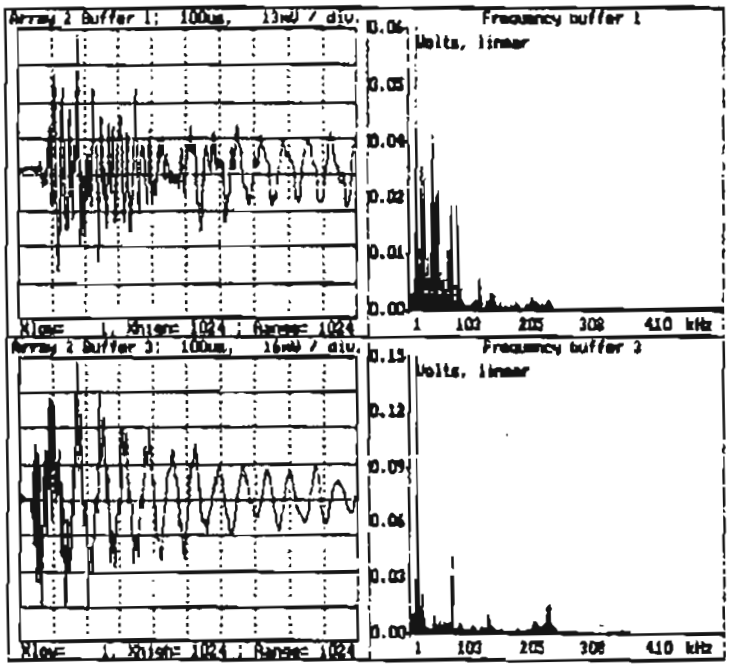

Figure D3.a

Direct

Indirect

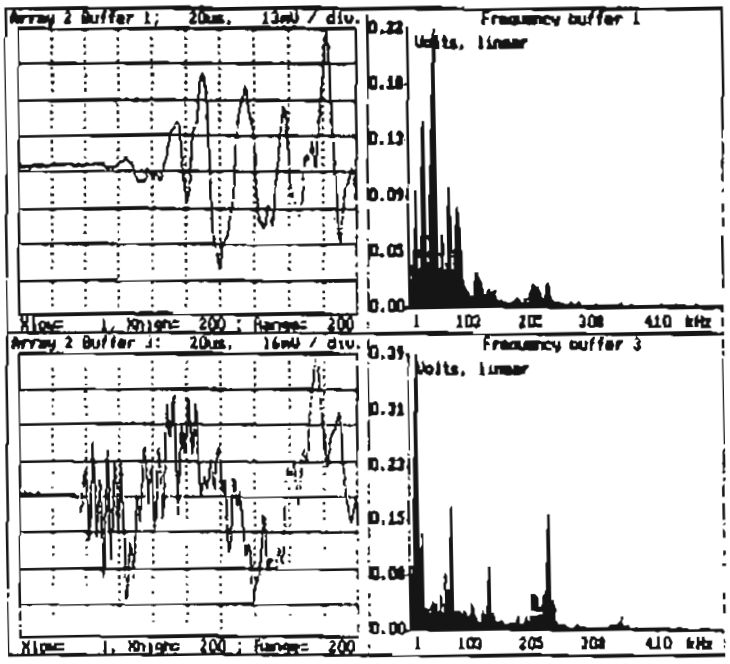

Figure D3.b

Direct, 1st 200us

Indirect, 1st 200us

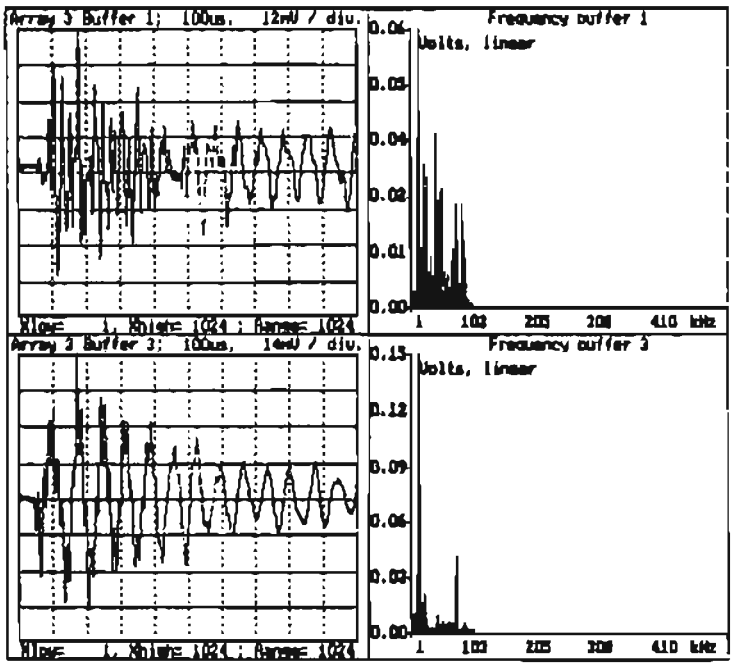

Figure D4.a

Direct, LF pass Filter

Indirect, LF pass Filter

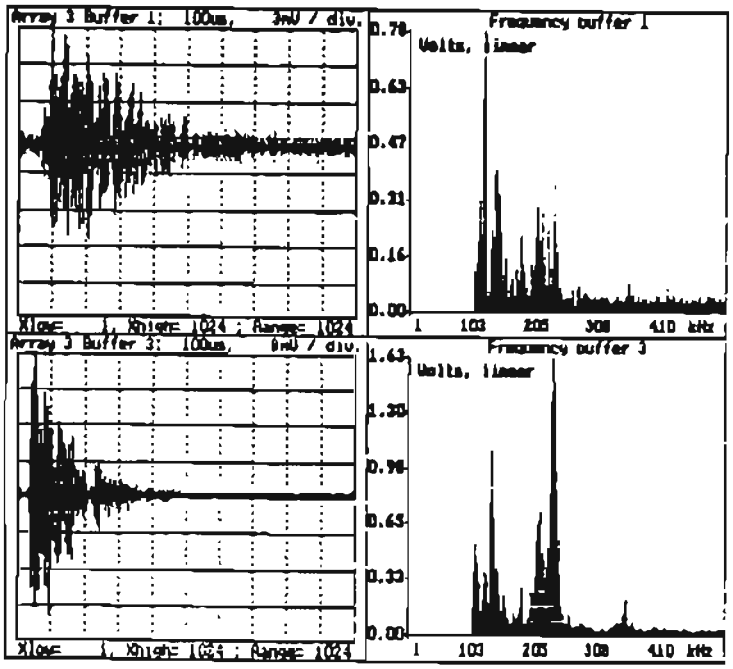

Figure D4.b

Direct, HF pass Filtr

Indirect, HF pass Fil

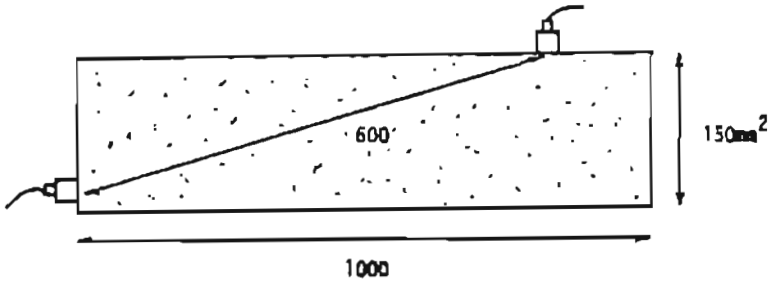

Figure D5

Beam Divergence Estimation

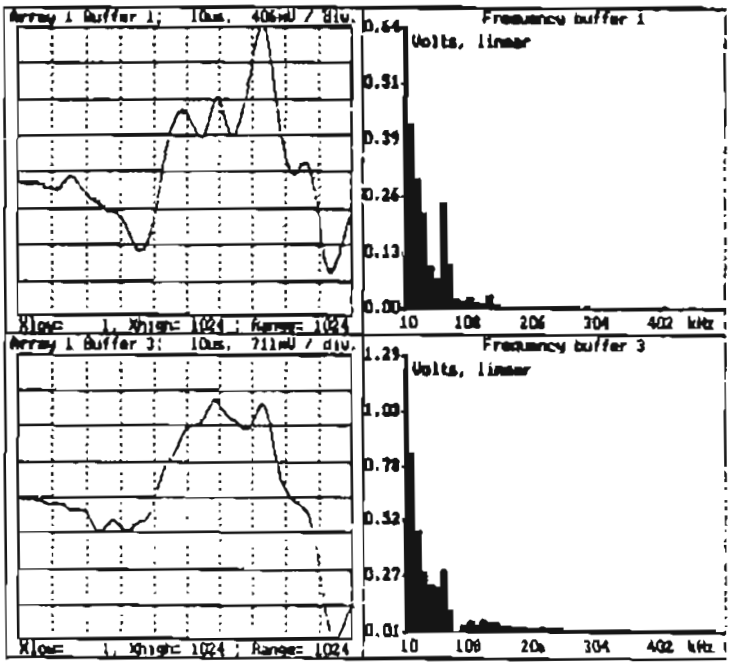

Fimure D6

a. Tx on top face

b. Tx on side fac

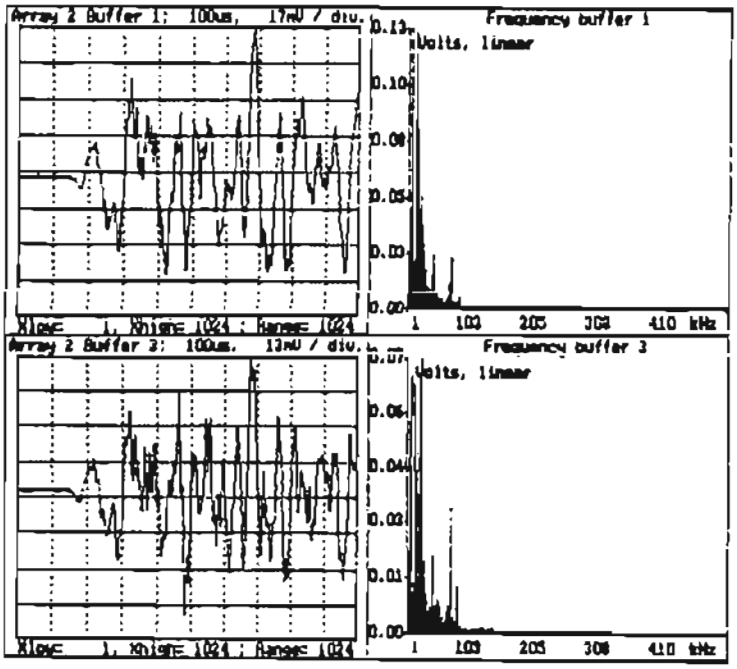

Figure D7

a. Tx on top face

b. Tx on side face

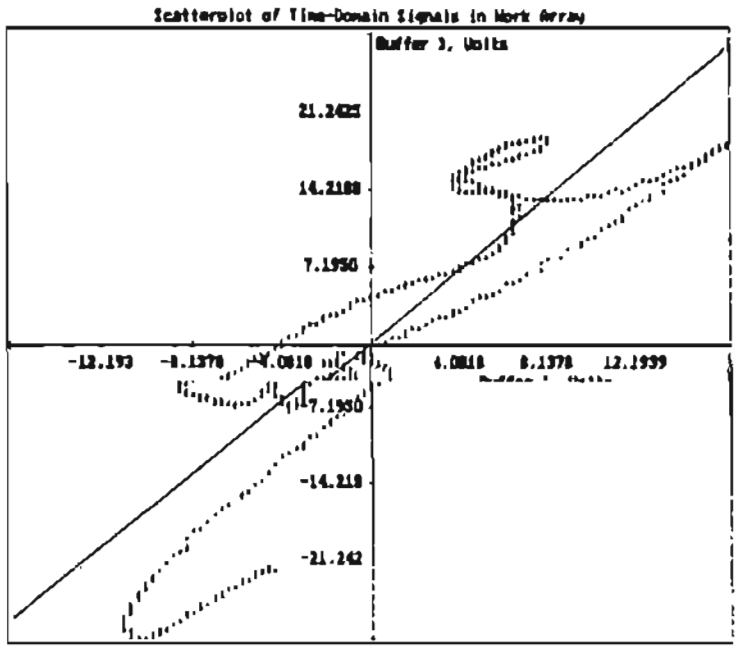

Figure D8

Coherence analysis
Trace 6b V Trace 6

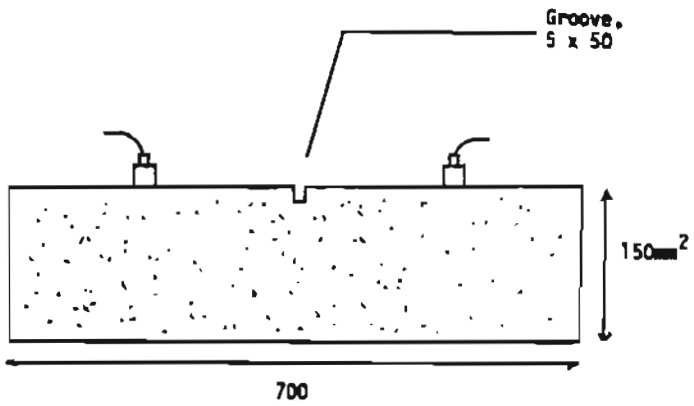

Figure D9

Groove effect determination

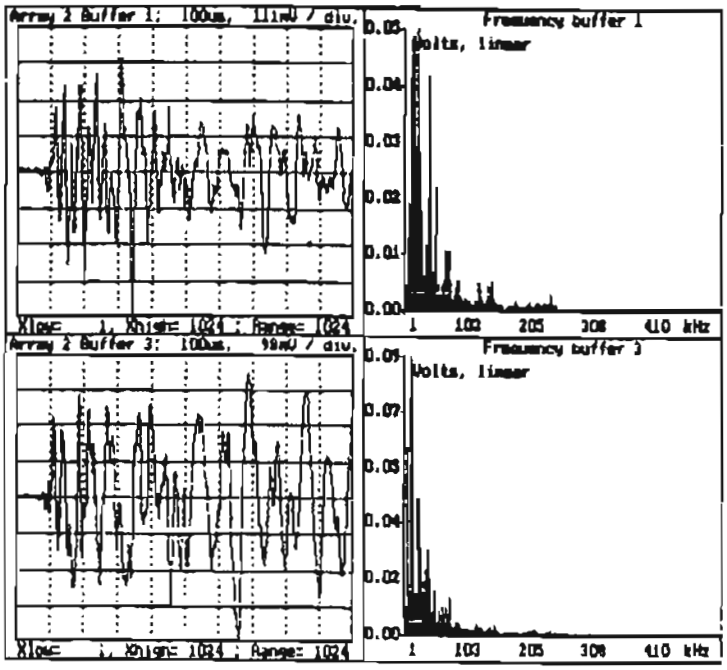

Figure D10

a. Intact Sampl
200mm

b. Grooved Sampl
200mm

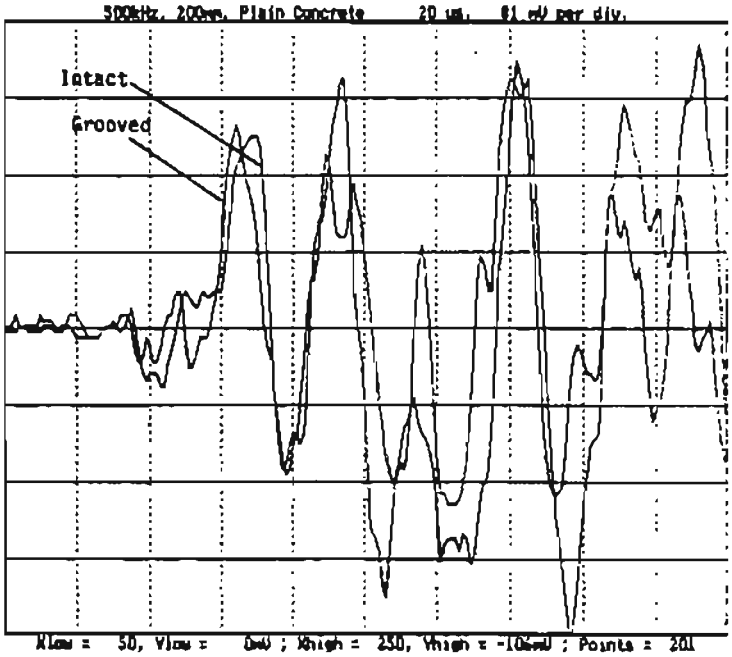

Figure D11

Intact and Groov
Samples, 1st 20C

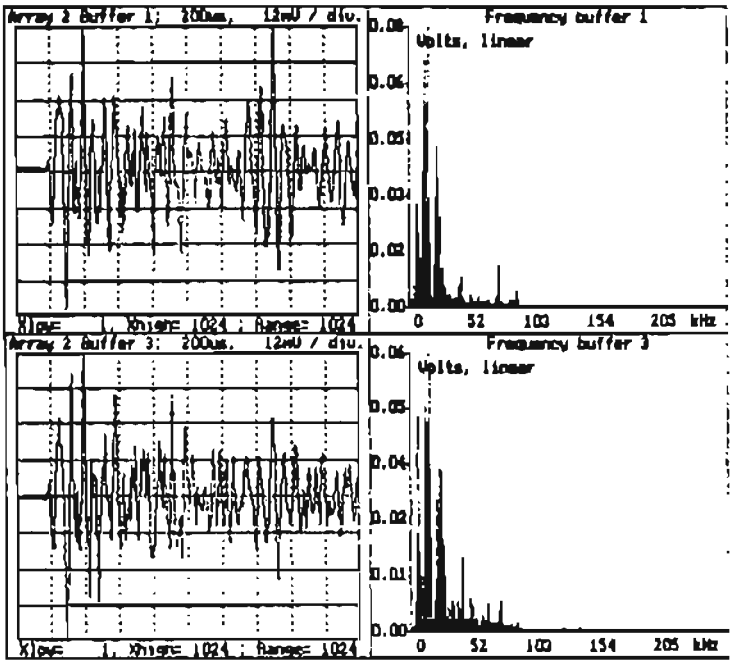

Figure D12

a. Intact, 500mm

b. Grooved, 500mm

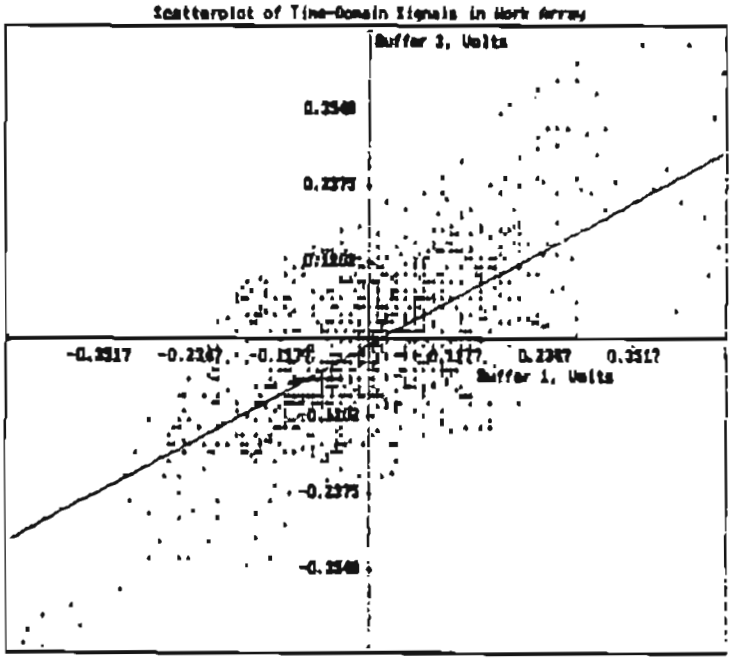

Figure D13

Coherence analysis
Grooved V Intact,
500mm

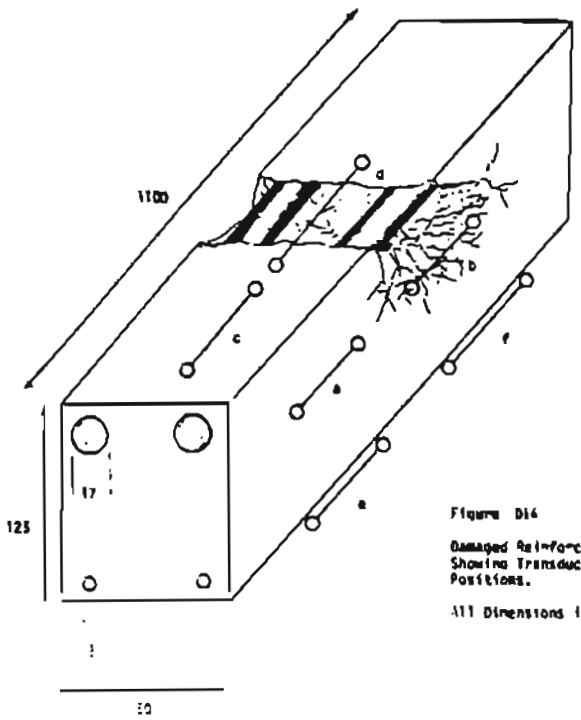

Figure D14

Damaged Reinforced Samp
Showing Transducer Test
Positions.

All Dimensions in mm.

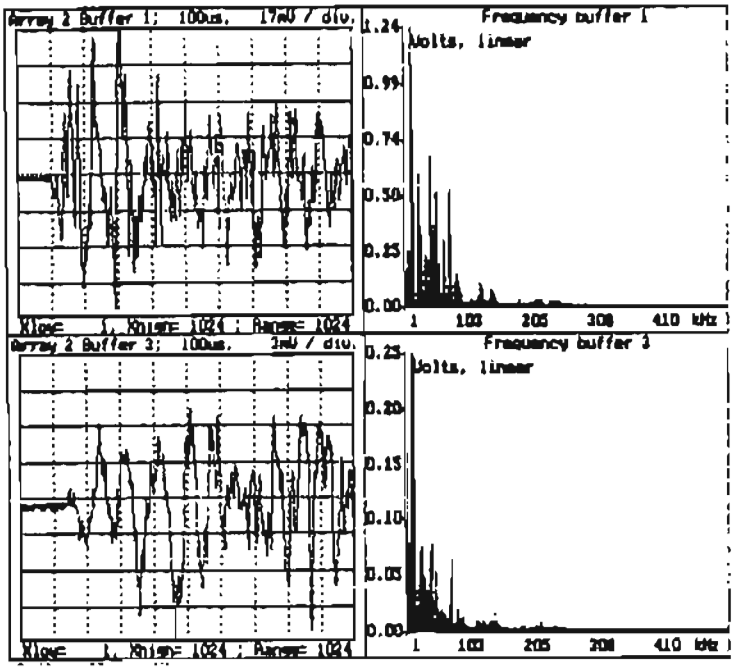

Figure D15

a. Position a.

b. Positiob b.

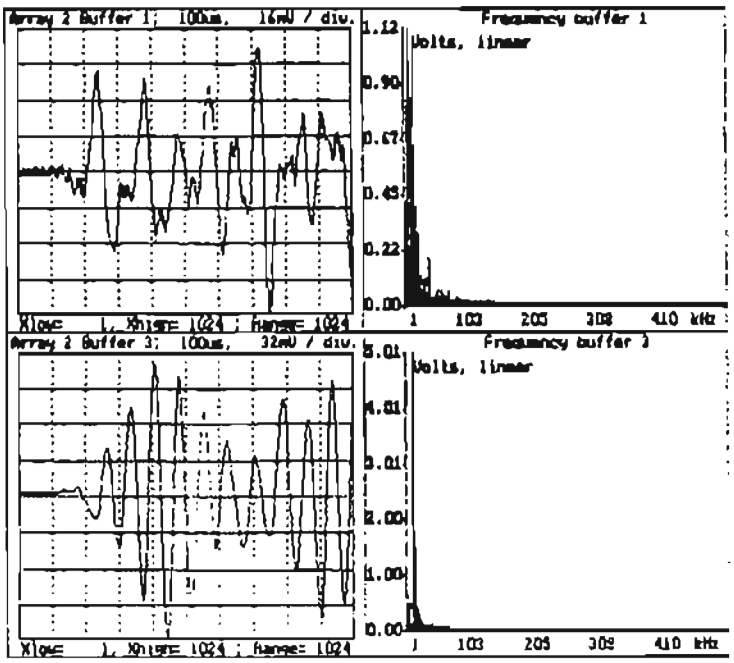

Figure D16

a. Position c.

b. Position d.

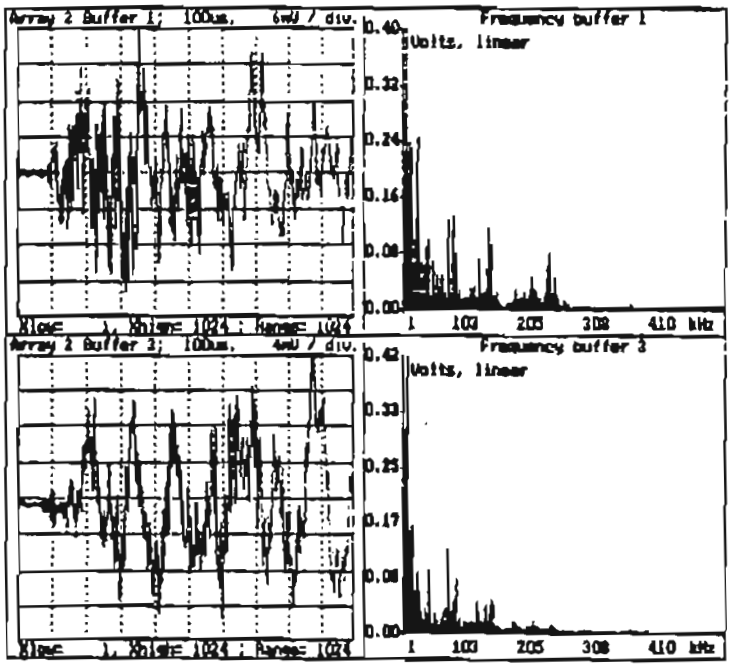

Figure D17

a. Position e.

b. Position f.

APPENDIX E: METHODS OF ANALYSIS: EARLY EXPERIMENTATION AND WATER SIMULATION TRIALS

E.1. Concrete Sample And Beam Tests

Prior to the introduction of frequency domain filtering and the energy calculations based on discrete frequency band, most of the analysis of ultrasonic signals was based, in the time domain, on signal velocity, rms voltage, energy, and dB attenuation. These calculations were usually carried out on data records 1024 bytes in length, using a sampling frequency of 1MHz and triggered to coincide with the excitation pulse sent to the transmitting probe. These basic calculations were made more reliable, under certain conditions (as in the presence of noise or low amplitude signals) by the application of signal averaging, smoothing, amplitude modulation and signal addition.

Given a discrete time signal x(t), its velocity is calculated using the identity:

$$c = \text{sample length/transit time} \qquad (E.1)$$

with length in metres, time in seconds and c in m/s.

The rms voltage of such a signal is given by:

$$V_{rms} = \sqrt{\left(\frac{\sum_{t=1}^{n} x(t)^2 . \delta t}{n}\right)} \qquad (E.2)$$

and the energy by:

$$E = V_{rms}^2 . T \qquad (E.3)$$

with E in volt-squared seconds, and T being the duration of the sample in seconds.

There are a number of methods that can be used to estimate signal-to-noise or attenuation statistics, but the method used predominantly in this research has been based on the decadic logarithm of the signal rms:noise rms ratio or signal rms:reference rms ratio, multiplied by 20, i.e. S/N is given by:

$$S/N\ (rms) = 20\text{Log}\left[\frac{S_{rms}}{N_{rms}}\right] \qquad (E.4)$$

and attenuation given by:

$$\alpha = 20\text{Log}\left[\frac{S_{rms}}{P_{rms}}\right] \qquad (E.5)$$

where P is the acoustic pressure generated by the transmitter, measured at a distance of 3 mm in water.

Addition of two discrete time signals is performed using the formula:

$$x_3(t) = x_1(t) + x_2(t), \quad t = 1 \text{ to } 1024 \tag{E.6}$$

and amplitude modulation by:

$$x_3(t) = x_1(t)[x_2(t)], \quad t = 1 \text{ to } 1024 \tag{E.7}$$

Signal smoothing was normally performed using a running mean algorithm. Given a running mean of i points, the implementation is simply:

$$x_2(t) = \sum_{n=t}^{t+i} x_1(n), \quad t = 1 \text{ to } 1024-i \tag{E.8}$$

If the running mean is weighted, equation (E.8) becomes:

$$x_2(t) = \sum_{n=t}^{t+i} x_1(n)g(n), \quad t=1 \text{ to } 1024-i \tag{E.9}$$

where g(t) is the weighting function.

The signals were also analysed in the frequency domain after Fourier transformation had been applied to the data. The signal x(t) may be expressed as the sum of an infinite set of harmonic components, thus:

$$x(t) = \frac{1}{2\pi} \int_{-\infty}^{+\infty} X(\omega)e^{j\omega t}d\omega \tag{E.10}$$

Because of the phenomenon of symmetry between time and frequency domains, the spectrum, X(ω), is given by:

$$X(\omega) = \int_{-\infty}^{+\infty} x(t)e^{-j\omega t}\,dt \tag{E.11}$$

The spectrum for all discrete time signals was calculated using a standard fast-Fourier transformation algorithm that derived 512 harmonics from a signal 1024 points in length, with a spectral resolution equal to the inverse of the sample length, i.e. if the sample lasted 1 ms, the spectral resolution became 1 kHz.

Most of the calculations made in the frequency domain involved finding the ratio of the integrated harmonic amplitude for a particular bandwidth using some reference band or the total spectrum. The general formula for such an operation is given by:

$$r_f = \frac{\int_b^a X(\omega)d\omega}{\int_d^c X(\omega)d\omega} \tag{E.12}$$

in which a and b define the band limits of the signal which is being measured and c and d define the band limits of the reference signal.

E.2. Water Simulation Trials

Most of the analysis of the data gathered from the water based experiments was based upon the detection of phase changes to indicate corresponding changes in the signal path length, which in turn suggested changes to the condition of the reflecting interface. Strictly speaking, this is not really an example of phase shifting, since such a phenomenon involves a change in the frequency characteristics of the signal. The phase discrepancy arises from the change in onset time of the echo. Because the shape of the waveform is unaffected, the disparity is ideally suited to cross-correlation analysis, a technique that is highly sensitive to two similar signals exhibiting displacement in the time domain.

The expression for the discrete time domain cross-correlation is given by:

$$y(t) = \sum_{T=-\infty}^{T=+\infty} x(t)z(t=T) \qquad (E.13)$$

where x(t) is the first input record,
z(t) is the second input record, and
y(t) is the output record.

In order to establish the onset discrepancy (given here in microseconds), the point of maximum correlation is subtracted from the time corresponding to that point in the function representing the correlation of the two signals when they are aligned, point for point, in the time record.

To highlight differences in the frequency domain, the polynomial functions and their respective correlation coefficients were calculated. These functions describe the degree of association between any two sets of readings, and are sensitive to both phase and amplitude. Unlike the cross-correlation function however, they are not sensitive to local changes but represent a method of testing general signal coherence. The general form of the polynomial equation is:

$$y = a_0 + a_1 x + a_2 x^2 + \ldots + a_n x^n \qquad (E.14)$$

and the correlation coefficient is calculated using the expression:

$$r = \frac{\sum (x-\bar{x})(y-\bar{y})}{\sqrt{[\sum (x-\bar{x})^2 \sum (y-\bar{y})^2]}} \qquad (E.15)$$

E.2.1 Notes to Tables

At the end of this appendix are included a number of tables containing the results of analyses performed on the data taken from the water based experiments, described in Section 2.5.8 of the main body of this report. In these tables, the symbols A and B refer to the signals detected by the left-hand receiver and right-hand receiver respectively, in clear water. A1 and B1 refer to signals reflected to the same probes from a good quality steel bar present in the tank, and A2 and B2 refer to the signals reflected from a bar that was defective in some way (see tables for details).

TABLE E1

TRANSDUCER CHARACTERISTICS, WATER ALONE

CHANNEL	RMS, V	ENERGY, V^2 µs	fo kHz	FREQ. INTEGRAL, V kHz	ESTIMATED VELOCITY m/s
A	0.0755	5.8353	122	0.7361	1476.1
B	0.0675	4.6678	117	0.6914	1467.8

Notes on Table 1:

1. Above figures calculated over a sample period of 1024 µs.

2. The propagation velocity for sound in water is usually given as 1482.3 m/s.

TABLE E2

ENERGY AND SPECTRAL CHANGE CHARACTERISTICS, CHANNEL B ONLY

EXPERIMENT	RMS, (V)	ENERGY, (V^2 µs)	FREQUENCY INTEGRAL, (V kHz)	AMPLITUDE AT 41 kHz, (V)	AMPLITUDE AT 121 kHz, (V)	HF:LF RATIO, (dB)
Good Steel	0.0359	0.4489	0.3245	0.0017	0.0102	15.6
Midway Cut	0.0256	0.2381	0.2379	0.0021	0.0076	11.1
Cut Near Tx	0.0470	0.8051	0.3840	0.0026	0.0136	14.4
Rotated Cut Force	0.0389	0.5514	0.3246	0.0027	0.0113	12.4
Corroded Bar Naturally	0.0139	0.0706	0.1481	0.0008	0.0041	14.2
Corroded Bar	0.0323	0.3805	0.2276	0.0005	0.0110	26.0

TABLE E3

GOOD STEEL V STEEL CUT MIDWAY BETWEEN TX AND CHANNEL B

CHANNELS	PHASE CHANGE, TIME DOMAIN, µs	FREQUENCY CORR. COEFFICIENT	FREQUENCY SPECTRAL SHIFT, kHz
A1 B1	In phase	0.9311	-1
A2 B2	- 0.6 (0.9 mm)	0.8844	In phase
A1 A2	- 0.1 (0.1 mm)	0.9325	In phase
B1 B2	- 0.7 (1.0 mm)	0.9001	In phase

TABLE E4

GOOD STEEL V STEEL CUT AND ROTATED THROUGH 90°, MIDWAY BETWEEN TX AND CHANNEL B

CHANNELS	PHASE CHANGE, TIME DOMAIN, μs	FREQUENCY CORR. COEFFICIENT	FREQUENCY SPECTRAL SHIFT, kHz
A1 B1	In phase	0.9311	-1
A2 B2	-1.2 (1.8 mm)	0.8650	-1
A1 A2	+0.5 (0.7 mm)	0.9421	In phase
B1 B2	-0.6 (0.9 mm)	0.9830	In phase

TABLE E5

GOOD STEEL V FORCE CORRODED BAR, POSITIONED MIDWAY BETWEEN TX AND CHANNEL B

CHANNELS	PHASE CHANGE, TIME DOMAIN, μs	FREQUENCY CORR. COEFFICIENT	FREQUENCY SPECTRAL SHIFT, kHz
A1 B1	In phase	0.9311	-1
A2 B2	+0.9 (1.3mm)	0.8471	-1
A1 A2	-0.2 (0.3mm)	0.9522	In phase
B1 B2	+0.7 (1.0mm)	0.8916	In phase

Notes to Tables E3 to E5.

1. Time Domain cross-correlation function derived from 1st 26.4 μs of a signal sampled at 10 MHz.

2. Frequency Domain cross-correlation function derived from 1st 200 harmonics of a Fourier transformed signal, the latter having been sampled at 1 MHz and windowed to the first 364 μs.

3. Phase changes are indicated by referencing the first Channel shown against the second. Hence in Table E5, row 3, Channel A_1, lags $_2$ by 0.2 μs.

APPENDIX F: CANDI SYSTEM: DESCRIPTION AND OPERATING PROCEDURES

F.1 System Description

i The CANDI hardware system comprises five major components:
ii The transducers
iii The pulser/synchronisation unit
iv The amplifier
v The waveform analyser
vi The host computer.

The heart of the system is the Analogic waveform analyser, which in turn comprises a model 630 analogue-to-digital converter and a model 6100 processing unit.

The A to D converter is a twin channel device, featuring independent time bases, a sampling rate ranging from 1.7 mHz to 35 MHz, a maximum record buffer length of 8192 points and built-in anti-aliasing filter at 5MHz. Standard sampling resolution is 9 bits (512 levels) with 12 bits in signal compression mode (4096 levels). The device can be triggered in a wide variety of ways, either internally or by an external source, or clocked for each sample point. Post and pre-triggering is available as standard.

The 6100 processing unit is built around the 16-bit 68000 microprocessor, and has three distinct processing modes:

i By single key stroke;
ii By execution of a user-written program, stored in the unit's own memory;
iii By the control of a host computer.

The unit has a very comprehensive repertoire of operations, with more than 50 waveform analysis, manipulation, signal processing and display functions. These include forward and inverse FFTs (typically 400 ms for a record length of 512 points), chirp-Z transforms, convolution, correlation and all the standard scalar calculations.

F.2 System Operating Procedure

The roller type transmitting transducer is connected to the 600V output of the pulser/synchronisation unit, and the synchronisation output of this device is connected to the trigger input of the 630 A to D converter. The roller type receiver is then connected to one channel of the amplifier, and the gain set to 40dB. Its output is connected to one input of the A to D converter. The analyser itself is connected to the host computer by means of a standard IEEE cable. The analyser, amplifer and computer are then switched on.

The supervisor software, CANDI 1.6 (see Appendix G), held in the computer, is activated by simply typing CANDI and pressing the return key. The program will automatically configure the analyser to the setup normally required for a standard scanning operation. This setup is as follows:

i IEEE address #4, EOI enabled, CR-LF as end-of-message delimiters.
ii Plotter RS232 interface at 4800 baud, no parity, 1 stop bit, full duplex.
iii External trigger, 640 mV positive going threshold, DC couple. Initialised to DISARM status.

iv Channel 1: 1MHz acquisition speed, 512 point record length, DC couple, +5V sensitivity, no time base offset, single record display.

v FFT outputs of magnitude and phase, hanning window.

Once the system has been configured, the concrete surface to be scanned is sprayed with water and the transducer bogie is positioned at the first scan point. The pulser is then turned on, and a reading is taken every 10 mm. The time records are then stored in the analyser's memory by pressing the COPY button after each successive reading. After the specimen has been scanned, the data are transferred to the computer's hard disc by using the program's file-handling sub-menu.

Once the data have been stored, they may be analysed in a variety of ways by simply accessing the data analysis sub-menu of the program. This sub-menu may instruct the analyser to calculate simple scalar measurements on each record and present them as a single trend trace; alternatively it can instruct the analyser to perform "brick-wall" filtering on the data and then make the above scalar measurements on the filtered data. Once the trends have been calculated, CANDI instructs the analyser to plot the traces on a Hewlett Packard (or HPGL compatible) plotter.

APPENDIX G: SOFTWARE AND EQUIPMENT PRODUCED

G.1 ULTRAMATH 1.6

This software package was written prior to the purchase of the Analogic waveform analyser and was used in conjunction with the Solartron digital storage oscilloscope to record and process ultrasonic signals in experiments performed before March 1989. It is a menu based system, written in Turbo-Pascal revision 4.0.

The command level menu comprises four categories - data acquisition, time domain analysis, frequency domain analysis and data display.

The data acquisition option allows the user to read the contents of the two channels of the solartron 5602 oscilloscope, with the time base and the sensitivity being automatically detected. The data are stored as real text values, and although there is an overhead in terms of storage requirements, this is largely academic given the hard disc capacities of most modern machines. Moreover, it allows the user to readily examine or edit the data using the Pascal editor, or enter the data through the keyboard if a suitable data acquisition unit is not available.

When the program is running, the data are held in the four storage arrays, that is, data arrays one to three and the work array. Each array comprises in turn four data buffers, 1024 bytes in length, each having the capacity to hold the data from one channel of the oscilloscope. Hence the program can hold a maximum of 16 time records at any one time in various stages of processing.

The time domain analysis menu has eight major options, involving operations on a specific time record or combinations of records.

The file-handling option allows the user to load or save data to or from the disc, from or to the program's data arrays.

Array translation provides options for the transfer of data within the program's data arrays.

The reset data facility enables the original data to be restored after a processing sequence without the necessity of re-reading the files from disc. This has obvious implications in terms of speed and efficiency.

If analysis is to be made of only part of the data, rather than the full 1024 bytes, the set window option provides the means of examining a specific segment of the time record.

The arithmetic operations menu contains a list of processes which may be carried out on a single buffer (time record). These include adding a constant, subtracting the DC component, adjusting the gain, squaring, differentiating, phase shifting or half-wave rectifying the signal.

By contrast, the signal combination menu contains operations which combine different signals in some way. These include waveform addition, subtraction, multiplication and division by other waveforms, cross or auto-correlation, and polynomial regression analysis between any two waveforms. This last option can handle polynomials up to the fourth order, and also provides the associated statistics such as standard errors and confidence limits.

The main time domain menu option 7, the rms feature, calculates the rms, mean and energy values of all waveforms in the work array. The energy is displayed in volt-squared micro-seconds, assuming a 1 ohm load.

The final option in the time domain menu, the filtering menu, enables the user to filter the data using either a running mean filter of up to 20 points or a sine-weighted running mean filter.

Like the time domain analysis menu, the frequency domain analysis menu has buffers assigned to the data. The program can hold up to four spectra simultaneously, as real, imaginary, magnitude and phase components. Although, strictly speaking it is really only necessary to hold the real and imaginary components for complete spectral description, the computer has more than enough memory to accommodate the other two components, and since this obviates the requirement for recalculation, the speed of processing is considerably enhanced.

The main menu includes a file handling facility similar to that of the time domain menu, for storage and retrieval of spectra.

The second option is the windows menu, allowing rectangular, triangle or hanning windows to be applied to the data prior to Fourier transformation.

As in the time domain menu, there is also a windowing facility to allow the processing of a specific bandwidth of data, and a data reset option.

Options five and six carry out fast Fourier transformation of the time domain data and inverse transformation of a spectrum to the time domain respectively. On a 286 AT machine operating at a clock frequency of 8 MHz, transformation of a 1024 point record (to obtain 512 harmonics) requires approximately 12 seconds.

The filter design option allows the user to filter a signal in the frequency domain by performing "brick-wall" filtering of up to 10 frequency bands and then re-transforming to the time domain. This of course is one of the key operations performed by the present CANDI system.

The arithmetic operation menu provides the user with the ability to multiply a spectrum by a constant, to take the spectral logarithm, to calculate it in terms of a self-referenced dB scale (maximum set at 0 dB), to square it or to calculate basic statistics on a spectrum such as the centre frequency and its standard deviation.

The last option in the frequency domain menu, the combinations menu, enables the addition, subtraction, convolution, deconvolution, cross-correlation and polynomial regression analysis of any two spectra.

The final option presented at the command level menu is termed the display processor, and in turn consists of a four option menu. This is a versatile sub-system of ULTRAMATH 1.6 which can generate a wide variety of graphical displays either on the screen or on paper using a printer. Option 1 configures the screen to a given display template, selected by the user; the user specifies which array buffers are to be assigned to which display mode. Once this has been done to the user's satisfaction, the template may be stored and recalled at a later date without the need for re-configuration. One of three screen modes may be selected for display at any one time, and these comprise the remaining menu options of the display processor. These modes are:

a **Mode 1**: full screen, single plot. In this mode the program can display a time record (a signal trace), a frequency spectrum (phase or amplitude), a scatter plot and its associated polynomial curve, or a cross-correlation plot. The last two may be the results from either a time or frequency domain operation.

b **Mode 2:** full screen, multiple plot. In this mode the program can display up to four overlayed signal traces.

c **Mode 3:** split screen, multiple plot. The screen is split into four quadrants, any one of which can display either a signal trace or a frequency spectrum (phase or amplitude).

In modes a and b, the screen is interactive. By using the function keys, the user can position bracketing cursors to window a specific trace or spectrum segment. This obviates the need to return to the windowing facilities provided in the time and frequency domain menus once a region of interest has been identified. The windowed region can then be redrawn, automatically enlarged to encompass the full area of the screen. All calculations are now referenced to the windowed segment only. If the plot is of a spectrum (amplitude component only), a third cursor travelling in the y plane can be manipulated to threshold the noise level of the plot. When the plot is redrawn, all values below the cursor are excluded since auto-scaling is performed.

G.2. CANDI 1.6

Like ULTRAMATH 1.6, CANDI 1.6 is a menu based program written in Turbo-Pascal revision 4.0. Its purpose is to provide the user of the system with a simple, powerful and rapid means of control of the analyser. For instance, many of the operations performed on the data, such as digital filtering of up to 100 records with subsequent energy calculations, would require a great number of key-presses (not to mention time) if they were executed using the analyser's front panel controls. By merely providing CANDI 1.6 with the basic information, i.e. which records are to be processed and in what manner, the program instructs the analyser to automatically sequence through the data, processing and storing the results of the analysis.

The command level menu has seven options. The first is a general control option, whereby specific commands may be sent to the analyser, e.g. 'DARM', which instructs the A to D converter to disable all trigger inputs.

The file utilities option is a sub-menu, enabling the user to transfer data from the analyser to the computer and vice-versa, transfer programs into the analyser's memory for execution, or to merge several data files into a single, large file. This last option makes for more efficient data processing.

The data analysis option is another sub-menu, giving the user the following choices:

a Trend template editing. CANDI 1.6 currently provides automatic calculation of up to 11 scalar measurements: rms, energy, duty cycle, maximum and minimum amplitude, peak-to-peak amplitude, mean amplitude, frequency, period, number of cycles and time of occurence of maximum amplitude. Not all of these will normally be used in an analysis run, so certain ones may be selected and the choice stored by the program to obviate the requirement of re-inputing the selection.

b Trend analysis. The scalar measurements, given by the trend template, are calculated using the scan data-set. The results are presented as a trend trace.

c Spectral analysis. Each record in the scan data-set is analysed using a chirp-z transform. This is similar to an FFT but provides unlimited spectral resolution, regardless of time domain record length. The user must enter the required centre frequency and bandwidth.

d Bandpass filtering. This is again performed for all records in the scan data-set. The user selects the filter bandwidth, and the analyser calculates the fourier spectrum for each record, filters it and re-transforms it to the time domain.

e Envelope detection. Many signals have a high frequency carrier wave modulated by a low frequency envelope. This function allows the envelope to be isolated by applying a Hilbert transformation to each record in the scan data-set.

The Data plotting option is the last sub-menu in the CANDI program. it provides the user with the ability to plot single trend displays or waterfall displays using a HPGL compatible plotter.

The remaining two options at the command level are not often used. These are the record auto-copy facility, which instructs the analyser to make copies of a number of traces (thus protecting the original data from accidental deletion or corruption), and the batch command sequence, a command used when setting certain segments of a data record to a specific value, for a given number of records.

In addition to the functions listed above, CANDI 1.6 provides the user with an on-screen note pad facility. By selecting this option, the user can enter text in a reserved area, for the purposes of making notes on an experiment or scan operation. This was added to the program to make the use of pens and note paper unnecessary in a field environment.

G.3. FOUR CHANNEL INSTRUMENTATION AMPLIFIER

This unit actually comprises four identical amplifiers, one of which is shown in Figure G1. The design is a significant improvement on the single stage differential amplifier, and constitutes the standard instrumentation amplifier configuration. The input stage is a subtle combination of two op-amps that provides high differential gain without any close resistor matching. Its differential output represents a signal with substantial reduction in the comparative-mode components, and it is used to drive a second stage conventional differential input amplifier circuit with a single ended output. Offset trimming is achieved with a trimming resistor connected to one of the input stages. The first stage gain is variable, being dependent on resistors R1, R2 and R3. normally, resistor R3 (665 ohm) is not switched into the circuit. In this case the first stage gain is given by:

$$G = 1 + 2(R2/R1) \qquad (G.1)$$

and is therefore x 11. Resistor R3 can be switched into the circuit by the FET switch (DG180) which shunts it in parallel with resistor R1. At first sight this may seem an unnecessarily elaborate way of connecting R3 into the circuit, since it could more easily be achieved by replacing the FET switch with a simple mechanical device. However, in doing so the signals that were being amplified would be taken, along wires, to the front panel of the instrument (where the switch would be located), thereby increasing the

likelihood of noise pickup. By employing a FET switch, the only voltages taken to the front panel are DC control voltages, used to turn the DG180 switch on or off. This is termed logic-switched gain or "cold" switching and is used whenever very low noise performance is required. When resistor R3 is connected into the circuit, the first stage gain becomes:

$$G = 1 + \frac{2(R2(R1+R3))}{R1 \cdot R3} \qquad (G.2)$$

With the values of the components in the design, the gain now becomes x 41. The second stage gain is fixed at x 10, given by R5/R4. Hence the overall gain of the amplifier is either x 110 or x 410, depending on the condition of the FET switch, i.e. approximately 40dB or 52dB.

In order to maximise the performance of this amplifier, a high grade op-amp was chosen for the input and output stages of the design. The op-amp that was used was the OP-37, a bi-polar device, which features the following specifications:

a Standard operating voltage of ±15 V.
b Output voltage swing of ±11 V.
c Noise figure of 3 nV/Hz at 1 kHz.
d Common-mode rejection ratio of 126 dB.
e 123 dB open-loop gain.
f Input bias current of ±15 nA.
g 17 V/µs slew rate.
h Small signal gain-bandwidth product of 63 MHz.

The most important features in this case are the low noise figure and the gain bandwidth product. By cascading the op-amps in the manner of the above, an amplifier is produced with a constant gain extending to several megahertz.

G.4 FOUR-TO-TWO CHANNEL MULTIPLEXER

This device was used when the signals arriving from four independent receiving probes were to be connected to only two channels of the waveform analyser. It operated by alternately switching between probes 1 & 2 and 3 & 4, deriving its synchronisation from the trigger pulse produced by the ultrasonic pulser. G2 shows the circuit design.

The trigger is input to a 311 comparator circuit, the purpose of which is to convert the signal to TTL levels. This in turn is fed to a 74HC123 timer, configured to produce a pulse in synchrony with the trigger pulse, but lasting for 0.2 secs. This is connected to a 74HC4024 7-stage ripple counter, which, at its 1st stage output (pin 12), changes state from logic high to low alternately at the end of each pulse sent from the 74HC123. The state change is used to select, for output, two of the four inputs to the FET switch, the AD792. The outputs are unity-gain buffered by the 351 op-amps, and the channels that have been selected are indicated by the LEDs driven by a 7437 high-current driver.

The sequence of events is as follows. When the 74HC4024 is reset, the output is set to logic low and pins 12 and 11 are selected on the AD792 (channels 1 and 2) for the output pins, 13 and 10. The status remains this way for 0.2 s after the reception of a trigger pulse, which also occurs at the

same instant the transmitting probe is fired. This time, 0.2 s, is more than enough for the system to acquire the signal. After this period, the 74HC4024 changes state to logic high and pins 14 and 9 are selected on the AD792 (channels 3 and 4) for the output pins. This process is repeated each time a trigger pulse is received.

G.5. SINGLE-CYCLE SINE WAVE GENERATOR

This unit was constructed in an attempt to drive transducers at other than their resonant frequencies, by exciting them in a controlled manner rather than shocking them into oscillation. This controlled driving took the form of a single sine wave whose period could be varied from DC to 1 MHz.

The circuit is shown in Figure G3. A conventional continuous sine wave generator is fed to the input of a 311 comparator, configured to change state at the zero-crossing points of the sine wave, in non-inverting mode. The sine wave generator is also connected to the input of a DG211 FET switch, which is normally open, i.e. the single is not transmitted to the output pin, pin 3. The output of the 311 comparator is connected to a 12 stage ripple counter, a 74HC4040. Every stage of its output is AND-ed together, resulting in a single pulse at the output of the 74HC30 after every 4096 pulses produced by the comparator, or 4096 cycles produced by the sine wave generator. This pulse lasts exactly for one period, synchronised to the start of the sine wave. Since the pulse is routed to the FET switch, one sine wave in 4096 appears at the output pin, pin 3. Hence for a frequency of 100kHz, One cycle is output every 40.96 mS.

G.6. LOW VOLTAGE PULSE-ECHO UNIT

This device was constructed to enable low frequency probes (below 500 kHz), to be operated in pulse-echo mode, rather than in pitch-catch mode, their usual method of usage.

Figure G4 shows the circuit diagram. The pulse repetition frequency (PRF) is generated by a single Schmitt gate of a 74HC14, configured as a square wave oscillator. By selecting one of three resistors in the feedback path, frequencies of 10 Hz, 100 Hz or 212 Hz can be generated. The PRF is buffered by a second Schmitt gate, and used to drive two 74HC123 monostable circuits. The first produces a pulse 10 us in duration in response to the leading edge of every square wave generated by the 74HC14. This is used to trigger the oscilloscope. The second produces a pulse 1 us in duration and forms the basis of the signal used to excite the transducer. It is amplified from 5 V to 15V by the 7667 high current driver. The 15 V pulse is fed via a 50 ohm resistor to the transducer. The 50 ohm resistor is used to raise the output impedance of the 7667 driver and reduce the damping of the transducer. The transducer is also connected to the input of an OP37 op-amp, with diode D1 used to ground the large input pulse which would otherwise saturate the output of the amplifier. The amplifier is configured as a non-inverting AC device with an input impedance of 22 kohms and a gain of x 93.

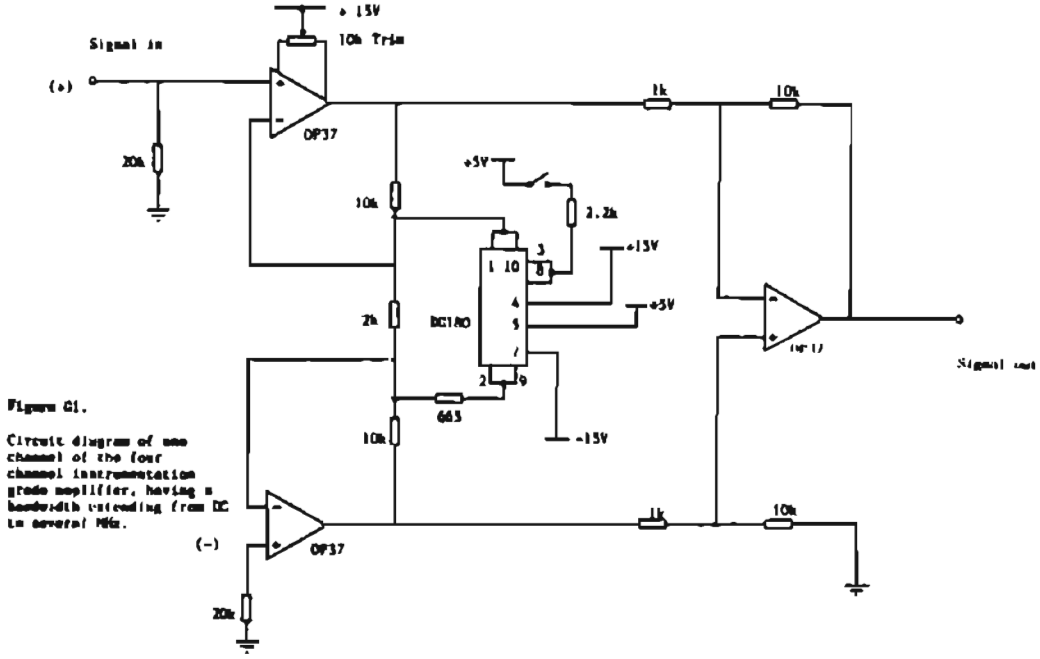

Figure G1.

Circuit diagram of one channel of the four channel instrumentation grade amplifier, having a bandwidth extending from DC to several MHz.

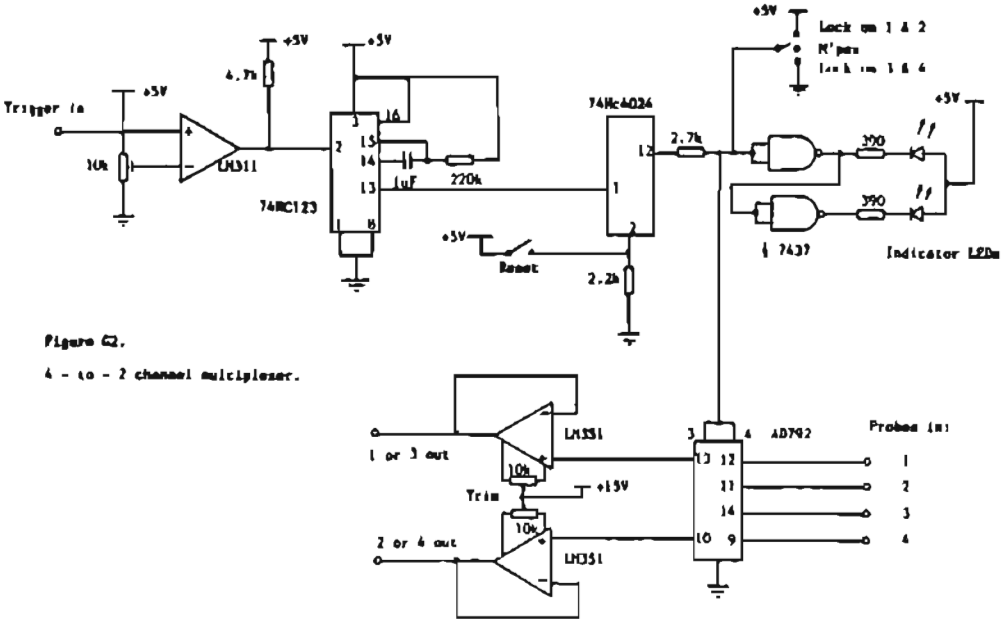

Figure G2.

4 - to - 2 channel multiplexer.

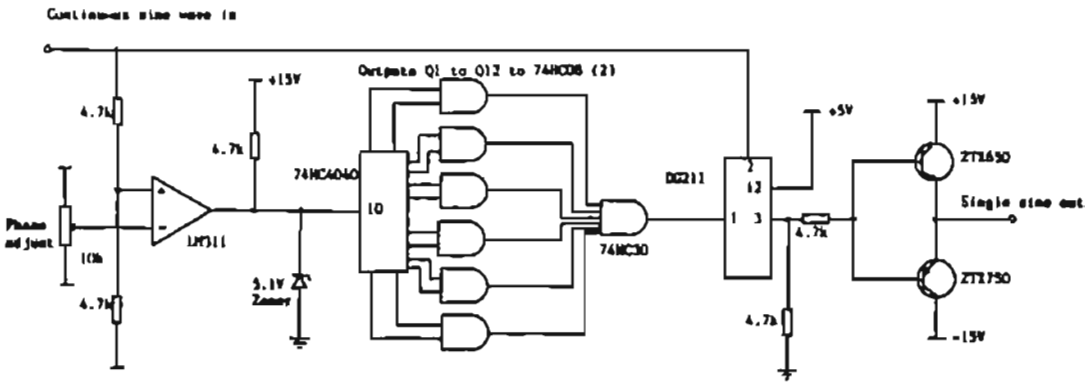

Figure C3. Circuit diagram for single-cycle sine wave generator.

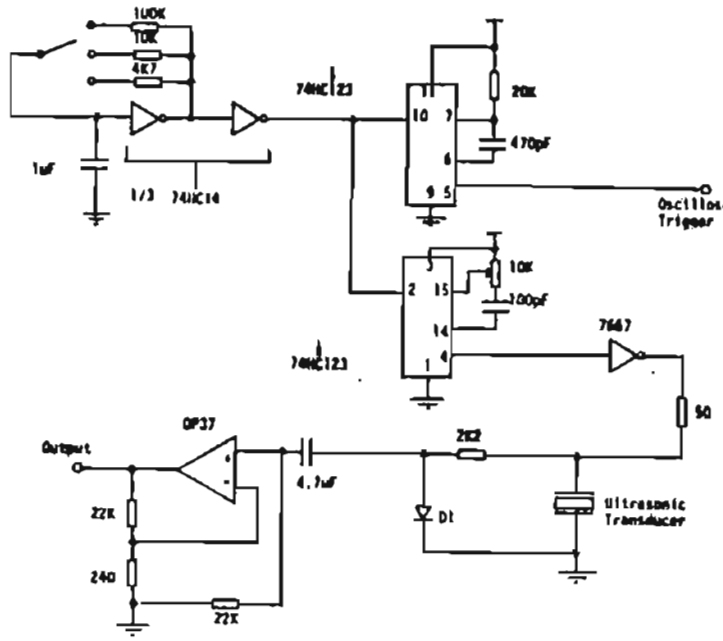

Figure C4.

Pulse-Echo System Circuit Diagram

Note: For purposes of clarity, decoupling capacitors and power supply connections have been omitted.